5. EXPERIMENTS AND MODEL VALIDATION*

5.1 Introduction

In order to apply the models presented in the previous chapter, effort has to be put on the validation of the developed numerical tools. The final objective for all tools developed in this context is to estimate the danger potential that can arise after a hypothetical release of hydrogen into the containment atmosphere of a NPP. Therefore, the results of numerical simulations need to be comapared with basic experiments.

The first part of this chapter describes the test facilities that were used to investigate various combustion phenomena. Although the experimental results, presented in this chapter, are not detailed enough to be used as input data for independent numerical simulations, they are intended to give code developers a comprehensive overview of what kind of experiments were performed in various test facilities. In particular, shock-induced ignition and transition to detonation, accelerating flames in obstacle arrays, and turbulent combustion in complex and large-scale geometries are addressed.

The second part of this chapter deals with the state of simulating hydrogen combustion phenomena as they are currently applied. A comparison of the state of the art in the application versus the state of the art of what is theoretically possible as shown in Chapter 4 shows that there is still a wide gap between the two. This is mainly related to the lack of sufficient computing memory and run time. Nevertheless, with increasing concerns regarding the system safety, the demand for more detailed and sophisticated modelling increases as well. However, for most of the everyday engineering tasks, it would be ineffective and unnecessary to employ the most-advanced and most-complex modelling tools. A compromise is to compile a hierarchy of models with an increasing level of detail, starting from coarse-grained lumped-parameter codes up to combustion modelling in Reynolds-averaged Navier-Stokes (RNS) field codes. The latter are concerned with computer resources, the most common method of simulating turbulent combustion today.

The examples of code validation presented in the second part of this chapter show the potential of a specific combustion model implemented in a certain type of code. An exemplary list of selected codes – classified into the categories lumped parameter, hybrid CFD-lumped-parameter, and CFD-Codes – is shown.

* Andreas Eder is the lead author for Chapter 5.

5.2 Experiments for Code Validation

5.2.1 Shock Reflections and Focusing *

5.2.1.1 Preliminary remarks

The problem of shock (or blast) waves reflections and focusing in combustible media is one of the key problems of DDT phenomena. Up to now, a representative review of main experimental and theoretical results (e.g., [5.1 – 5.17]) in this field does not exist.

5.2.1.2 Experimental set-up and description of the reflectors used

3D reflectors. The experiments on shock focusing near 3D reflecting endplates were conducted in a horizontally placed laboratory shock tube. A general scheme of the experimental set-up in [5.3, 5.4, 5.12 – 5.14] is shown in Figure 5.2.1.2-1. The low-pressure chamber (LPC) had a circular cross-section diameter of $D = 54$ mm and the high-pressure chamber (HPC) was 50 mm in diameter. The lengths of LPC and HPC were 1 m and 0.5 m respectively. The initial pressure in LPC, p_1, was varied in the range 0.8 to 6 bar. The maximum pressure in HPC reached $p_4 = 100$ bar. Helium, nitrogen, and argon were used as driver gases. Initially, the HPC was separated from the LPC by a hermetically mounted bursting membrane. Six reflectors of various shapes were available in the experiments. The end part of the LPC was properly designed to allow easy replacement of the reflector, including the installation of the plane-surface end flange. The photographs and charts of the reflectors used are presented in Appendix C in Figures. C.3.1(a-e).

These 3D surfaces can be described as follows: two cones with a length/diameter ratios $L/D = 1.5$ and 0.5 respectively (Figures C.3.1 a,b); two parabolic reflectors with length/diameter ratios $L/D = 1.5$ and 0.5 respectively (Figures. C.3.1 c,d); pyramid with 90° angles between the top ridges and ratio of the height L to the diameter D of base-inscribed circle being 0.7 (Figure C.3.1e). The same experimental procedure for 3D spherical reflectors was used in Reference [5.8], but in that work, the cross-section of spherical cavity (F) was only part of the full channel cross-section as in the scheme shown in Figure C.3.1.f.

2D reflectors. The tests on shock focusing near 2D reflecting end plates were realized in laboratory shock tubes with a rectangular cross-section [5.3,5.4,5.12,5.13,5.15]. The geometry of used 2D reflectors and the scheme for the arrangement of pressure and radiation gauges are shown in Figure 5.2.1.2-2. The displacement of 2D reflectors was the same that used in Reference [5.6] and [5.8]. As shown in Figure C.3.2 the reflecting wedge did not fully cover the channel cross-section. The exhaustive information about main initial parameters in different series of experimental research is presented in Table 5.2.1.2-1. The table contains information about the type of gaseous mixture, volume concentration of H_2 (% H_2), type of reflectors used, size of the cross-section of the test channel S_t, range of initial pressure p_0, length of reflector L_r, content of nitrogen in the mixture, volume concentration of steam (% $\mathrm{H_2O}$), initial temperature T_0, and ratio of reflector-covered area (F) to the cross-section of the test channel F/S_t.

* Contributed by Professor B. E. Gelfand

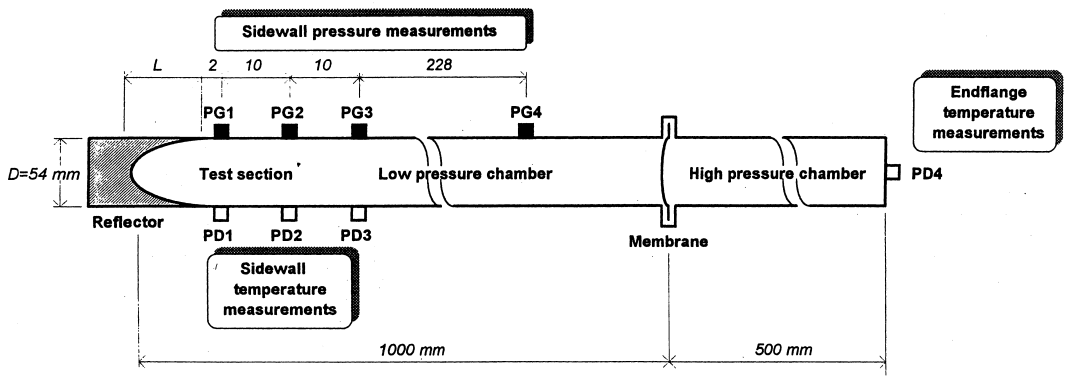

Figure 5.2.1.2-1 Scheme of the shock tube and the arrangement of the pressure and temperature measurement systems

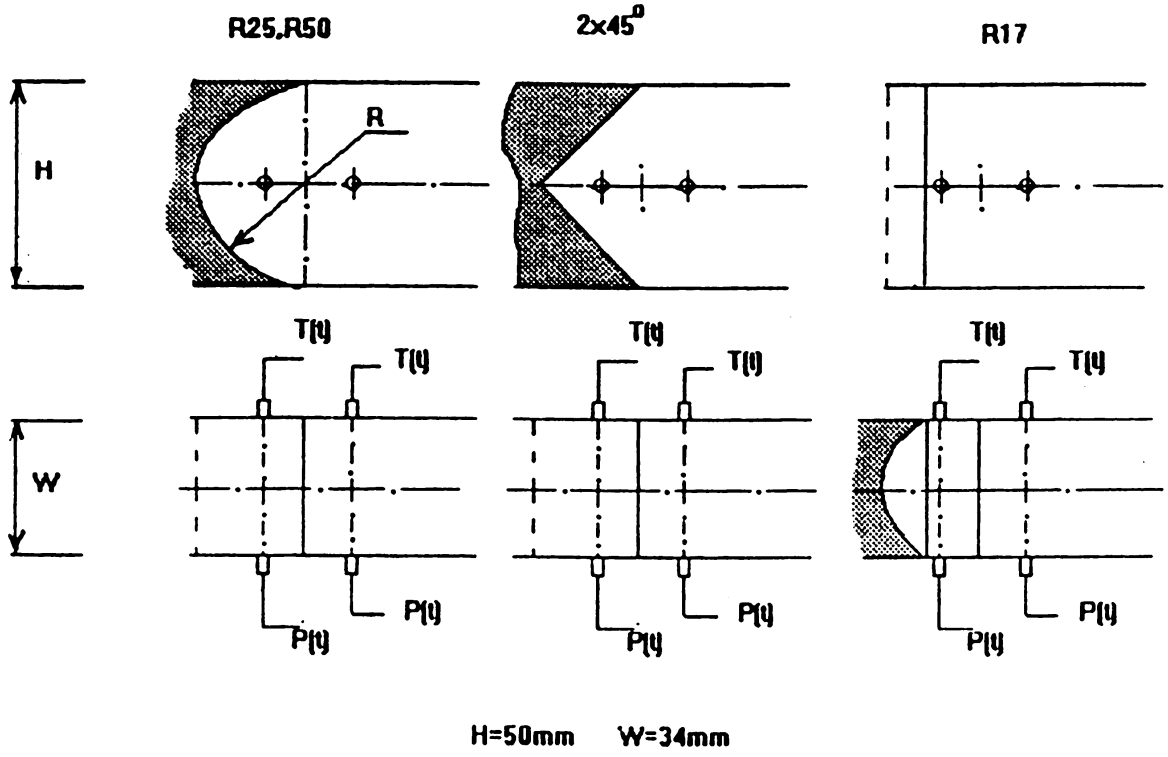

Figure 5.2.1.2-2 The main 2D reflectors and the scheme for the arrangement of pressure and radiation gauges

Table 5.2.1.2-1 Main initial parameters of shock focusing research

Mix	$\%H_2$	Refl.	S_t [mm^2]	P_0 [bar]	L [mm]	N_2/O_2	$\%H_2O$	T_0 [K]	F/S_t	[ref]
$2H_2 + O_2$	66%	wedge $15°$,$30°$,$45°$	90×90	0.05 - 0.2	12.7 - 60	0	0	293	$< 100\%$	[5.6]
H_2 + Air	15% - 60%	cylinders / radii $17, 25, 50$ mm, $45°$ wedge angle	34×50	1.0 - 3.0	$L = R$ $R = 36$ mm	3.76	0	293	$< 100\%$	[5.12, 5.13, 5.15]
H_2 + Air	15% - 60%	sphere: $R = 27$ mm cone: $R = 27$ mm parabola: $R = 27$ mm pyramid	$\pi \times 54^2/4$	1.0 - 3.0	$L/D = 1.0$ $L/D = 0.5, 1.0$ $L/D = 0.7$	3.76	0	293	$< 100\%$	[5.13]
H_2 + Air $2H_2 + O_2$	15% - 60% 66%	cylinders / radii $15, 22, 24$ mm	90×90	0.04 - 0.14	L= R	2.0 - 7.0	0% - 30%	293 - 393	9% - 28%	[5.8]
$2H_2 + O_2$	66%	sphere: $R = 35.7$ mm cylinder: $R = 22.5$ mm	$\pi \times 78^2/4$ 45×40	0.1 - 0.5	$L = 78$ mm $L = R$	0	0	293	83% 100%	[5.9]

5.2.1.3 Shock wave intensity, self-ignition regimes, mixture composition, and reflector type

A strong dependence was found experimentally between mixture composition and the type of reflectors installed near the end plates of the ignition-test shock tubes and the resulting shock wave intensity corresponding to different self-ignition regimes. Here, we discuss some important related observations.

3D reflectors One can plot the experimental dependence of Mach numbers corresponding to different self-ignition regimes in the mixture composition for each reflector used. A conical reflector $L/D = 1.5$ was chosen as a basis for the comparison. The dependence corresponding to this reflector is shown in Figure 5.2.1.3-1. A no-ignition region is shown below the curve 1. Curve 2 corresponds to the start of the self-ignition, which results not necessarily in flame front formation and propagation. Nevertheless, region A between curves 1 and 2 is potentially hazardous. Only the detonation-like strong ignition regimes take place in region C above the curve 3. Region B between curves 2 and 3 is responsible for mild ignition. As the ignition model approaches curve 3, it becomes transient and, finally, strong. These curves are U-shaped. Region B is extended when the hydrogen concentration approaches the limits. This is important for hazard assessments. Also, it is to be noted that stoichiometric mixtures are ignited at the reflection of shock perturbations propagating with a Mach number of about $M_{\min} = 1.1$. Therefore, a flame front moving with a velocity 330 m/s generates pressure disturbances that correspond to this shock wave intensity. These disturbances, being reflected from the obstacles, can cause secondary ignition, thus favouring the escalation of explosion.

Now let us consider the parabolic reflector with the same ratio $L/D = 1.5$. These data are presented in Appendix C, Figure C.3.3a. The results of conical and parabolic reflectors $(L/D = 1.5)$ are similar to each other except that for a parabolic reflector, the transition to strong ignition takes place at higher Mach numbers. Data for 3 reflectors with $L/D < 1$ are shown in Figure C.3.3 (b-d) of Appendix C. The incident shock wave Mach numbers at which self-ignition takes place are higher than those for the reflectors described above. This effect is more pronounced for near-limit mixtures. When the L/D ratio of the conical reflector changes from 1.5 to 0.5 (mixture with 15% H_2), the transient mode is replaced by the mild one at $M_{\min} = 2.13$, and, the strong regime changes to transient at $M_{\min} = 2.29$. Note that the

range of Mach numbers $M = 0.9$ to 1.0 is typical for the mild ignition regimes for near-limit mixtures ($M = M_{\rm tr} - M_+$), where $M_{\rm tr}$ and M_+ are respectively the Mach number corresponding to the transient regime of self-ignition and to the appearance of the self-ignition). This range is narrower for the 2D reflectors and is equal to $M_{\rm min} = 0.2$ to 0.5. Another specific feature of the ignition at the reflectors with $L/D < 1$ is the expansion of the domain of the mild ignition for stoichiometric mixture. For example, the strong mode occurs at $M_{\rm min} = 1.9$ for the pyramid, whereas the cone $L/D = 1.5$ requires $M_{\rm min} = 1.39$. The experiments performed confirm the conclusion [5.8] about the independence of critical shock wave intensity (i.e., Mach number) on the initial pressure in the range of 1 to 5 bar. The same results were obtained in tests conducted with a spherical reflector and described in Reference [5.8]. The domains of main explosion regimes are presented in Figure 5.2.1.3-2 for stoichiometric H_2 + O_2 mixture in the range of initial pressure $p_0 = (0.3$ to $14)$ kPa. Figure 5.2.1.3-3 demonstrates the dependence of low boundary of detonation domain for H_2 + air on mixture composition at elevated initial temperature. Figure 5.2.1.3-4 confirms the weak influence of initial pressure on the value of minimal Mach numbers for shock wave triggering detonation by focusing of the shock wave. Figures 5.2.1.3-5 and 5.2.1.3-6 represent the inhibition of self-ignition near spherical reflectors with additives of nitrogen or steam in a gaseous mixture.

2D reflectors. The tests performed allow us to present the dependence of the critical Mach numbers upon mixture composition and also for 2D reflectors. The typical dependence is presented in Figure 5.2.1.3-7 for a cylindrical reflector with radius of curvature $R = 17$ mm. No ignition occurs in the region below line 1. Zone A between lines 1 and 2 corresponds to the spotty ignition regime. Zone C above line 3 is responsible for the detonation explosive regime. In region B, between curves 2 and 3, transition regimes were observed. All 13 curves have a U-shaped form that is responsible for a known dependence of critical ignition and detonation parameters upon the mixture composition. A similar dependence was obtained for cylindrical reflectors with $R = 25$ mm, $R = 50$ mm, and for dihedral corner reflector 2, 4, 5 (see Figures C.3.4 a-c in Appendix C). The comparison of results for plane shock focusing at 3D (hemispherical) and 2D (cylindrical) reflectors is shown in Figure 5.2.1.3-8. As stated earlier, line 13 divides zones A, B, C for reflector $R = 17$ mm. Lines 1, 2, 3 demonstrate a significant decrease of critical Mach numbers at which the spotty and transition ignition regimes take place in the case of 3D reflectors. To summarize, the following observations are made from the results of these tests:

1. Shock or blast wave focusing, [5.18], inside 2D or 3D cavities essentially extends the range of parameters of pressure waves that can trigger explosion phenomena in H_2 + air mixtures.
2. The critical conditions for self-ignition in H_2 + air mixtures are determined for the wide nomenclature of focusing cavities. Three-dimensional cavities with conical and parabolic geometry are the most efficient for self-ignition in H_2 + air mixtures.
3. The dependence of critical Mach numbers responsible for self-ignition and the transition between ignition modes on the mixture composition have a characteristic U-shape.
4. Initial pressures in a range 0.1 to 5 bar do not affect the critical Mach number.

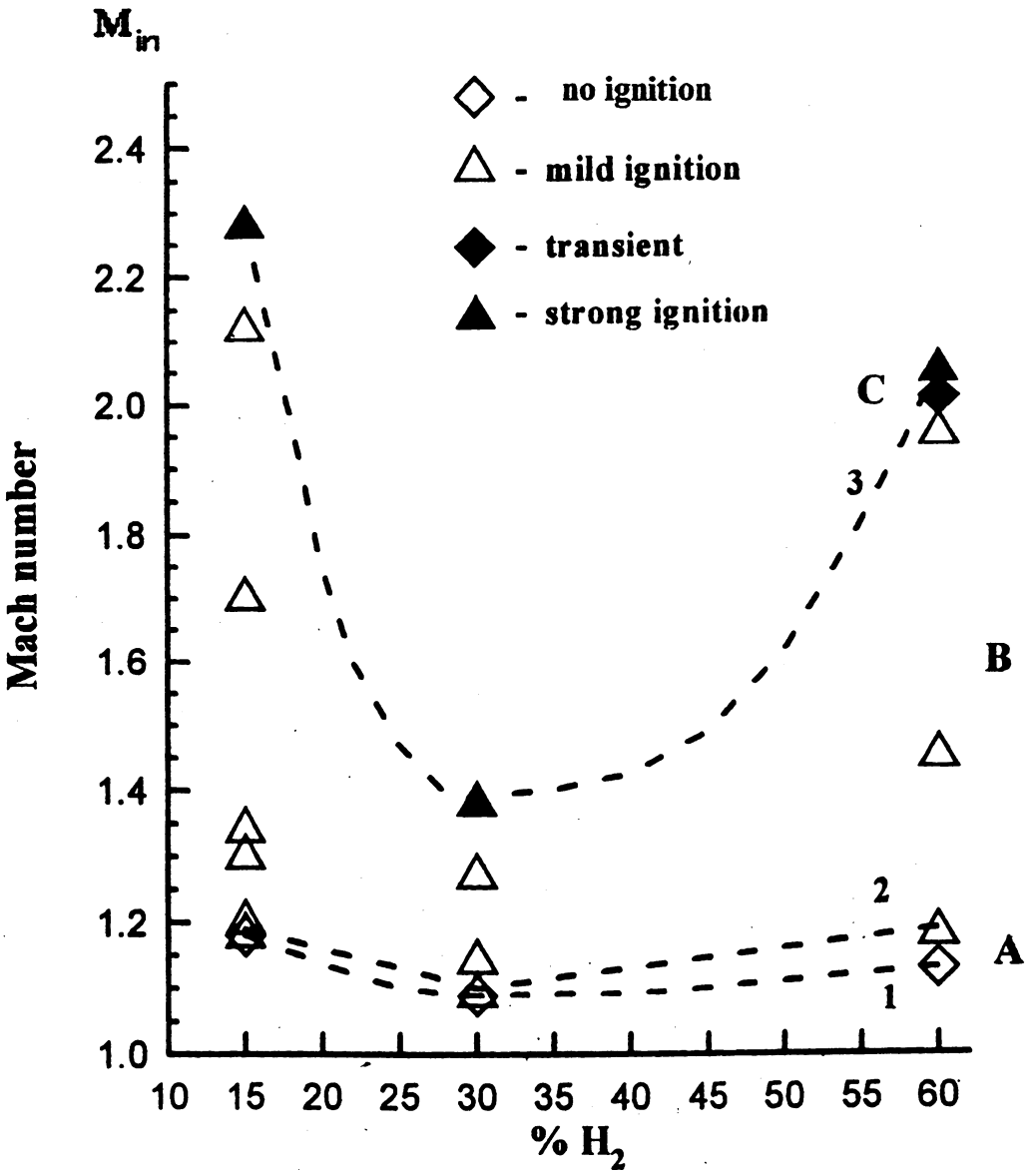

Figure 5.2.1.3-1 The incident shock Mach numbers corresponding with various modes of self-ignition versus hydrogen-air mixture composition. Reflector Cone $L/D = 1.5$. Curve 1 shows no ignition; curve 2 shows mild ignition with hot spot formation; curve 3 shows strong ignition; A shows the danger zone, where there is a possibility of ignition in the hot spots type; B shows the region of the mild-to-strong transient ignition; and C shows strong ignition zone.

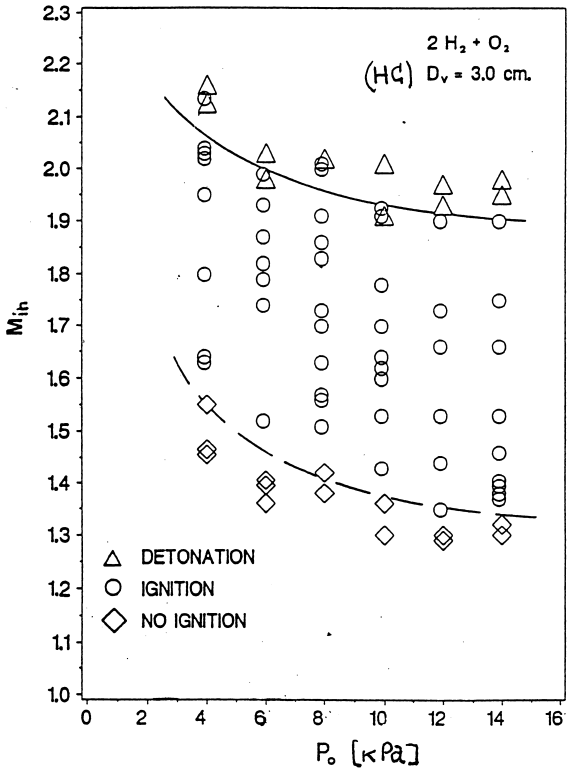

Figure 5.2.1.3-2 The influence of pressure on main self-ignition regimes near hemispherical reflector in $2H_2 + O_2$ mixture

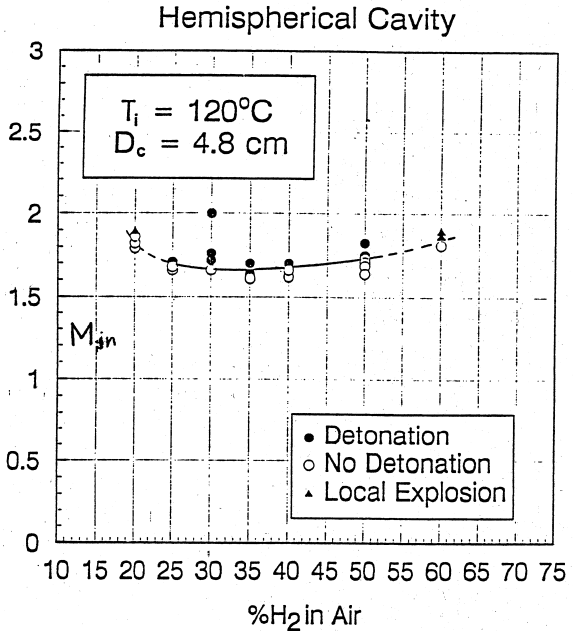

Figure 5.2.1.3-3 The influence of mixture composition on self-ignition near 3D reflector

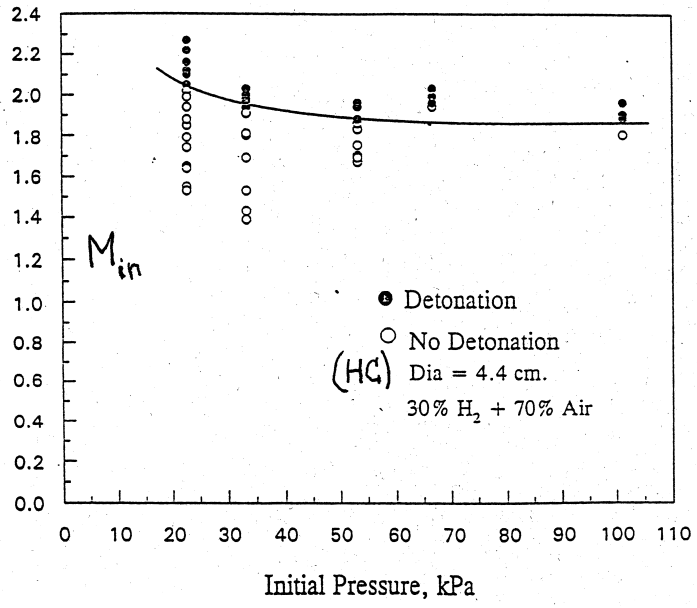

Figure 5.2.1.3-4 The influence of pressure on detonation domain boundary in 30% H_2 + 70% air mixture

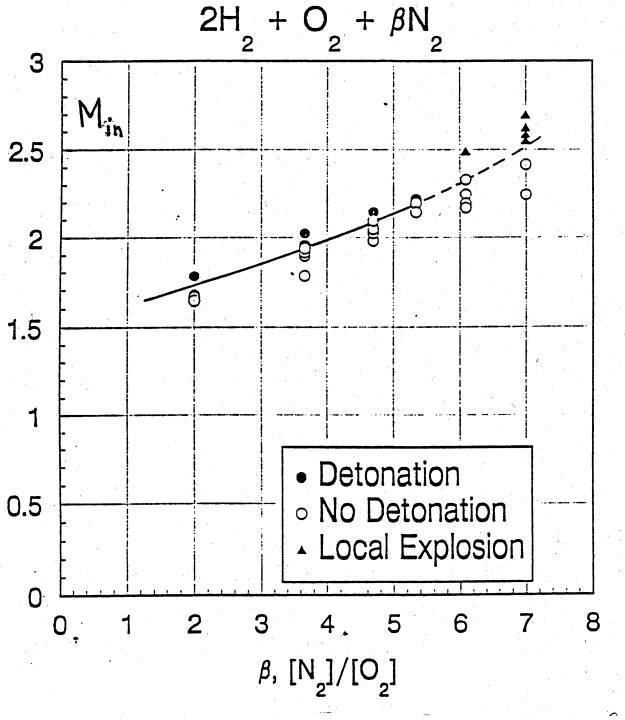

Figure 5.2.1.3-5 The influence of N_2/O_2 ratio on detonation domain boundary

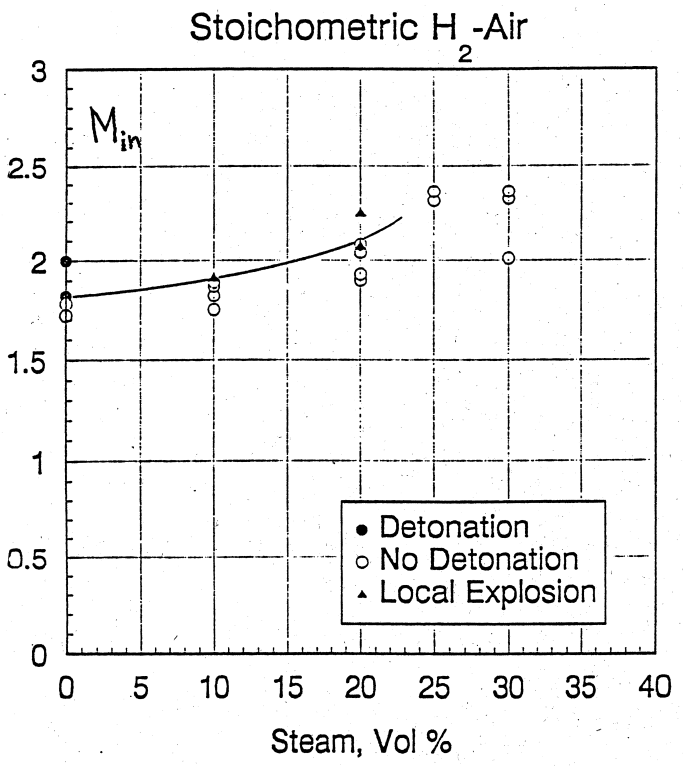

Figure 5.2.1.3-6 The influence of steam additive on detonation domain boundary

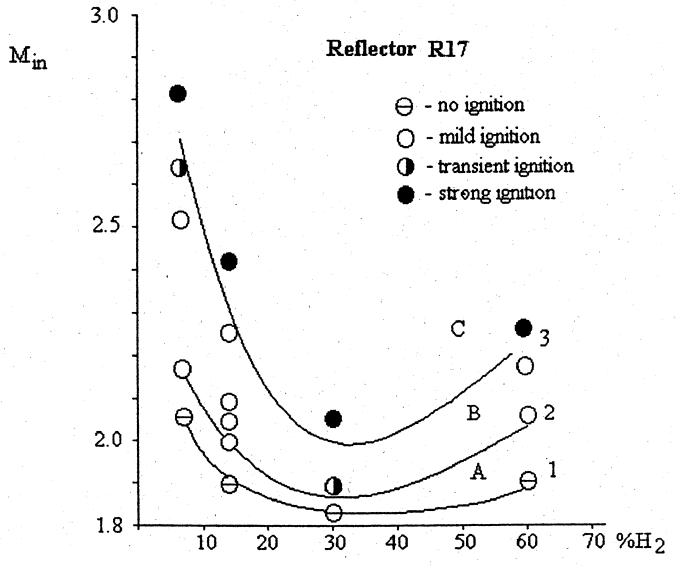

Figure 5.2.1.3-7 The critical incident shock Mach number versus the H_2-air mixture composition, spherical reflector R17. The regions A, B, and C and the curves 1, 2, and 3 correspond to Figure 5.2.1.3-8 for reflector R27.

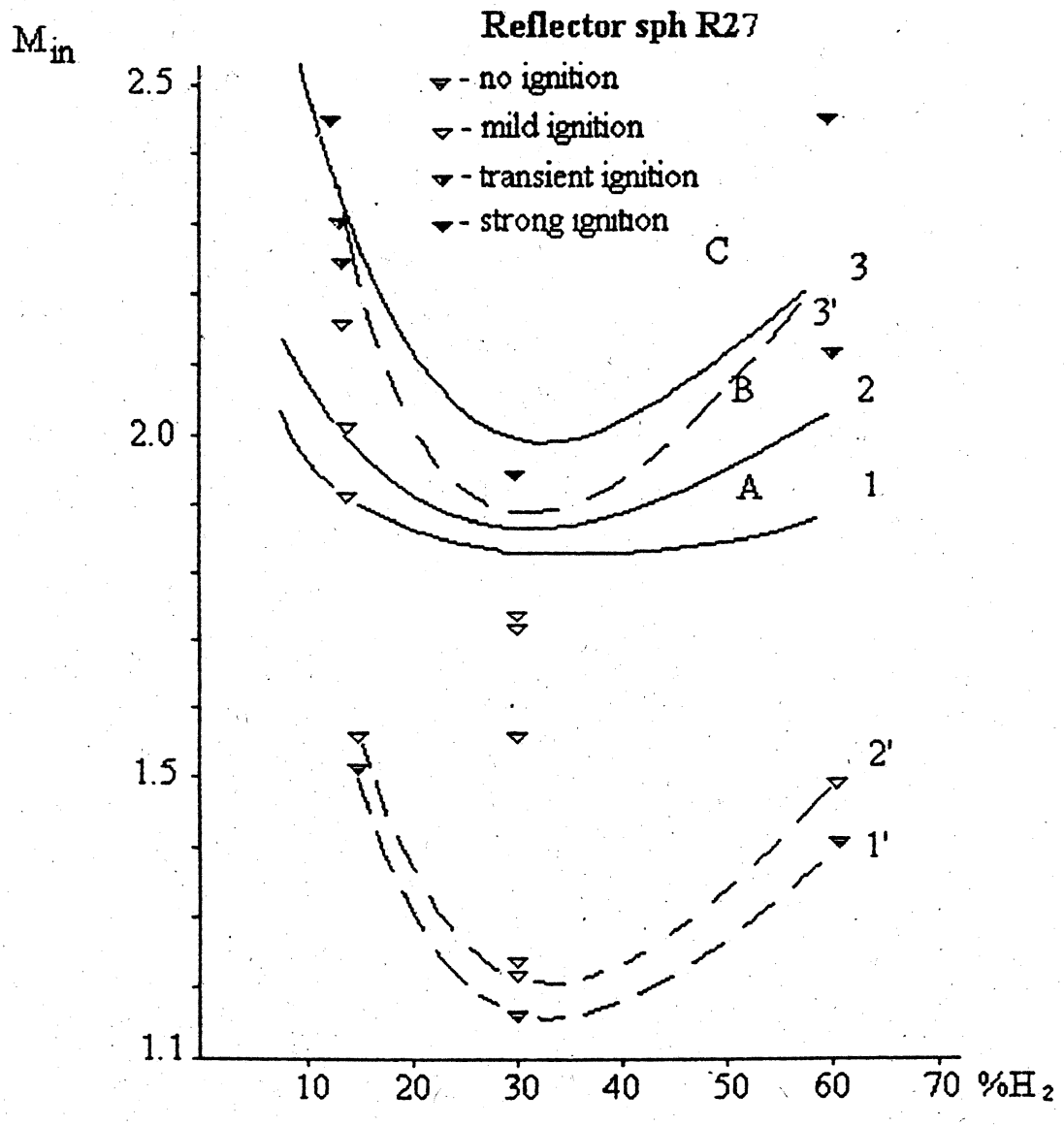

Figure 5.2.1.3-8 The critical incident shock Mach number versus the H_2-air mixture composition, spherical reflector R27. The regions A, B, and C and the curves 1, 2, and 3 correspond to Figure 5.2.1.3-7 for reflector R17.

5.2.1.4 Preliminary calculations of pressure and temperature time histories during shock wave focusing

The probability of self-ignition and the type of the subsequent mode of combustion in a reactive mixture depend on the change of temperature and pressure in space and time. From preliminary computations described in References [5.4,5.6,5.9 – 5.11,5.16,5.17], it follows that focusing of shock waves in a cavity causes fast changes of temperature and pressure in time, which are not typical of normal reflection at a flat surface. The sizes of the "hotest" zones, together with fields of pressure and temperature inside them, become larger after a series of complex interactions between reflected and attached wave structures. Thus the history of explosion regime depends on a ratio of characteristic times both linear gas dynamic scales and chemical processes. In particular, the time at which increased temperature τ will occur in a local zone corresponds to a certain extent with the characteristic time of a chemical reaction θ.

At $\tau < \theta$ ignition will not occur.

At $\tau > \theta$ ignition takes place in a local zone of the size δ.

At small δ the transition from deflagration to detonation is unlikely. Then the outcome of the development of explosion processes because of focusing of shock waves depends on the linear sizes of the focusing cavities. Another aspect of applying a numerical modelling technique to a problem under consideration is an investigation of complex wave dynamics during the self-ignition process under focusing conditions. It allows one to predict the "points of interest", i.e., positions of probes where the flow reveals specific features, and therefore, significantly facilitates the experimental method. With this aim, a special computer code was elaborated. The code uses a set of 2D Euler gas dynamics equations of conservation, coupled with a detailed scheme of chemical reactions between hydrogen and air. The Lax-Wendroff solution method was used, together with the flux-corrected transport (FCT)-algorithm for shock capturing. The chemical part of the solution was computed using the CHEMKIN package. To resolve the peculiarities of a flow near reflection surfaces, a special procedure of grid refinement was used. The code was verified by results of experimental findings shown above, and known theoretical and experimental data on the subject done by other authors.

An example of the preliminary calculation results is presented in Figures 5.2.1.4-1 and 5.2.1.4-2. The case considered is a computer visualization of an initiation of a combustion regime. Figure 5.2.1.4-1 presents a computer shadow-graph of the combustion process (i.e., modulus of density gradients), and Figure 5.2.1.4-2 shows pressure spatial distributions for inert and reactive cases (lower and upper parts of the pictures), respectively. The case considered has the following initial conditions: $p_0 = 0.0263$ MPa, $T_0 = 293$ K, initial shock Mach number $M = 2.0$. The mixture used was 15 % H_2 + 85 % air (reactive case) and 15 % H_2 + 85 % N_2 (inert case). Frames are presented after each 10 μs. Spatial sizes are shown in centimetres. The first four frames are the same both for inert and reactive cases. It is especially evident from Figure 5.2.1.4-2 that ignition takes place in the time interval between the fourth and fifth frames. After that, a fast combustion mode starts to propagate in the direction opposite to the gas flow. The temperature at the front is about 2400 K, and the temperature in the combustion products is steady at about 2000 K. The following specific features of the process could be noted:

1. A combustion wave accelerates fast (in 25 mm) after the primary explosion occurs. Further propagation proceeds at approximately the same radial speed.

2. The pressure distribution at the front is very non-uniform. Along the reflector boundaries, at the

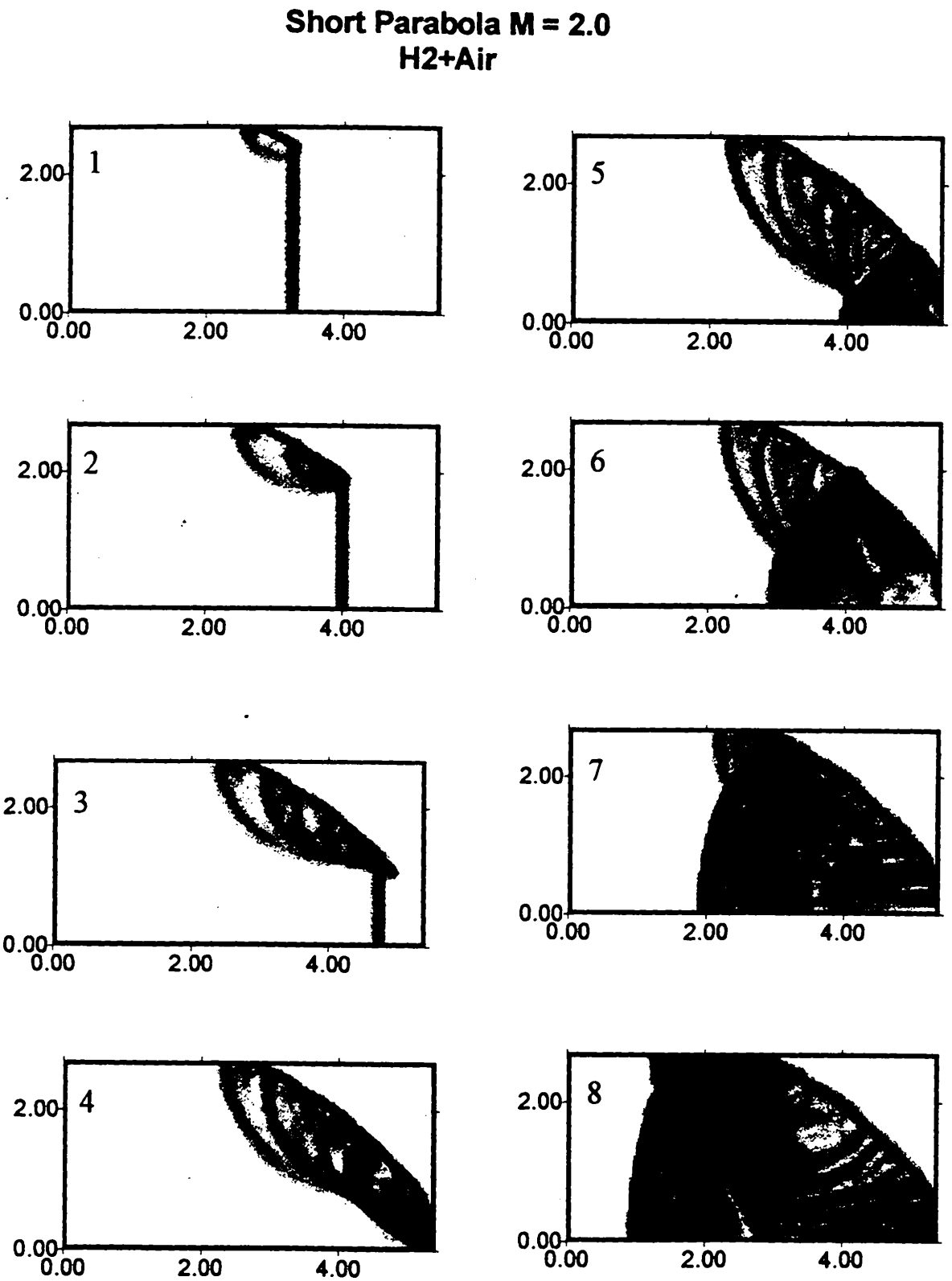

Figure 5.2.1.4-1 Combustion simulation of shock focusing

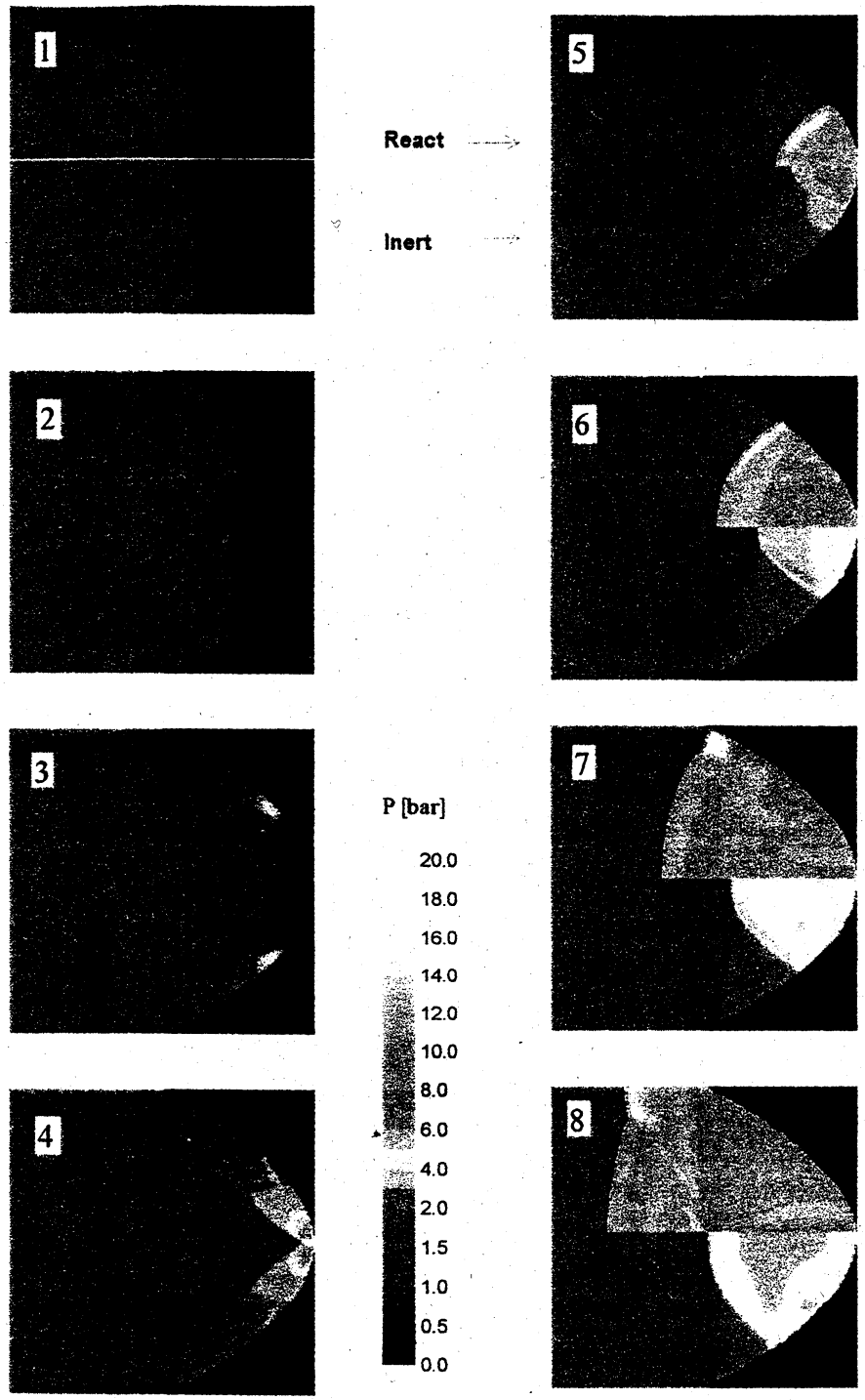

Figure 5.2.1.4-2 Pressure distribution

point where the reflection of incident shock wave changes its mode from a Mach number to a regular number, a sharp pressure rise is detected. Thus at the time that the combustion front leaves the reflection cavity (7th frame), the region with maximal pressure is located at the borders of the reflector.

3. At the same time (7th frame) behind the flame front in the combustion products, a secondary shock wave reaches its axis of symmetry (see Figure 5.2.1.4-1). This wave is formed at the point where the reflection mode changes.

Thus the combustion wave that leaves the reflection cavity has a noticeable non-uniform spatial structure. Evidently, at later times, depending on the size of a channel and the reactivity of the mixture, the wave can be transformed into a detonation with cellular structure.

5.2.1.5 Investigation of H_2 + air flame propagation and DDT in a channel with multi-dimensional end plates

As a logical final stage of separate research on shock waves focusing phenomena and fast deflagration in the congested area, a set of combined tests was performed in a cylindrical tube channel (filled by H_2-air) with a partially obstructed part and a multi-dimensional end plate. Three main regimes of loading from explosive combustion of H_2 - air mixtures near the obstructed space were distinguished on the basis of tests performed [5.14]:

First Regime: At a hydrogen concentration in air of 20% by volume, a non-decaying quasi-steady complex (QC) is emitted from the congested space. This complex consists of the pressure wave (SW1), followed by a combustion zone (FF1). The speeds of SW1 and FF1 are close to each other. The reflection of the QC at the end wall causes a reflected wave (RW) to appear in the combustion products, and the loading process does not depend on the reflector type.

Second Regime: At hydrogen concentrations in air in the range of 15% to 20% by volume, a decoupling complex, consisting of a shock wave (SW2) + decelerating delaying flame front (FF2), is emitted from a congested part of the channel. The reflection of SW2 results in reflected shock wave RSW moving in the unburned mixture ahead of flame front FF2. The reflection of SW2 at the flat end wall is not accompanied by additional self-ignition phenomena. Instead of that the reflection at the concave reflector gives the rise to secondary explosion waves (SEWs) or DDT from exothermic centres created by focusing SW2 inside the non-flat reflector. Other variants of the mentioned complex focusing briefly near an elliptical end plate are described without detailed analysis is described in Reference [5.19].

Third Regime: At hydrogen concentrations in air below 10% to 11% by volume, the speed of the deflagration front (FFi) inside a congested space is sufficient only for supporting a weak compression wave before the flame front in the congested part and a fan of acoustic waves ahead of the decelerating flame (FF3) in free space. The reflection of these waves at any type of reflector does not lead to the significant effect on the overall pressure increase during combustion in a channel.

5.2.1.6 Common conclusions

1. The shock (blast) wave-type disturbances with Mach numbers of $M < 1.2$ being reflected from focusing surfaces and the obstacles cannot cause secondary ignition.
2. The shock (blast) wave-type disturbances with Mach numbers of $1.2 < M \leq 1.4$ being reflected from the obstacles and concave surfaces can cause secondary ignition, thus favouring the escalation of explosion.
3. The shock (blast) wave-type disturbances with a Mach number of $M > 1.4$ being reflected from the obstacles can cause the detonation initiation in the vicinity of reflecting surfaces.

5.2.1.7 Experimental verification of reaction kinetic models relevant to self-ignition phenomena

The transition from deflagration to detonation of the hydrogen-air system and the hydrogen-water (steam, fog)-air system depends on the physico-chemical properties of an explosive mixture, the characteristics of the ignition process, and the interaction of ensuing deflagration waves with the environment. Critical for failure of the containment will be the pressure and time history and the resulting effective structural load. Recent investigations of the H_2-air (or O_2) self-ignition [5.20 – 5.26] have shown that the measured ignition delay times are partially in contradiction with the calculated data obtained with the established kinetic mechanism. Up to now, it has been assumed that the kinetic mechanism of the hydrogen-air system is one of the best-known reaction schemes [5.27 – 5.31]. However, the experimental results from References [5.20 – 5.22] and [5.32 – 5.34] show that in the region of "low" temperatures and also in the region of practically interesting high-pressure deviations of calculated and measured ignition delay times of more than 2 orders of magnitude occur. Figure 5.2.1.7-1 shows the typical example of the dependence of the ignition delay time τ_i on pressure p for different calculations and experiments in the form of a diagram $\tau_i = f(p)$ at a fixed level of temperature $T = \text{const.}$ ($T = 1000$ K for Figure 5.2.1.7-1).

There seems to be good agreement between theory and experiment for $p < 3$ bar, whereas for higher pressure, the devations are unacceptable. Figure 5.2.1.7-2 indicates a similar behaviour for the standard dependence of ignition delay times $\tau_i = f(T)$ at $p = \text{const.}$. The τ_i-values predicted for $T < 1100$ K are up to 10 times longer than those that were experimentally observed. The same results were obtained by comparison of calculated and measured values of τ_i taken behind oblique shock waves in stoichiometric H_2-air mixtures [5.30, 5.35].

The same features are typical for $H_2 - O_2$ mixtures. Figure 5.2.1.7-3 compares calculated and measured values of τ_i [5.20, 5.24] as a function $\tau_i = f(p)$ for several fixed levels of temperature in range $800 \text{ K} < T < 1200$ K. The figure also shows some experimental points representing $\tau_i = f(p, T)$. Numbers at the data points specify the temperature at which the corresponding τ_i values were measured. The summary of these results, including recent data from Reference [5.29] is as follows:

- At $T \approx 700$ K – 800 K, the measured τ_i value differs from calculated values by a factor of $O(10^3)$.
- At $T \approx 800$ K – 900 K, the difference amounts to a factor of $O(10^2)$.
- At $T \approx 900$ K – 1000 K, the difference is more than tenfold.
- At $T > 1100$ K, the calculated dependence $\tau_i = f(p, T)$ agrees satisfactorily with the measured results.

The comparison of the calculated and measured dependence of $\tau_i = f(p,T)$ shows that available kinetic schemes fail to give a correct prediction for reactivity of H_2-air and H_2-O_2 mixtures in definite p/T ranges even when the latest recommended rate constants from, say, Reference [5.36] are used for the elementary reactions. For the DDT process, this observation is of greatest importance because it demonstrates the evidence for substantially higher reactivity of H_2-N_2-O_2 mixtures at "low" temperature, ranging from 800 K to 1000 K at pressures $p \geq$ 1MPa.

A further decisive influence is exerted by the high water vapour content present in the reactor containment under conditions of failure. Self-ignition of this H_2-air-steam mixture deviates from that of the H_2-air system. The calculated ratio $\tau_i(H_2O)/\tau_i = f(p,T,x_{H_2O})$ at fixed levels of temperature $T = 860\,\mathrm{K}$, $T = 1000\,\mathrm{K}$, $and\, T = 1100\,\mathrm{K}$ is presented in Figure 5.2.1.7-4. The time delay $\tau_i(H_2O)$ applies to "humid" H_2-air systems. Some reasonable experimental data from Reference [5.37] are given in Figure 5.2.1.7-4. A dotted line indicates a temperature $T \approx 860$ K and $x_{H_2O} = 0.07 \pm 0.03$. Again, as for "dry" mixtures, the theoretical predictions deviate significantly from the experimental data. Theory predicts an inhibition of self-ignition by addition of steam at a lower pressure than that used in the experiments.

Another important influence upon the physico-chemical processes in hydrogen oxidation is exerted by additives of NO_x, CO and CO_2, which may be formed during reactor accidents. The NO_x may be produced by the projected spark-ignition systems, and carbon-oxides will occur subseqent to oxidation of hydrocarbon compounds and concrete. The experimentally observed decrease of the τ_i value for small amounts of NO_x additives, 0.5% to 1%, can be predicted quite well for low-pressure self-ignition regime at $p < 10$ bar as is shown in Figure 5.2.1.7-5. Accordingly, it is found experimentally, [5.23, 5.33], that small (less than 1% by volume) additives of NO_2 to the lean H_2-air mixture reduce the lower detonation limit from 15.5% H_2 to 13% H_2 (in a tube of 41 mm diameter). Additives of CO did not change the value of τ_i, but transformed the type of self-ignition from mild to strong, [5.33], and promoted DDT behind the reflected shock wave. Additives of CO_2 inhibit the self-ignition not only by increasing the τ_i value but also by the transformation of strong self-ignition regime to mild regime, [5.34]. The dynamics of self-ignition phenomena was practically the same in shock waves with constant pressure and temperature and in blast waves with decreasing pressure and temperature, [5.32].

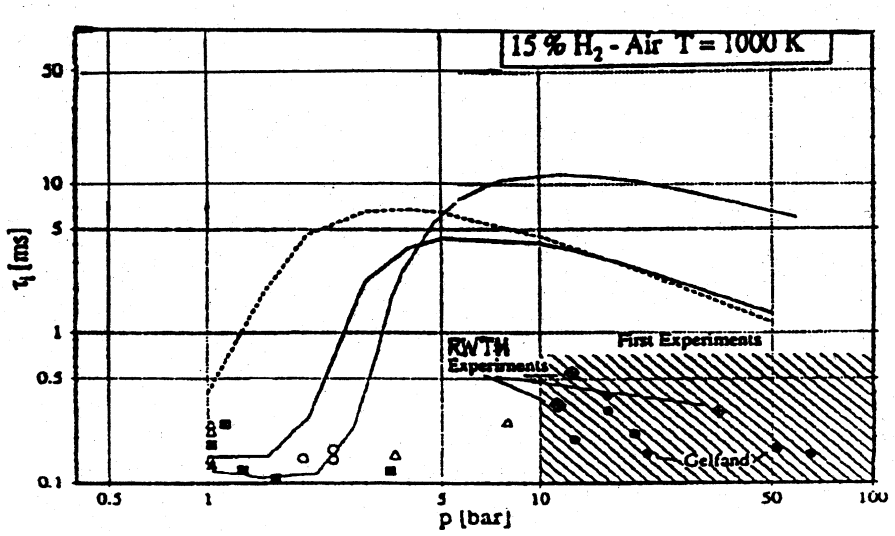

Figure 5.2.1.7-1 Ignition delay time $\tau_i = \tau_i(p)$, $T = 1000$ K (calculations and different experimental data)

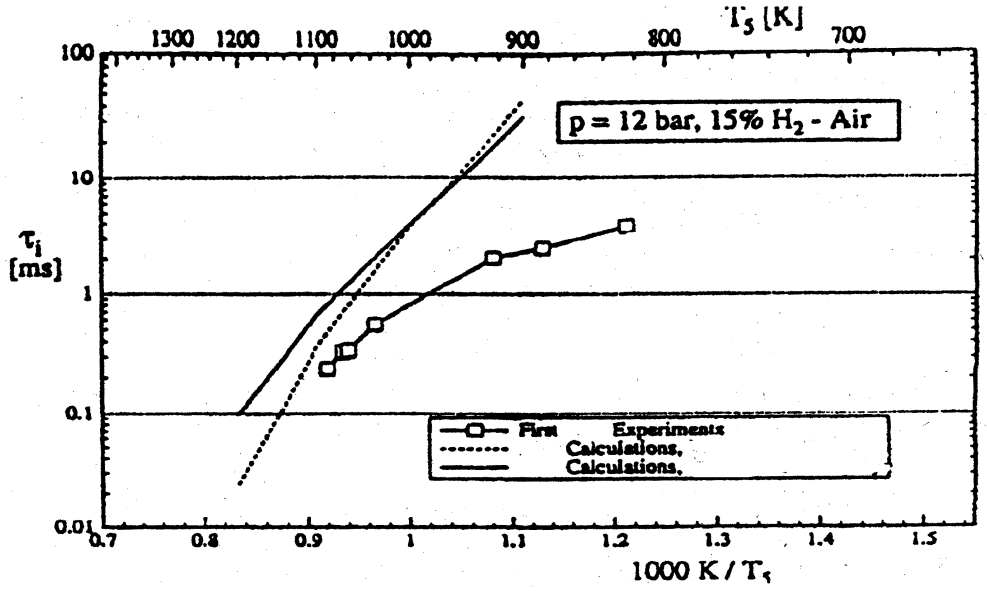

Figure 5.2.1.7-2 Ignition delay time $\tau_i = \tau_i(T)$, $p = 12$ bar (calculations and different experimental data)

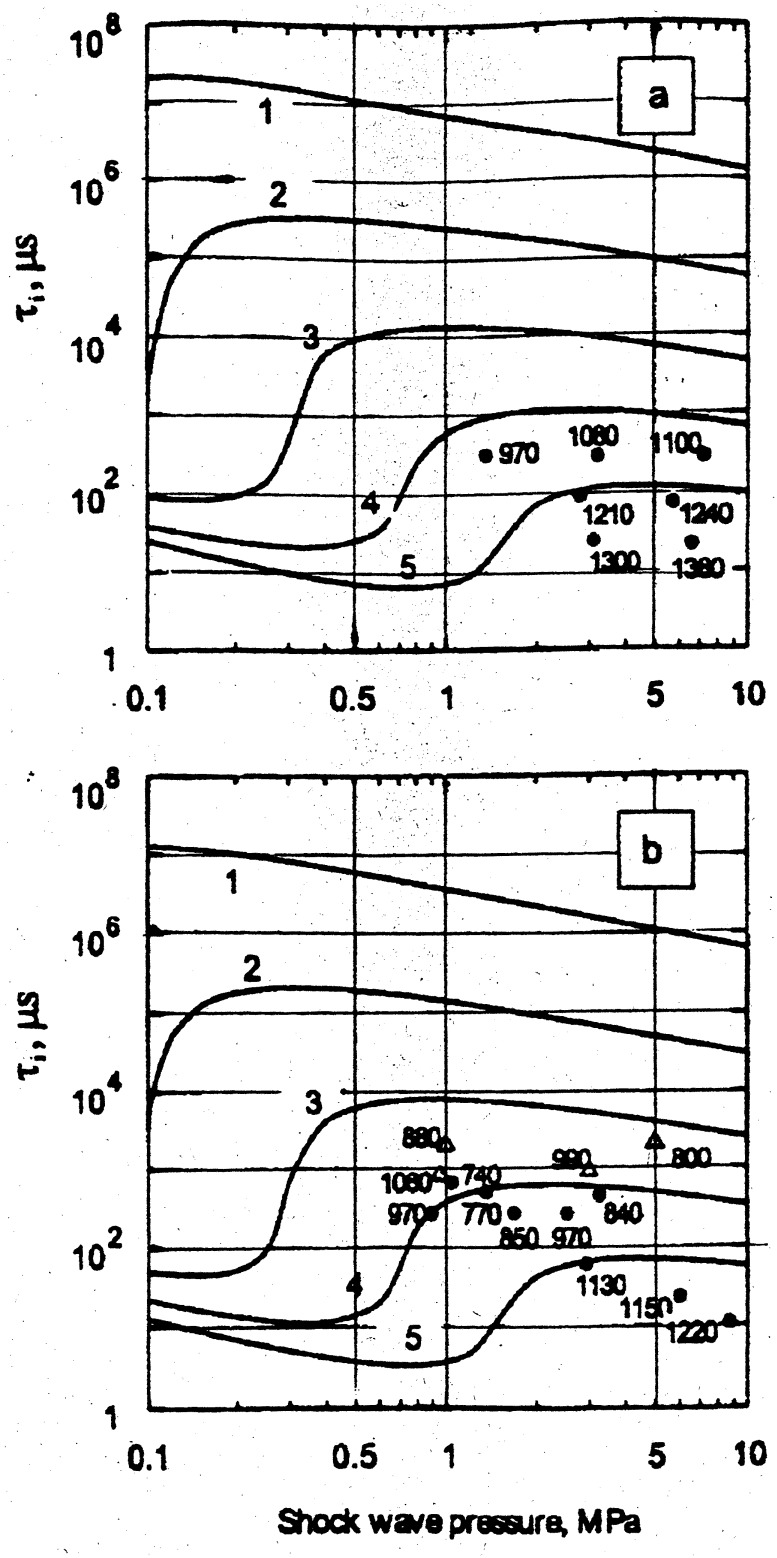

Figure 5.2.1.7-3 Comparison of measured with calculated ignition delays for (a) $0.05H_2 + 0.95O_2$ **and (b)** $0.15H_2 + 0.85O_2$ **mixtures as functions of pressure at temperartures (1)** 800 **K, (2)** 900 **K, (3)** 1000 **K, (4)** 1100 **K, and (5)** 1200 **K**

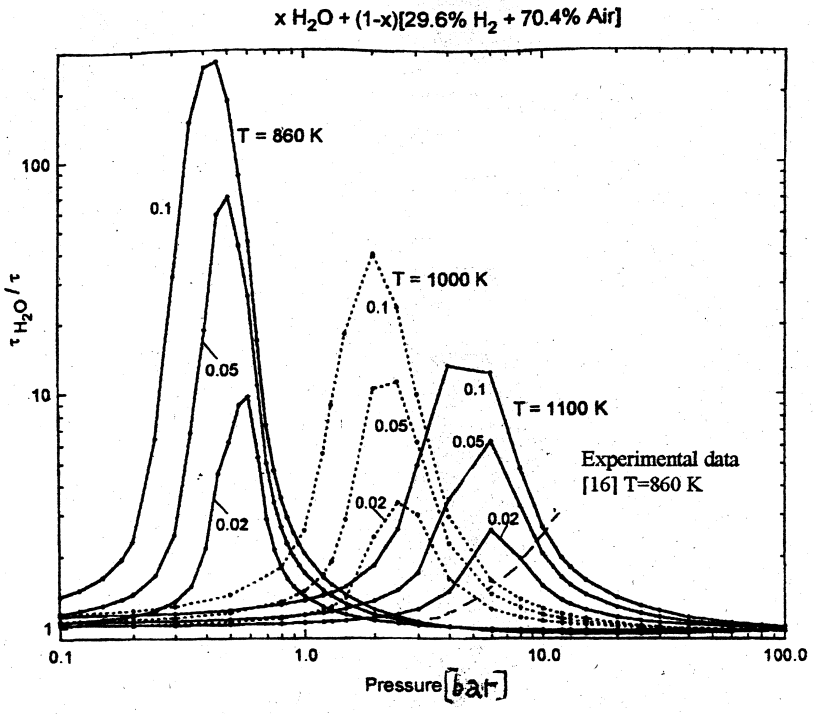

Figure 5.2.1.7-4 Influence of steam on self-ignition time delay of stoichiometric H_2-air mixtures

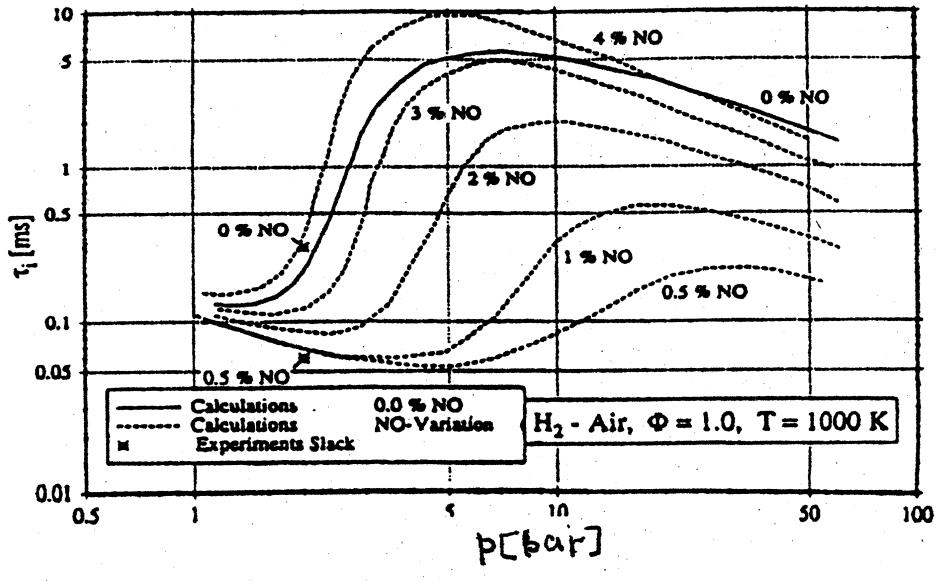

Figure 5.2.1.7-5 Ignition delay time $\tau_i = \tau_i(p)$, $T = 1000$ K; calculations were performed by RWTH Aachen and by [5.14] in comparison to experiments by Slack

5.2.1.8 *Volumetric oxidation and operating temperature limit experiments*

If a combustible mixture temperature is sufficiently high, the mixture may ignite without an external ignition source. Even at temperatures below the "auto-ignition temperature", chemical reactions occur that would tend to change the mixture composition with time. In Reference [5.38] preliminary experiments were conducted to determine the maximum vessel temperature that would result in the test mixture being injected into a heated vessel without burning. A stoichiometric H_2-air mixture at an initial pressure of 0.1 MPa was used for these experiments since it is the most sensitive mixture and thus would yield the lowest temperature limit. The results suggest that no "significant" chemical reaction occurred at $T \approx 588$ K. At $T = 700$ K, burning was observed in all cases, independent of mixture fill time. The experimental results were compared with corresponding calculated "reaction time" using CHEMKIN, a chemical kinetic code [5.39]. The measured time for ignition of the mixture upon injection was significanly shorter (about 1000 times) than the reaction times predicted by the CHEMKIN code. This indicates that either wall effects, which are not modelled in the CHEMKIN calculation, play an important role in the ignition of a mixture [5.20] or the constants used in the chemical kinetic equations are not accurate at the initial pressure and temperature conditions of the experiment as described in Reference [5.39].

5.2.2 Flame Propagation in Obstructed Areas[*]

5.2.2.1 *High-speed deflagration of gaseous mixtures*

Usually, shock waves are generated if the combustion velocities in hydrogen-air mixtures exceed $S > 100$ m/s. However, it is a well-known fact that in any mixture of gaseous fuel and air, the normal flame velocity u_n and visible flame velocity $u_v = \sigma u_n$ are well below 100 m/s. Here $\sigma = \rho_u/\rho_b$ is the expansion ratio, ρ_u is the density of the unburned mixture, and ρ_b is the density of combustion products. The investigations in References [5.40 – 5.51] showed that velocities $S > 100$ m/s in hydrogen-air mixtures can be achieved if forced turbulence of gaseous flow in an obstructed channel is used. The high speed of flame propagation is associated with the increase of the surface burning because of turbulence at obstacles. The kinetic differences in chemical processes in the case of combustion in obstructed channels are not significant.

To study the effect of obstacles on gaseous combustion various systems were used: separate perforated screens, a set of rods, spirals, and a system of screens with orifices. The obstacles were placed in a channel with diameters up to 2.5 m and in volumes with cylindrical symmetry. A set of tests was done in a series of concentric perforated spheres. The simplest types of obstructed channels are tubes with repeated steps or obstacles, or rough tubes. These constructions were used for the investigations of accelerating or quasi-stationary regimes of combustion with velocities $S > a$, where a is the speed of sound in the unburnt mixture, in tubes with diameters $d = 50 - 300$ mm and lengths $L = 3 - 12$ m. The appearance of pressure waves capable of causing self-ignition [5.40 – 5.51], expands the range of dangerous situations and requires special investigations.

5.2.2.2 *Main results of studies of explosion regimes*

To select the method of investigation and determine the range of initial conditions for possible future research, it is necessary to analyze the main results from previous studies on combustion regimes of hydrogen-air mixtures in (fully or partially) obstructed volumes. Unfortunately, up to now most of the

[*] Contributed by Professor B. E. Gelfand

Table 5.2.2.2-1 Initial experimental conditions from References [5.40 – 5.55]

P_0[bar]	T_0 [K]	%H_2	%H_2 =	%CO_2	%N_2	L_Ξ	L_{obs}	BR	δ [mm]	s [mm]	s/δ	L_{obs}/s	Obst.Type	[ref]
1	293	10 – 45		0 – 15	0 – 15	9	3	0.28 – 0.6	50 150 300	50 150 300	1 1 1	60 20 10	spiral rings	[5.42]
1	293 – 353	10 – 75	6 – 40			6	3	0.29 – 0.7	66.6	35 60 81 120 140 242 325 490	0.52 0.9 1.2 1.8 2.1 3.6 4.87 7.35	85 50 37 25 21 12 9 6	rings	[5.44] [5.45] [5.46]
1	293 – 353	10 – 62	0 – 30			6.4	6.4	0.3	280	280	1	23	buffles	[5.52]
1	293 – 400	12 – 20	0 – 30			5.7	5.7	0.1 – 0.28	1500	1100 550 275	0.73 0.36 0.18	5 10 21	cylindr. tubes	[5.48] [5.49]
1	293	10 – 25				2	0.9 – 1.35	0.5 – 0.71	54	50 – 480	0.93 – 0.89	12 24	rings	[5.50]
1	293	10 – 25				12	6	0.6	350	500	1.43	12	rings	[5.50]
1	293	9.8 – 12.5				34.6	34.6	0.3 – 0.6	2300 • 2500	2500 5000 •		12 6 •	concr. blocks	[5.51]
1	300 – 650	10 – 30	9 – 25			21.3	21.3	0.43	270	270	1	78	rings	[5.43] [5.54] [5.55]

data cited were from Reference [5.42]. Table 5.2.2.2-1 presents the data on the initial conditions in the investigations [5.40 – 5.51] on fast combustion regimes in hydrogen-air mixtures for a wider spectrum of tests.

The following information about combustible mixture properties is helpful for further discussion:

- normal flame velocity - u_n
- sound velocity in unburned mixture - a
- expansion ratio after burning - σ

Figure 5.2.2.2-1 presents the dependence of the above-mentioned parameters on the hydrogen volume content in air [5.46]. The values u_n and σ characterize the ability of the reaction. The sound speed a is a reference value for propagation regime classification in obstructed channels through the expression S/a.

The measurements in Reference [5.42] showed that the main parameter responsible for flame propagation velocity is the composition of the mixture. Figures 5.2.2.2-2 and 5.2.2.2-3 show the dependence of flame velocity in hydrogen-air mixtures in a channel containing obstructed and smooth parts. The obstructed part has blockage ratios of $BR = 0.4 \text{ to } 0.6$. The volume fraction of hydrogen was varied in a range $10\% \text{ to } 30\%$, but for practical applications the data with hydrogen content $10\% \text{ to } 20\%$ are especially important. No detonation was obtained for mixtures with hydrogen volume fractions of $< 12\%$, but at a length of $\approx 1\text{m}$, the acceleration of a flame up to a quasi-steady value of $S \approx 700\text{m/s}$ was detected; i.e. $S/a > 1$.

Subsonic regimes of fast deflagrations were pointed out in mixtures with hydrogen volume fraction of 10% to 30% in air. Figure 5.2.2.2-4 gives an overview of the measured levels of maximum flame velocities in obstructed channels with different types of obstacles (Schelkin spiral, a system of perforated screens with step $s = \delta$ in tube with diameter $\delta = 50\text{mm}$). At $s/\delta = 1$ and hydrogen volume fraction of $< 20\%$ neither the type of obstacles, nor the level of obstruction influence the explosion process. Further investigations showed that the diameter of the channel has also only a small effect on the combustion if the holding blockage ratio (BR) and the ratio s/δ are kept constant.

The studies in References [5.40,5.41,5.47] revealed the influence of the obstacle step height on the change of flame velocity. Figure 5.2.2.2-5 summarizes the results of experiments from References [5.44 – 5.47] for the mixture with hydrogen volume content of 16% and 24% in a channel with $BR = 0.69$. At $s/\delta < 1.8$ and hydrogen volume fraction of $< 16\%$, the distance between obstacles influences the flame velocity very slightly. Note that the effect of s/δ parameter on the maximal flame velocity in a channel at $10 > s/D > 3$. A summary of the effect of parameter s/δ is presented in Figure 5.2.2.2-6. Using various spacings between obstacles, one can change the type of explosion process. Figure 5.2.2.2-5(a,b) also presents the effect of a single diaphragm on the flame velocity. The diaphragm is placed at a distance of $100\ \text{mm}$ from the source of ignition in mixtures containing 16% and 24% hydrogen. Horizontal lines in Figure 5.2.2.2-5(a,b) represent the sound velocities in an unburned mixture. The change of explosion dynamics of a stoichiometric mixture diluted by a water-steam mixture in an obstructed channel [5.47] is shown in Figure 5.2.2.2-7. Dilution by more than 30% (vol) steam results in a drastic deceleration of the flame down to subsonic values at the exit of the obstructed part. In Reference [5.47] contradictory data are presented about the influence of initial temperature on fast flame propagation in a congested channel. Beauvais et al. [5.47] concluded that an increase of the initial temperature of a given mixture can have enhancing or damping effect on turbulent flame acceleration, depending on the geometrical boundary conditions. The length of the obstacle field in these experiments was likely insufficient to fully investigate the DDT phenomenon at elevated temperatures [5.53, 5.54]. The detonation run-up distance was found to decrease with increasing hydrogen mole fraction and with decreasing initial temperature.

All experimental results, obtained in a laboratory-scale facility, were confirmed by large-scale tests [5.48, 5.49, 5.51]. Quite recent results of large-scale tests are presented in Reference [5.49]. Flame acceleration tests were performed over a range of hydrogen-air-steam mixtures, obstacle spacing, blockage ratios, and igniter locations in a 1.5-m-diameter, 5.7-m-high cylindrical vessel (volume $\approx 10\ \text{m}^3$) . It was found that the flame speed increased as the hydrogen concentration increased, but decreased as the steam content increased. For accelerating flames, the flame speed rapidly increased with distance, reached a peak value, and then rapidly decreased. The peak flame speed was attained at approximately midheight. Of the diluents tested, steam was more effective than CO_2, and CO_2 was more effective than nitrogen in suppressing flame acceleration. The initial pressure had no significant effect on the flame speed. An increase in the obstacle spacing in range $0.18 < s/\delta < 0.73$ was found to decrease the peak flame speed nearly linearly. In small-scale tests [5.44, 5.45, 5.47], flame speeds did not depend on the spacing of obstacles in the range $s/\delta < 1$. Experiments performed with blockage ratios $0.1 < BR < 0.28$ indicated that peak flame speed increased as the obstacle BR increased. The direction of flame propagation did not have a significant effect on the peak flame speed.

The main result of observations in References [5.40 – 5.51] is a proof of the possibility of fast combustion regimes in obstructed channels. These regimes are accompanied by the generation of pressure waves, overtaking combustion waves. Thus the problem should be considered in the framework of unsteady interactions within a complex pressure wave-fast deflagration front system.

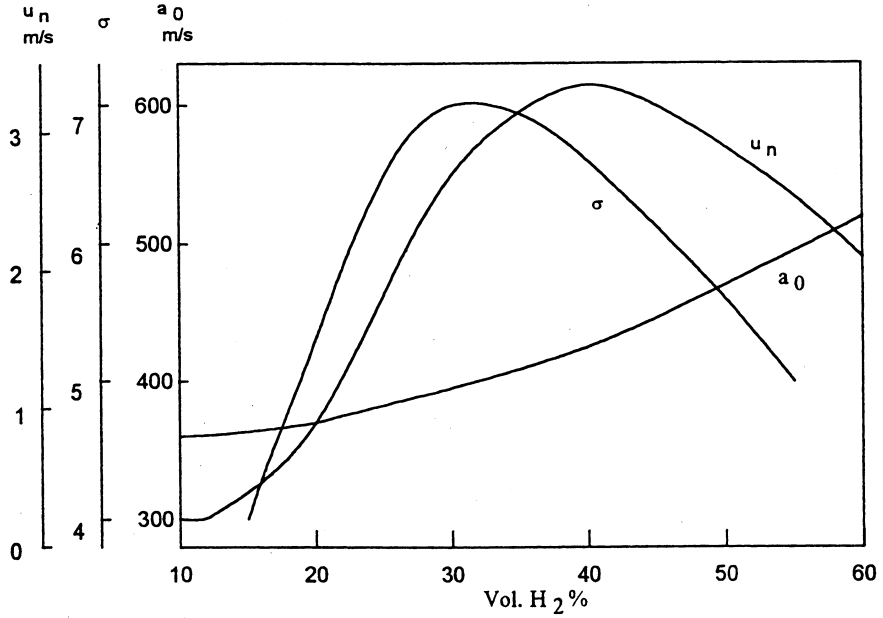

Figure 5.2.2.2-1 Normal burning velocity, speed of sound and expansion ratio of hydrogen-air mixtures

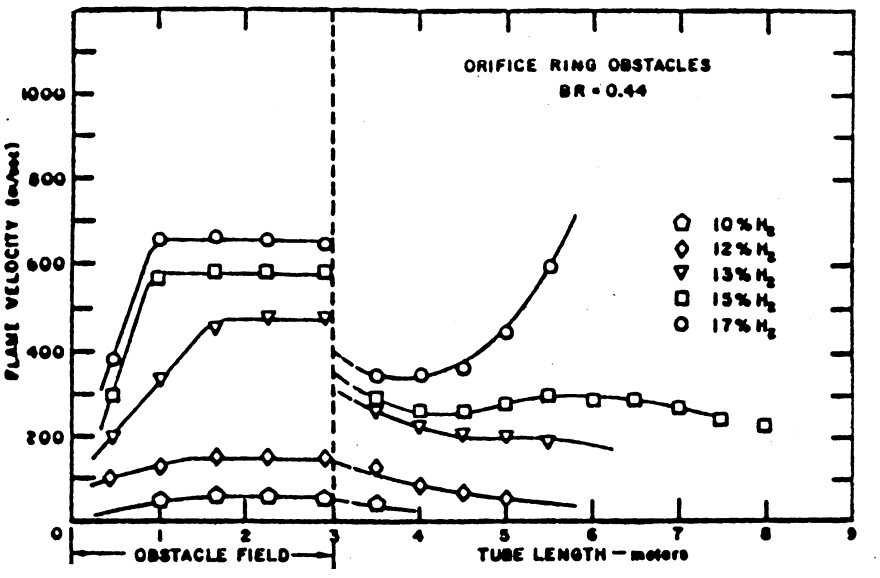

Figure 5.2.2.2-2 Variation of flame velocity along the flame tube for the orifice ring obstacles with a blockage ratio of $BR = 0.44$

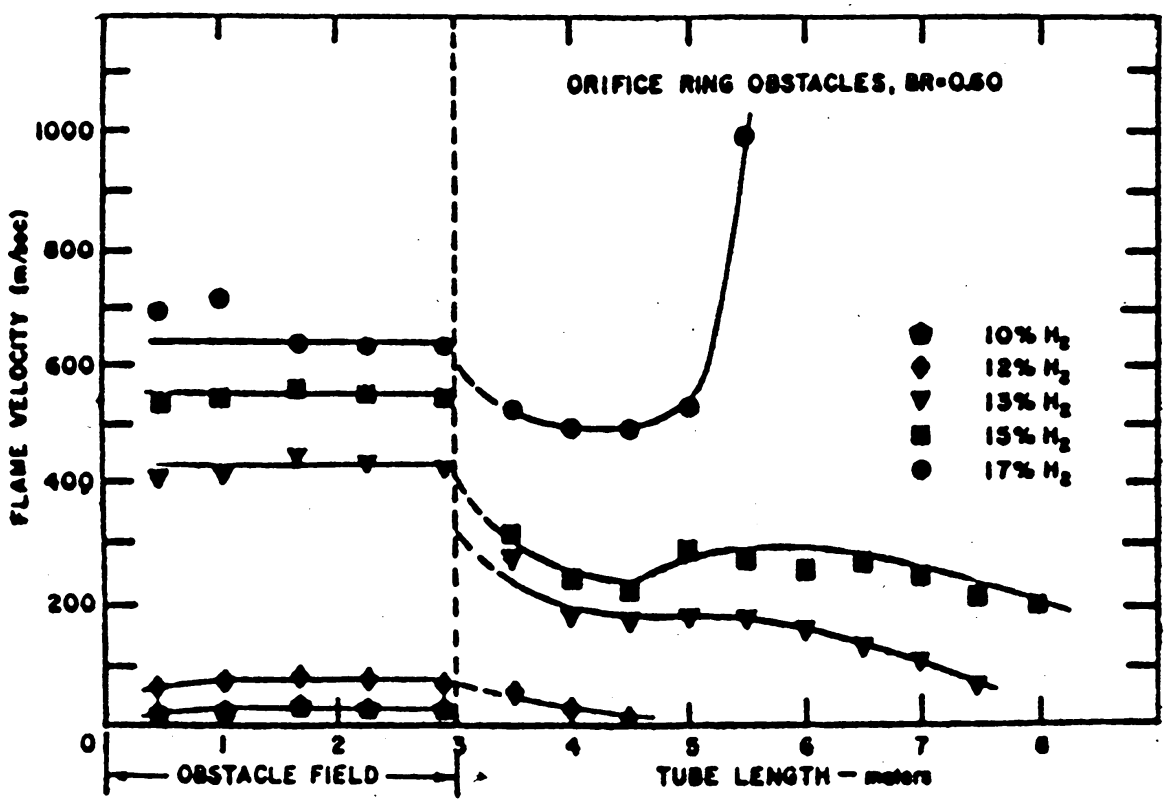

Figure 5.2.2.2-3 Variation of flame velocity along the flame tube for the orifice ring obstacles with a blockage ratio of $BR = 0.60$

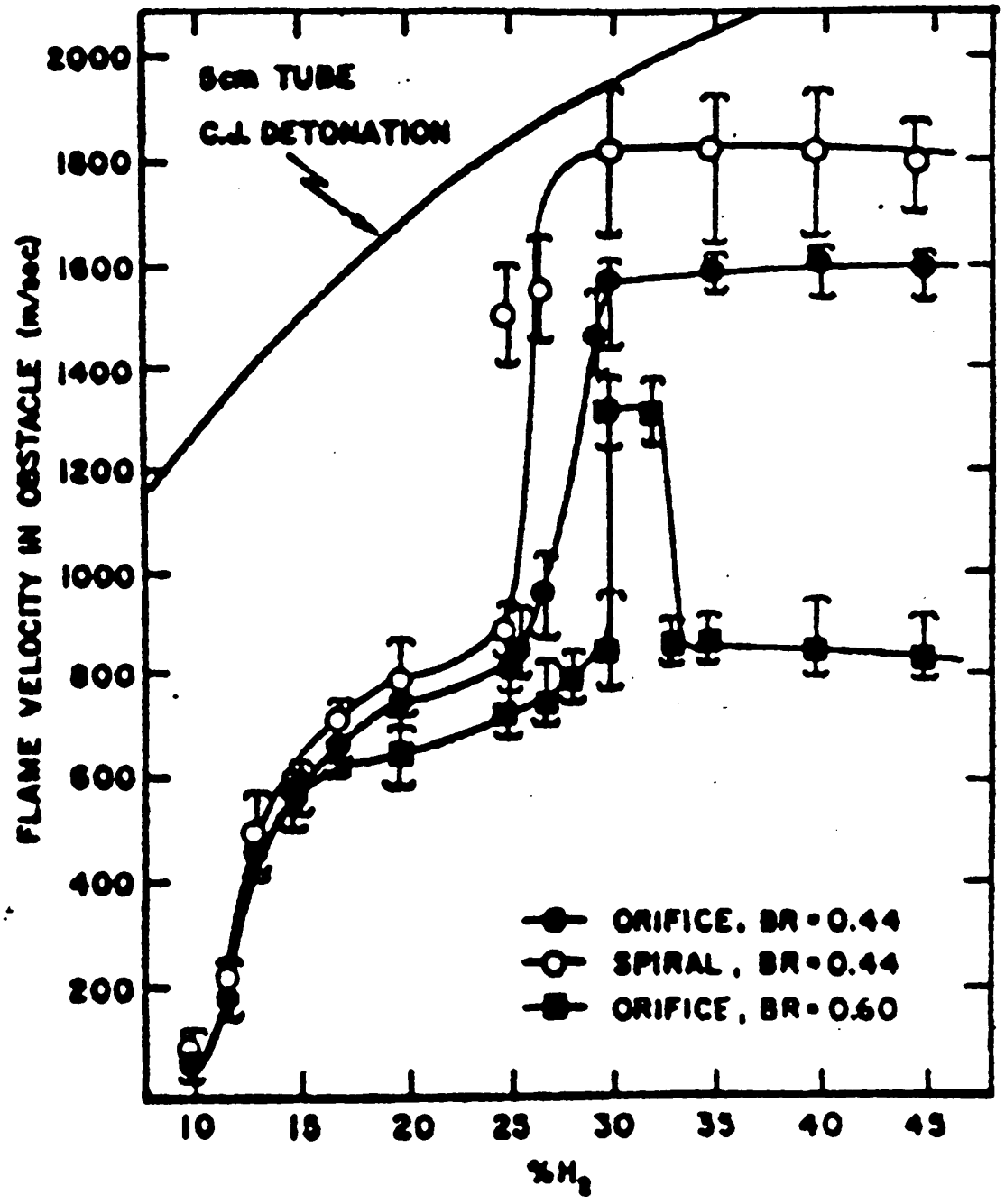

Figure 5.2.2.2-4 Variation of maximum steady-state flame velocity with composition of the H_2-air mixture

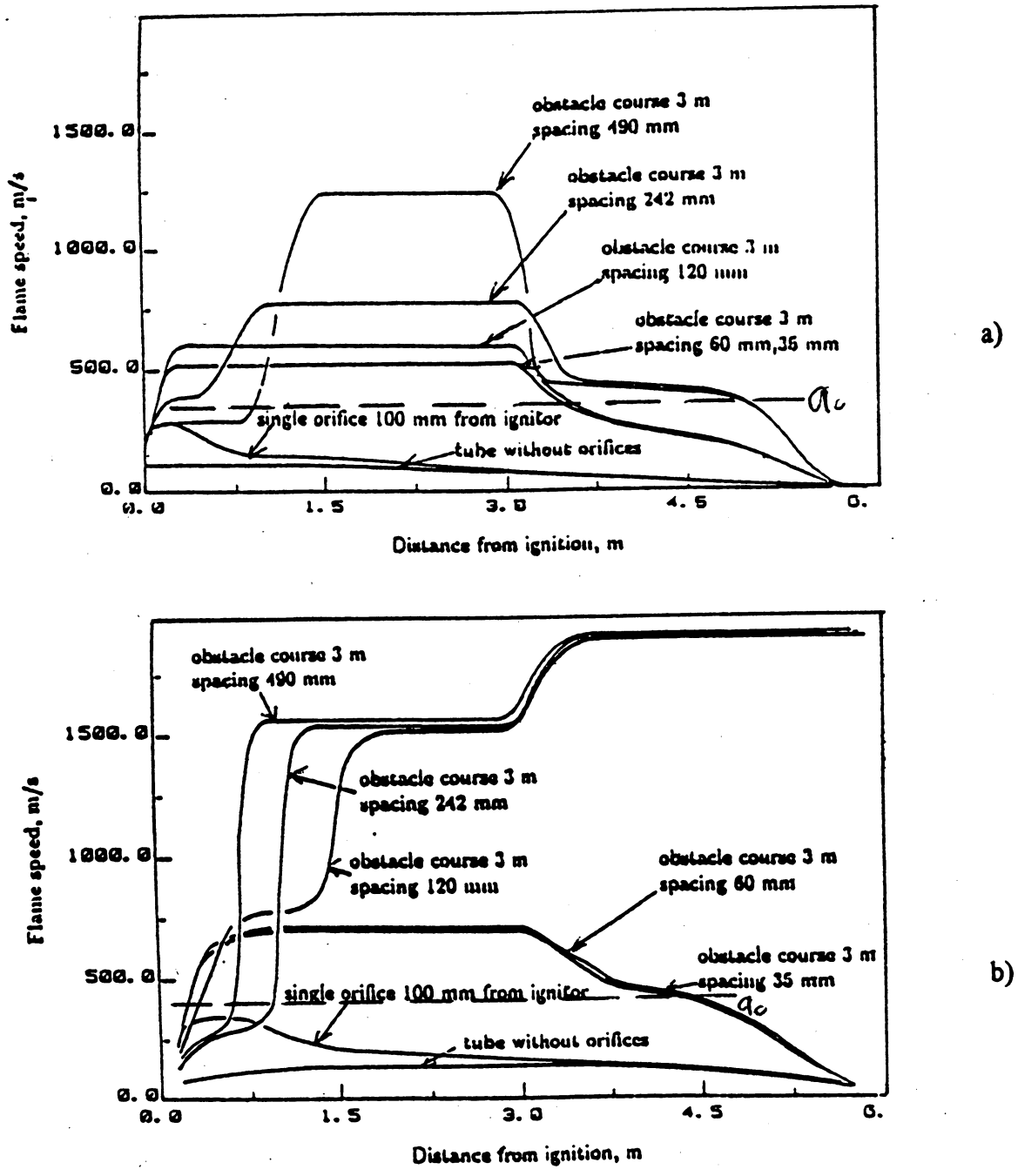

Figure 5.2.2.2-5 Flame profiles in the explosion tube for hydrogen-air mixtures. (a) $16\%H_2$**, (b)** $24\%H_2$**,** $BR = 0.7$

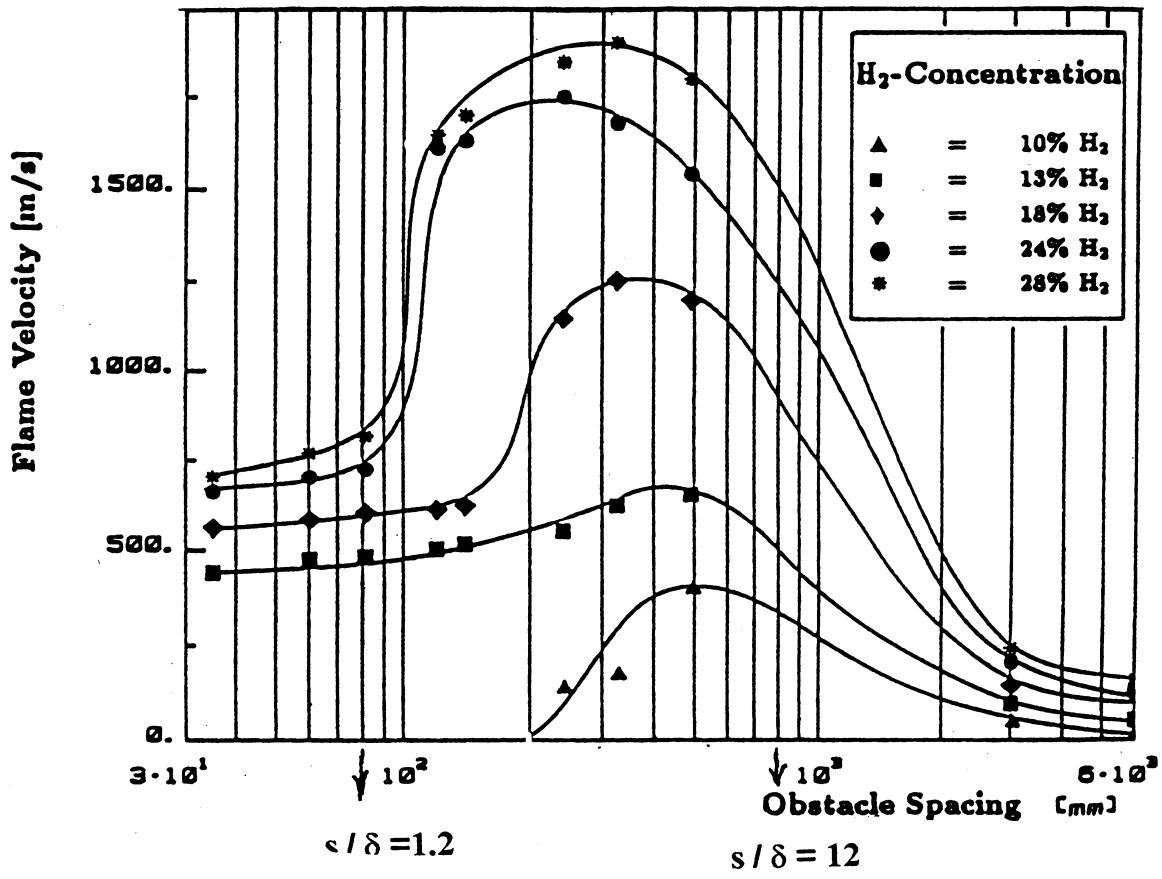

Figure 5.2.2.2-6 Maximum flame velocity as a function of obstacle spacing

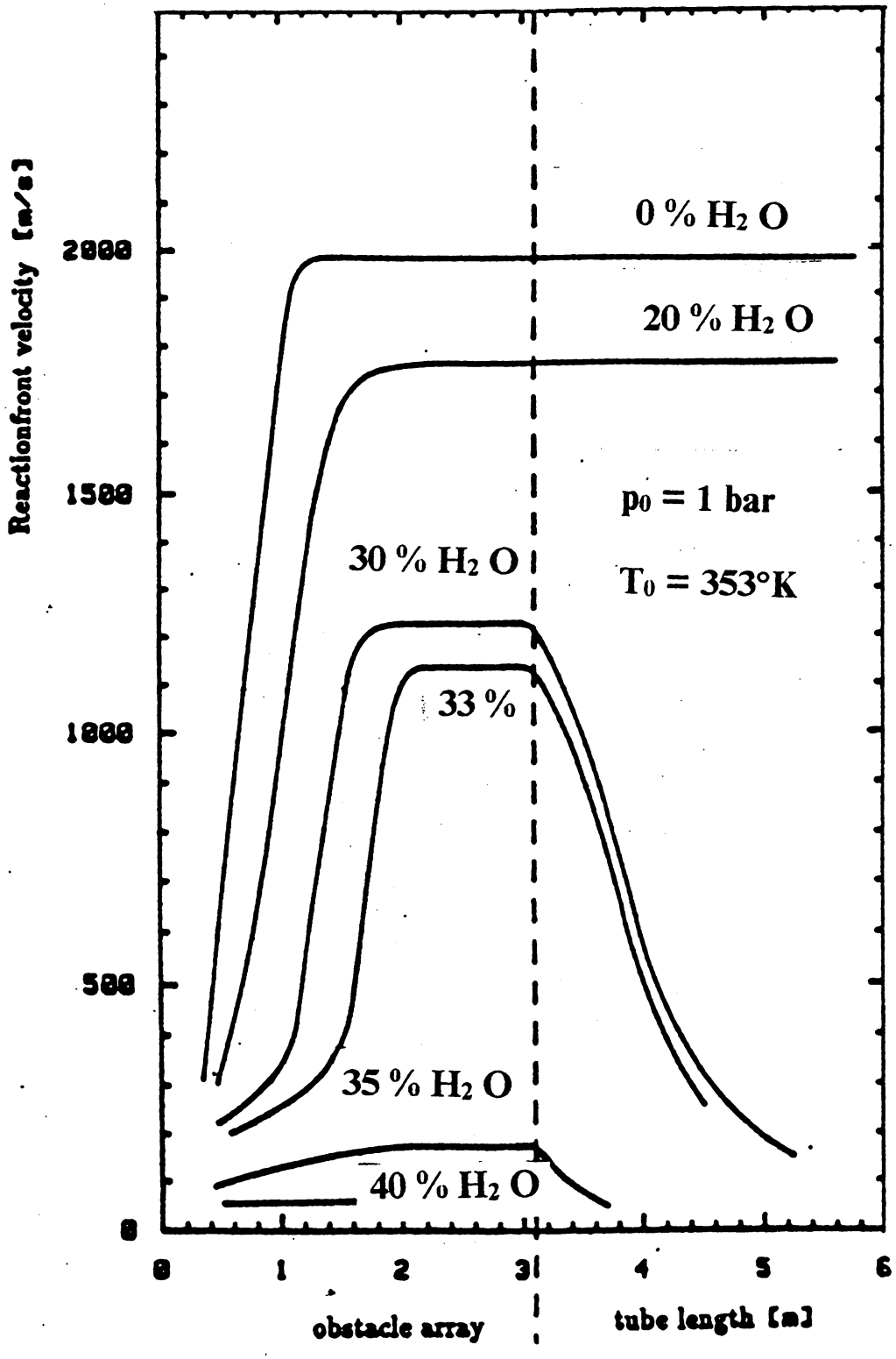

Figure 5.2.2.2-7 Variation of flame velocity along the partially obstructed tube

5.2.2.3 *Influence of venting on flame propagation in obstacle-laden channels* *

Experiments were performed at the Brookhaven National Laboratory (BNL) in the High-Temperature Combustion Facility (HTCF) to study the influence of venting on the propagation of deflagration . The experiments were jointly funded by the United States Nuclear Regulatory Commission (USNRC) and the Japanese Nuclear Power Engineering Corporation, which is sponsored by the Ministry of International Trade and Industry (MITI). The HTCF detonation tube, which can be heated up to a maximum temperature of 700 K with a temperature uniformly of $\pm 14K$, is 21.3 m long and is constructed from sections of stainless steel with an internal diameter of 273 mm. (see Figure 5.2.2.3-1). The test gases are mixed in a chamber fed with two pipes: one flowing air at room temperature and on the other a heated mixture of hydrogen and steam. The desired mixture composition is achieved by varying the individual constituent flow rates via choked venturis.

In the experiments investigating the DDT phenomenon, a flame is ignited and it subsequently accelerates as a result of turbulence generated in the induced flow ahead of it. For certain mixtures, this FA could lead to the initiation of a detonation wave. In order to promote flame acceleration, periodic orifice plates are installed down the length of the entire detonation tube. The orifice plates have an outer diameter of 273 mm (equivalent to the inner diameter of the tube), an inner diameter of 206 mm ($BR = 0.43$), and have a spacing of one tube diameter. A standard automobile diesel engine glow plug is used to ignite the test mixture at one end of the tube.

For venting experiments, the main modification of the detonation vessel was the addition of four vent sections that were inserted between non-vented pipe sections. Figure 5.2.2.3-2 shows a photograph of the detonation tube equipped with vent sections, and Figure 5.2.2.3-3 shows a schematic sketch of a vent section. These vent section consist of two standard pipe-crosses butt-welded together, with each pipe-cross having the same inner diameter as the detonation tube. The total vent area per vent section is thus 4 times the detonation tube cross-section area (5.1% of the total vessel surface). The vent openings are initially closed by vent covers that are dislodged when the vessel pressure increases as a result of combustion. The welded pipe-crosses are matted to the straight pipe sections using compatible flanges. The length of a vent section is 1.52 m, which is exactly half the length of a standard HTCF straight pipe section. In order to maintain the same total vessel-length-to-diameter ratio (e.g., 78) as the vessel without the vent sections, two of the straight sections are not utilized in the present experiments. In this way, five straight sections are not utilized in the present experiments, and five straight pipe sections are separated from each other by one of the four vent sections.

The parameters that most influence the FA process are the mixture composition, which includes the hydrogen concentration and the steam dilution, and the mixture's initial temperature. The hydrogen concentration was varied from a minimum where benign flames were produced to a maximum where vent covers were dislodged from their tethers. The initial temperature was varied between 300 K and 650 K, and the initial pressure was 0.1 MPa for all tests. In general, for the test apparatus configuration studied, venting reduced the likelihood of DDT at all initial temperatures tested. Flame propagation in the vented tube geometry consists of an initial FA phase followed by a quasi-steady-state phase where the combustion front velocity oscillates about a mean. The various flame propagation regimes have been classified as (1) slow deflagrations, (2) choking, and (3) detonation.

Slow deflagrations. The flame propagation in these various regimes is qualitatively similar to that observed in the test without venting, except for local perturbations induced by the vent sections. In the

* Contributed by Dr. A. Malliakos

slow deflagration regime, the flame accelerates to a maximum velocity of $100 \text{ to } 200 \text{ m/s}$ around the first vent section and then for the remainder of the tube decelerates to a velocity on the order of metres per second. No significant pressure is generated in this propagation regime.

Choking regime. In the choking regime, flame acceleration is followed by an oscillatory propagation mode where the flame accelerates in the tube section and decelerates across the vent section. The mean flame velocity during the oscillatory propagation is just under the speed of sound in the burnt products. The structure of the combustion front consists of a turbulent flame preceded by a weak precursor shock wave and a stronger leading shock wave. The leading shock wave is generated as a result of the coalescing of compression waves generated ahead of the turbulent flame. This leading shock wave has a typical pressure rise just under the adiabatic isochoric complete combustion (AICC) pressure. The weak wave is generated by decoupling of the leading shock wave and the flame during their passage through the vent section. Therefore, the weak precursor wave is a product of the leading shock wave after it emerges from the vent section.

Detonation regime. In the detonation propagation regime, which exists for particularly sensitive mixtures, a detonation wave is initiated at some point during FA. In all the cases tested, the detonation wave failed before the end of the vessel as a result of wave diffraction in the vent section. However, one would expect that if the mixture cell size is small enough, a detonation wave could propagate through the entire vessel unimpeded by the orifice plates at the venting.

The influence of venting on the combustion phenomenon could be measured by the magnitude of change in the choking and the DDT limits from tests without venting to tests with venting. The choking limit, which is in effect the minimum hydrogen composition where significant FA takes place, increased for all initial temperatures and steam dilution in the experiments with venting. The DDT limit, which in this case is defined as the minimum hydrogen composition where a detonation is observed, was equally affected by venting. For example, for hydrogen-air mixtures at 500 K, the DDT limits increased from 12% hydrogen with no venting to 15% hydrogen with venting. The study without venting had shown that for hydrogen-air mixtures at 500 K, the DDT limit criterion was $d/\lambda = 1$. In the present study with venting, for hydrogen-air mixtures at 500 K, the DDT limit is $d/\lambda = 5.5$.

Table 5.2.2.3-1 Choking and DDT limits for hydrogen-air mixtures

Temp (K)	Choking Limit		DDT Limit			
	No Venting	Venting	No Venting		Venting	
	Hydrogen [vol %]	Hydrogen [vol %]	Hydrogen [vol %]	d/λ [–]	Hydrogen [vol %]	d/λ [–]
300	11	12	15	1.0	N.A.	
500	8	11	12	1.5	15	5.5
650	11	13	11	5.5	13	11.9

Table 5.2.2.3-1 shows the choking and DDT limits for hydrogen-air mixtures for test with and without venting. Table 5.2.2.3-2 shows the same limits for hydrogen-air-steam mixtures for tests with and without venting. Figures 5.2.2.3-4 and 5.2.2.3-5 show a comparison of the combustion front velocity versus distance for a 10% and a 15% hydrogen-air mixture at 500 K with and without venting respectively.

Table 5.2.2.3-2 Choking and DDT limits for hydrogen-air-steam mixtures

Temp (K)	Choking Limit			DDT Limit			
	H_2O [vol %]	No Venting	Venting	No Venting		Venting	
		Hydrogen [vol %]	Hydrogen [vol %]	Hydrogen [vol %]	d/λ [–]	Hydrogen [vol %]	d/λ [–]
400	10	12	12	18	0.7	N.A.	
500	25	14	15	24	1.5	N.A.	
650	25	16	18	19	0.8	23	5.7

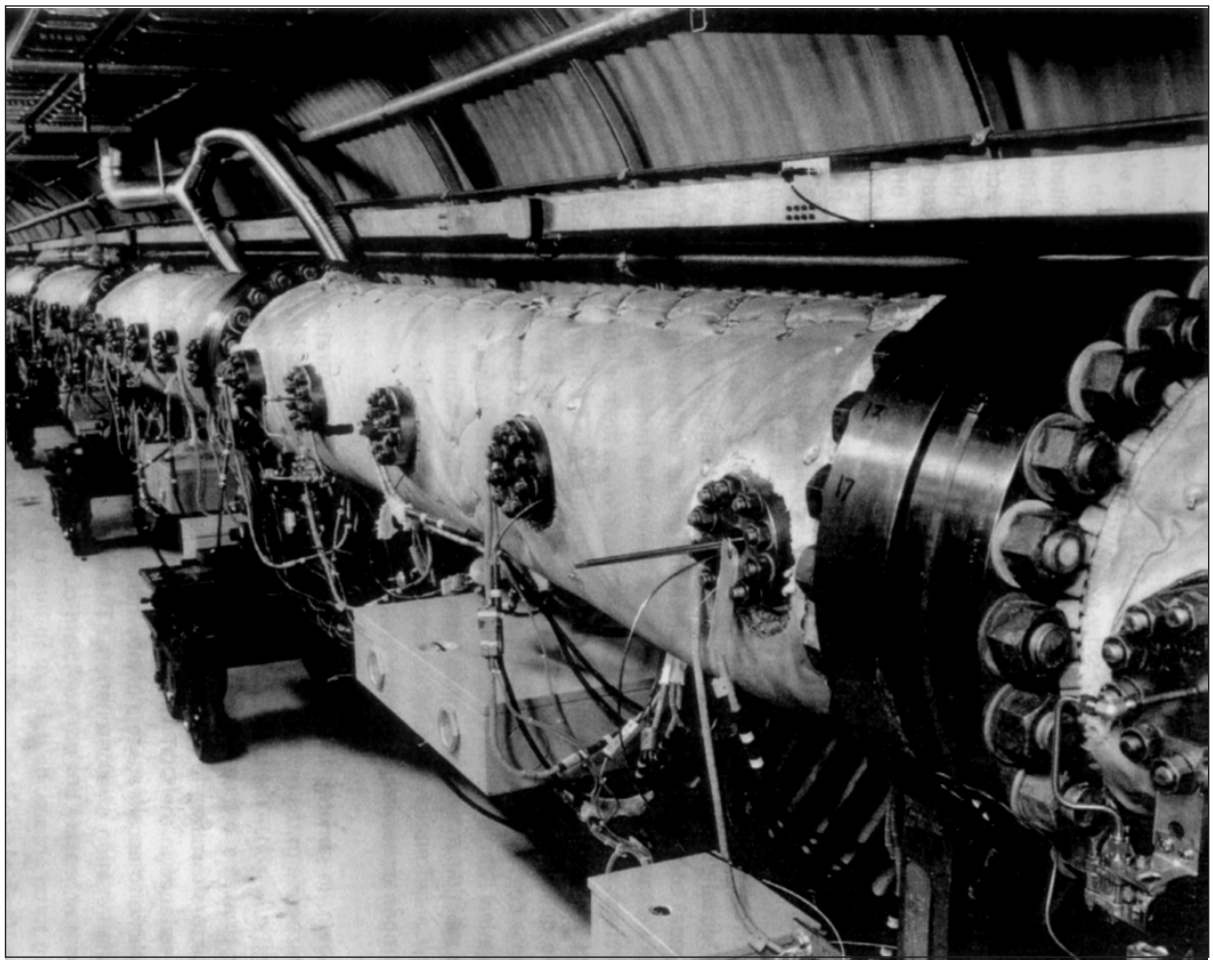

Figure 5.2.2.3-1 Photograph of the HTCF detonation tube located inside the 3.05-m tunnel

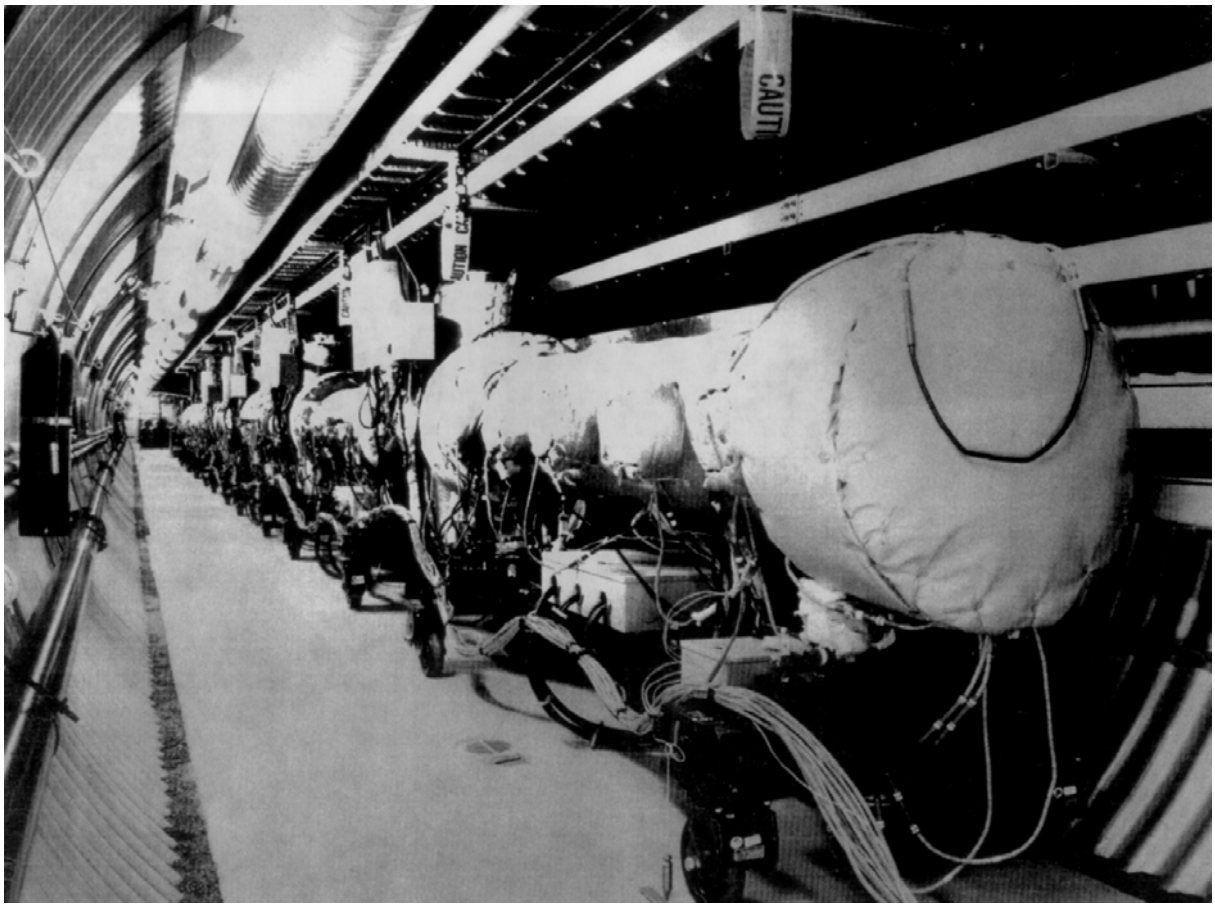

Figure 5.2.2.3-2 Photograph of the HTCF detonation tube equipped with vent sections

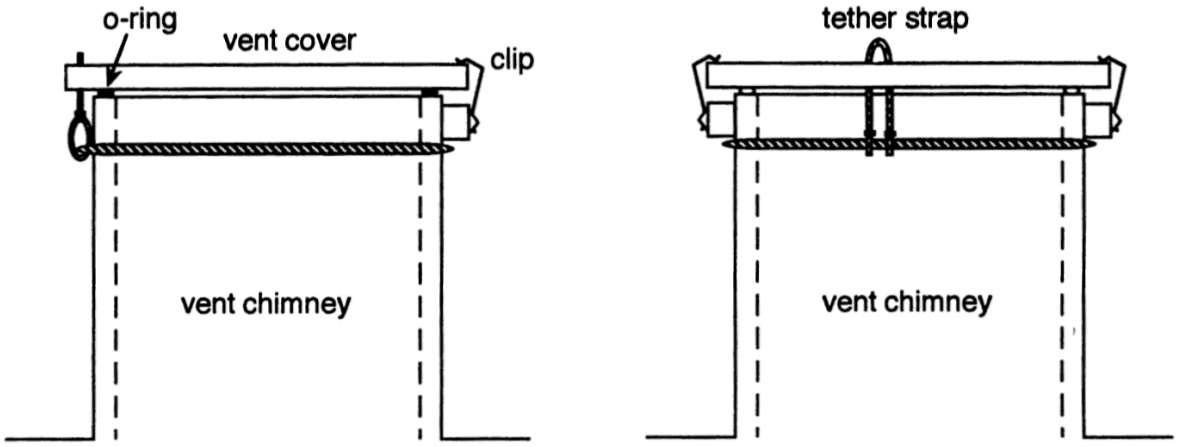

Figure 5.2.2.3-3 Schematic of vent cover tether strap and clip assembly, HTCF Facility

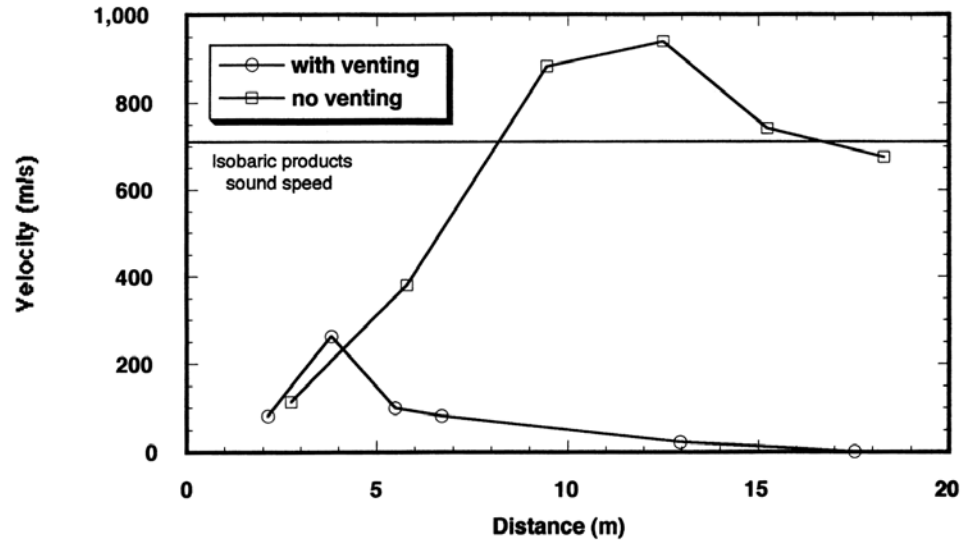

Figure 5.2.2.3-4 Comparison of the combustion front velocity versus distance for a 10% hydrogen-air mixture at 500 K with and without venting, HTCF Facility

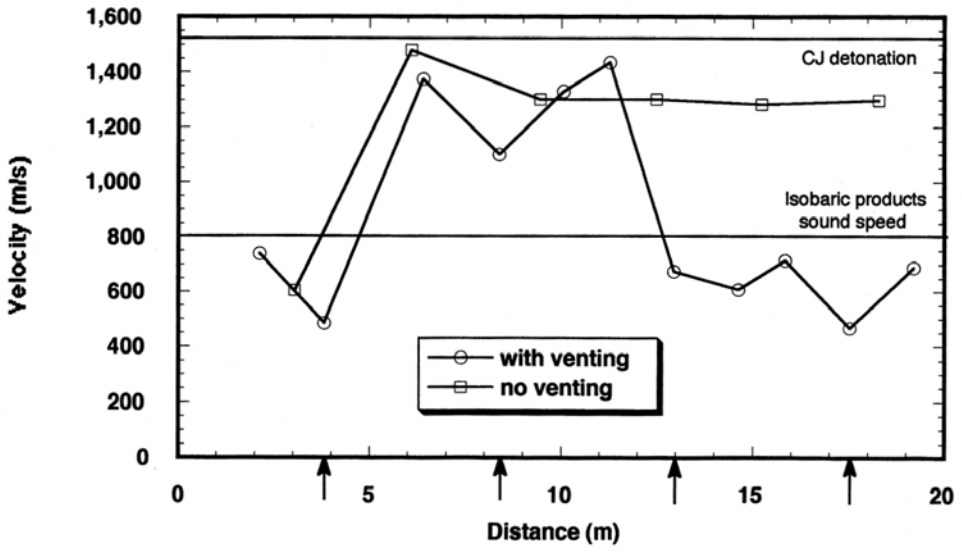

Figure 5.2.2.3-5 Comparison of the combustion front velocity versus distance for a 15% hydrogen-air mixture at 500 K with and without venting, HTCF Facility

5.2.2.4 He-air turbulence tests and modelling

In Reference [5.43] the 12-m tube was modified to allow inert tests in a shock tube mode, where a 3-m-long section can be pressurized (Figure 5.2.2.4-1). After bursting of the membrane, a shock wave travels in the remaining 9-m-long part, which is initially at low pressure (e.g., 1 bar) and contains circular rings as obstacles. The shock wave loses velocity and pressure amplitude by partial reflection and turbulence generation. The measured pressure signals at different locations can then be compared with numerical simulations using different turbulence models. These data allow us to verify the turbulence modelling under inert conditions without interference from combustion process, which is exemplarily shown for the COM3D-code in Section 5.3.3.

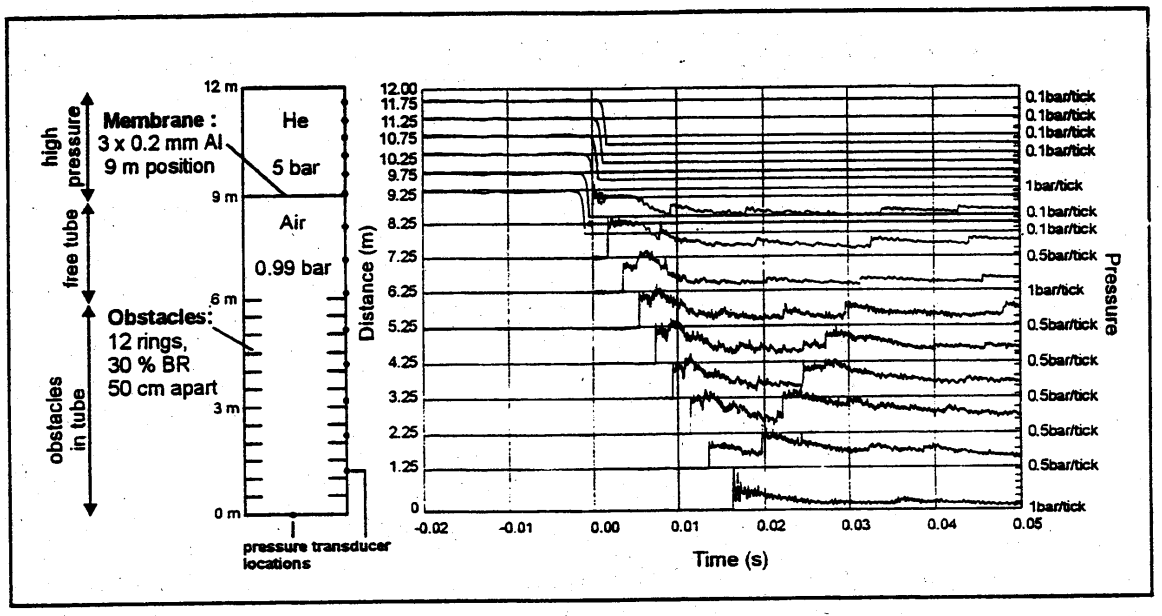

Figure 5.2.2.4-1 Inert shock tube experiments in FZK "12-m tube". The measured pressure data contain information about turbulence generation and dissipation without combustion.

5.2.3 Experiments in Large-scale and Complex Geometries[*]

5.2.3.1 Preliminary remarks

The explosion tubes, described in the previous sections, are very suitable for a first validation of computational tools for several reasons. The scale of the applied test facilities is relatively small (usually up to a volume of 1 m^3), which facilitates a very detailed investigation of the respective combustion phenomenon by means of a conventional measurement technique, with a high resolution in time and in space or optical measurement techniques. The geometries of these facilities are, in most cases, very simple (e.g., periodic obstacles in a tube) and can, therefore, be easily modelled at a very detailed level. In order to apply the numerical codes for the simulation of propagating flame fronts in realistic geometries, they have to be validated with experiments that have been performed in facilities with a scale of several magnitudes larger compared with the scale of a small-scale explosion-tube. In Figure 5.2.3.1-1, the sizes

[*] Contributed by A. Eder and Dr. M. Heitsch

Table 5.2.3.1: Recent experiments in complex and large-scale geometries

Test Facility	Country/ Operator	Geometry	Mixture	Instrumentation	Test Parameters
MuSCET	Germany, TU-Munich	286×286 mm, $L = 6.7$m	9%-16% Hydrogen	LIPF, LDV, schlieren, pressure gauges, thermocouples, photodiodes	Visualization, flame-acceleration due to obstacles
L.VIEW	Italy/ University of Pisa, TU-Munich	670×670 mm, $L = 3.2$ m	8.5%-10% Hydrogen	Video, LDV, schlieren, pressure gauges, thermocouples, volume fraction	Vizualisation, ignition and opening location, jet ignition, turbulence
AECL Interconnected Vessels	Canada/ AECL	$V_{sphere} = 2.3m^3$, $V_{cyl.} = 10.7m^3$	6-20 vol % H_2	pressure gauges	Jet ignition, independent hydrogen conc. in sphere and cylinder
LSVCTF	Canada/ AECL	$10 \times 4 \times 3m, V = 120m^3$	$8 - 14\% H_2$, Steam	Pressure gauges	Vented Combustion with different ventareas
HTCF	USA/ BNL	ID 273 mm, $L = 21.3$ m	H_2-Air-(Steam)	Photodiodes, smoked foils, fast response thermocouples and piezoelectric pressure transducers	Effect of mixtures's composition and high initial temperature on mixture's sensitivity to detonation and DDT, as well as effect of venting on DDT
Battelle Model Containment BMC	Germany/ Battelle	$D = 10$ m, $H = 10$ m, $V = 40 - 200$ m^3	7-14% Hydrogen, 0-50% Steam, (CO2)	Pressure gauges, thermocouples, IR-diodes, volume fraction, (Hot wire turbulence)	Slow and fast combustion, vented combustion, jet ignition, realistic obstacles
DN-400	Germany/ Battelle	Diameter 0.4m, $L = 8$ m, $V = 1$ m^3	8.5-17% Hydrogen, 0-40% Steam	Pressure gauges, thermocouples, IR-diodes, volume fraction, hot wire turbulence	Scaling to BMC, realistic obstacles
PHDR	Germany/ FZK	Typical L=10m,$V = 535m^3$	8-12% Hydrogen, 34-30% Steam	Pressure gauges, thermocouples, volume fraction	Scaling to BMC
NUPEC Large Scale	Japan/ NUPEC	Diameter 8m, $V = 270m^3$	8-15% Hydrogen, 0-60% Steam	Pressure gauges, thermocouples, volume fraction, video	Ignition location, spray, elevated initial pressure, transient behaviour
RUT Facility	Russia/ Kurchatov Inst.	Channel: $L = 34.6$ m, $W = 2.5$ m, $H = 2.3$ m, "Canyon:" $L = 10.55$ m, $H = 6.3$ m, $W = 2.5$ m, $V = 480$ m^3	$H_2 - Air - H_2O$-Mixtures	Photodiodes, Pressure-Gauges	Influence of mixtures sensitivity to detonation and DDT

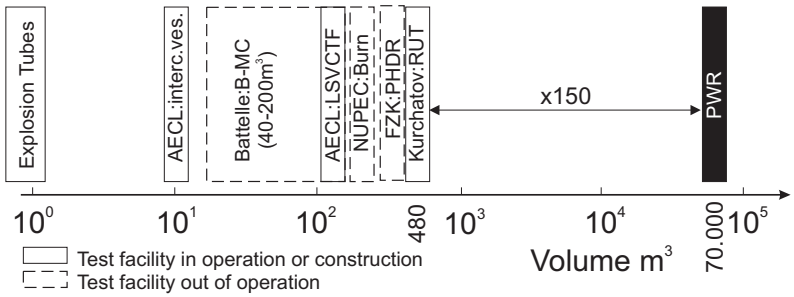

Figure 5.2.3.1-1 Scale of large-scale test facilities

of several large-scale facilities, presented among others in this section, in comparison to the size of a PWR containment are shown.

It is not possible to model realistic geometries with a full level of detail because of the enormeous requirement of computer memory. On the other hand, each grid-iron or tube in a room has, possibly, a significant influence on the propagation speed of a flame and, therefore, on the resulting pressure load on the containment structure. Nevertheless, the influence of these geometries has to be taken into account. Hence additional experiments are presented in this section, which focus on the influence of complex and realistic geometries for a containment in different scaled test facilities.

Table 5.2.3.1-1 summarizes the main parameters of the test series, which were conducted at different test facilities. A short summary of the investigated combustion phenomena, as well as the applied instrumentation, is described in this table, in order to give a general idea of which experiments should be used for a specific code validation.

5.2.3.2 Recent experiments applicable to code validation

The influence of obstacles, typical for a reactor containment (tubes, grid-irons, and doors) on the flame propagation was examined in the MuSCET Facility [5.56, 5.57] at the Technische Universität München (Figure 5.2.3.2-1). This explosion tube is equipped with a window section with an optical access for the application of optical measurement techniques (schlieren and laser-induced predissociation fluorescence (LIPF) for the investigation of the flame propagation and flame shape, laser Doppler velocimetry (LDV) for the determination of the flow velocity of the expansion flow and the turbulence-quantities). The investigated obstacles (see Figure 5.2.3.2-2) are classified into 3 categories: tubes (single tubes and tube-bundles, $BR\ 7.5\%$ to $-\ 17\%$); grid-irons ($BR\ 25\%$); and a door-opening ($BR\ 85\%$).

The maximum pressure for several obstacle configurations at different hydrogen concentrations is plotted in Figure 5.2.3.2-3. The maximum pressure rise of the three obstacle categories can be summarized as follows:

- Because of the low blockage ratio of the tube obstacles, the influence on the flame velocity is low (see below). Therefore, the pressure rise for all investigated tube-shaped obstacles is low, and the differences between the tube obstacle can be neglected.
- At the grid-type obstacles, a big difference was found depending on the angle of the grid blades. With the grid blades having an angle of 45^o to the main axis of the tube, the change of the flow

direction leads to an increased turbulence intensity. This results in a higher pressure rise compared with that in the rectangular grid-iron. It is of interest to note that because of buoyancy effects the blades of the 45^o grid iron are almost rectangular to the surface of lean hydrogen-air flames.

- The highest pressure was measured in the case of the highest blocking obstacle with a blockage ratio of 85%. With this obstacle configuration, a jet was formed, leading to a strong increase of the flow velocity and the intensity of the turbulence .

The maximum measured flame velocities for different types of tube-shaped obstacles, different types of grids, and the highly blocking obstacle are shown in Figure 5.2.3.2-3. The principle behaviour of the maximum flame velocity can be directly compared to the pressure measurements shown in Figure 5.2.3.2-4.

By means of the optical measurement techniques, the flame structure in the area near the orifice could be visualized in order to identify the important physical effects responsible for FA. The investigations were performed by means of the high-speed schlieren technique as well as the laser-induced predissociation fluorescence (see References [5.58 – 5.63]). Examples of schlieren images of the flame propagation inside the empty tube without obstacles are shown in Figure 5.2.3.2-5. At low hydrogen concentrations, the flame propagation is dominated by the influence of gravity. At 9 vol % H_2, the flame merely burns at the upper part of the tube and does not propagate to the bottom of the facility. Even at 12 vol %, the gravitational effect can still be clearly identified. At the highest investigated concentration of 16 vol % ,the burning velocity dominates the gravitational effect, which leads to a spherical flame front.

The visualization of the flame propagation shows a considerable difference in the flame structure, depending on the hydrogen concentration. These differences can be explained by the instability effects that occur at hydrogen-air flames, e.g., the Rayleigh-Taylor instability or the Darrieus-Landau instability.

Nevertheless, the structure of a 9 vol % hydrogen-air flame is not as smooth as it appears to be in the schlieren images. The application of the laser-induced predissociation fluorescence (see Figure 5.2.3.2-6) identified a distributed reaction zone. Because of the instability effects (see Chapter 2), the combustion process is completely quenched at the negatively curved areas and enhanced at the positively curved cusps.

The L.VIEW Facility [5.64 – 5.68] offers the opportunity to perform medium-scaled deflagration tests with complete optical access from 2 directions simultaneously (from the front and the top side by means of a mirror placed above the test facility). The apparatus consists of a regular test section with the inner dimensions of 677 mm $\times 677$ mm $\times 3200$ mm, divided into 2 chambers, which simulate 2 connected rooms, e.g., by a door or a window. The first chamber has a length of 1050 mm and is separated from the second chamber by a wall with a central round orifice (see Figure 5.2.3.2-7). The blockage ratio of the orifice can be varied from 96% up to 99.6% in order to investigate the influence of blockage ratios on the flame propagation. The second chamber is equipped with a weak rupture disk to the ambient atmosphere with the dimension 300 mm $\times$ 300 mm at the end flange.

The conventional instrumentation consists of 7 high-speed piezo-capacitive pressure transducers and 7 thermocouples. The visualization of the flame propagation is performed by means of a standard video camera with a frame rate of 25 Hz as well as a high-speed video camera with a maximum frame rate of $40\,000$ Hz. In addition, the velocity of the expansion flow can be measured without inertia and non-intrusively for the horizontal and the vertical component with a two-component LDV system.

A representative example of the flame propagation can be seen in Figures 5.2.3.2-8 and 5.2.3.2-9. In the experiments, areas of direct ignition in the second chamber, ignition after a certain delay time, or even total flame extinction without ignition in the second chamber at all were observed, depending on the hydrogen concentration and the blockage ratio of the obstacle.

In the case of a direct ignition in the second chamber, the measured burning velocity can be compared with the velocity that is calculated with a turbulent burning correlation (e.g., Koroll et al. [5.69], Peters [5.70], Beauvais [5.71]). Because of the high turbulence intensities, which were measured in front of the flame in the middle of the second chamber, the product of the Karlovitz flame stretch factor K and the Lewis number Le exceeds the value of 0.3. Therefore, local flame quenching effects during the flame propagation in the second chamber have to be expected, as described in Abdel-Gayed and Bradley [5.72].

The integral length scale, which is an essential quantity either for the classification of the combustion process according to Borghi (see Chapter 2) or the calculation of the turbulent burning velocities (see above) could not be measured at the L.View Facility. Literature data (e.g., Lindstedt and Sakthitharan [5.73]) reveal that the integral length scale can be determined to have a value of 0.125 times the hydraulic diameter of the chamber behind a plate having a blockage ratio of 50% for combustion processes of stoichiometric methane-air flames. In Figure 5.2.3.2-10, the measured turbulent burning velocity in the second chamber is plotted versus the hydrogen concentration of the initial mixture as well as the calculated burning velocity (according to Beauvais [5.71]).

Measurements of the flame-structure during the combustion process in the second chamber by means of the laser-induced predissociation fluorescence were performed in a comparable small-scale facility at the Technische Universität München (PuFlaG Facility, [5.64]). These measurements showed that in case of a direct ignition the combustion is initiated from several ignition kernels. At a later stage, the leading flame contour, which was observed during the combustion in the first chamber, is replaced by a volumetric reaction. This corresponds to the classification of different combustion regimes as suggested by Borghi. As it can be seen in Figure 5.2.3.2-11, the combustion in the second chamber in this case is located within the regime of the "well-stirred reactor", which corresponds to the experimentally observed volumetric reaction, where similar conditions exist over a large volume.

In case of an ignition after a delay, burned gas is blown into the second chamber where it is mixed with the unburned gas. The ignition occurs with a delay of up to 1 s after the flame in the first chamber has reached the orifice. It could be observed that the flame has approximately a constant velocity over the entire length of the second chamber and that the flame velocity does not vary significantly over the cross-section of the chamber (flat shape of the flame, see example in Chapter 2), although the gas-mixture is highly inhomogeneous.

This can be explained by the transport from the first into the second chamber together with the burned gas. Once mixed with the unburned gas, these free radicals decrease the chemical induction time and, consequently, increase the burning velocity. As a result, the flame velocity reaches a high value, although the flow velocity and, thus the turbulence before the ignition is rather low (see Figure 5.2.3.2-12).

In Figure 5.2.3.2-13, the maximum pressure in the second chamber is shown as a function of the hydrogen concentration and the ignition delay. It can be seen that the direct ignition in the second chamber causes the highest pressure rise in the second chamber. This is explained by the fact that during the longer ignition delay, more exhaust gas is blown into the second chamber, which leads to a leaner mixture. Moreover, it was observed that the burning velocity is a decreasing function of the ignition delay. In case

of a longer ignition delay, a higher amount of radicals is recombined, which results in a lower radical concentration before the igntion.

The flame quenching at high turbulence intensities has been studied in detail by various authors. According to Abdel Gayed and Bradley [5.72], turbulent flame quenching occurs when the product of the Karlovitz flame stretch factor K and the Lewis number Le exceeds a value of 1.5. In case of quenching that is due to a turbulent jet, this value has to be modified to fit the conditions that have to be expected during the flame propagation between to rooms connected by an opening. This value was determined to be $K \cdot Le = 0.9$; see Figure 5.2.3.2-14.

The maximum design pressure of the L.View Facility did not allow one to perform experiments with hydrogen concentrations of more than 11 vol %. However, an increased hydrogen concentration leads to an increased laminar burning velocity that reduces the probability of flame-quenching. Small-scale experiments at the Technische Universität München (PuFlaG Facility, see above) showed that higher hydrogen concentrations lead again to a direct ignition in the second chamber (Figure 5.2.3.2-15). Because of the smaller dimension of the PuFlag Facility (diameter 80 mm), the flame quenching takes place at lower hydrogen concentrations. The reason for this can be found in the smaller integral length scale that is an important parameter for the occurrence of quenching effects.

The total extinction of the flame depends on both the initial mixture and the blockage ratio of the central orifice. A critical hydrogen concentration, at which no ignition in the second chamber occurs, was determined to be 11 vol % for an orifice diameter of 70 mm, and 9 vol % for an orifice diameter of 52 mm.

The burning of near-flammability limit hydrogen-air mixtures in interconnected vessels was examined in a Large-scale Interconnected Vessels Facility at AECL, Whiteshell Laboratories [5.74]. Figure 5.2.3.2-16 shows a schematic of the experimental apparatus. It consists of a 6-m-high and 1.5-m-diameter cylindrical vessel (volume = 10.7 m^3) and a 2.3-m-diameter sphere (volume = 6.3 m^3). The 2 vessels are joined together by a 2.7-m-long pipe with an inside diameter of 0.45 m. The entire system is rated for a pressure of 10 MPa. To vary the size of the opening between the 2 vessels, orifices of different hole diameters (30 cm and 15 cm) were mounted between the pipe and the cylinder. The hydrogen concentration was independently varied from 6 to 20 vol % in the sphere and 0 to 20 vol % in the cylinder. The initial pressures in the vessels were atmospheric. The gas mixture in the sphere was ignited at the centre by an electric spark. The facility was equipped with a gas sampling and analysis system allowing gases from various locations in the 2 vessels to be sampled and analyzed.

Upon ignition, the expanding flame kernel propagated through the pipe and subsequently emerged into the cylinder, igniting the gas mixture. Results showed that, depending on the size of the orifice, the combustible mixture in the downstream vessel was not always ignited by the flame jet emerging from the upstream vessel. These critical conditions for 8 to 14 vol % H_2 in the sphere are illustrated in Figure 5.2.3.2-17. This figure shows that for 10 vol % H_2 in the sphere, complete burning was achieved for all H_2 concentrations higher than 14 vol % in the cylinder. Since 10 vol % H_2-air mixture is above the downward flammability limit, the mixture in the sphere should be completely burned. However, for H_2 concentration in the cylinder between 8 and 12 vol %, unburned hydrogen was observed in both vessels. It is reasonable to speculate that for all these cases, the hydrogen in the sphere was completely burned, but the flame emerging from the connecting pipe failed to ignite the gas in the cylinder. The hydrogen detected in the sphere was caused by the back flow of the gas from the cylinder after the steam in the sphere had condensed. This result implies that the turbulence induced by the vent flow is capable of

causing total extinction of the flame emerging from a 15-cm-diameter hole. Since the flow velocity at the orifice depends on the opening area and the mixture composition in the upstream vessel, the critical conditions (in terms of H_2 concentration in the cylinder) should also depend on these parameters. For extinction of the 12 vol % and 14 vol % H_2 flames as they emerge from the orifice, the H_2 vol % in the cylinder needs to be less than about 10 vol % and 8 vol % H_2 respectively. It should be pointed out that no flame extinction was observed for 8 vol % H_2-air mixtures. We speculate that since the burning rate of a 8 vol % H_2-air mixture and the resulting vent flow velocity were very low, the turbulence in the vicinity of the orifice was probably not sufficient to cause a total extinction of the flame. As a result, burning may have occurred in both vessels.

The Large-scale Vented Combustion Test Facility (LSVCTF) is located at the Whiteshell Laboratories in Pinawa, Manitoba, Canada. Figure 5.2.3.2-18 shows a cutaway schematic of the facility. The facility is a 10 m long, 4 m wide, and 3 m high rectangular enclosure with an internal volume of $120\ m^3$. It is constructed of 1.25-cm-thick steel plates welded to a rigid framework of steel I-beams. The entire structure is anchored to a 1-m-thick concrete pad. Two roller-mounted movable end walls are provided to open the vessel for internal modifications or to move in bulky experimental equipment, when needed. The combustion chamber, including the end walls, is electrically trace-heated and heavily insulated to maintain temperatures in excess of 100^oC for extended periods of time. The entire combustion chamber is enclosed in an insulated metal Quonset, which houses the gas analysis and hydraulic fan systems on one side and all the process piping on the other side. Venting occurs through openings in the end walls. The end walls are covered with removable rectangular steel plates bolted to the end-wall structure. Hydraulic fans in the combustion chamber are used for mixing and to generate turbulence during ignition and combustion. The test chamber is instrumented for pre-test gas analysis, pressure transients, flame tracking, and vent velocity. The facility is located in a fenced area and is remotely operated.

The LSVCTF has been used to perform a wide variety of experiments. Some of these are

- unobstructed vented combustion experiments in 30, 60, or $120\ m^3$ volumes to evaluate the effects of scale,
- turbulent vented combustion experiments to study the effects of initial turbulence,
- flame propagation studies between interconnected compartments, and
- catalytic recombiner testing for hydrogen mitigation applications in large enclosures.

Figures 5.2.3.2-19 and 5.2.3.2-20 show some results obtained from the Large-scale Vented Combustion Test Program. Results in both figures are from experiments performed in the $120\ m^3$ geometry ([5.75], [5.76]). Figure 5.2.3.2-19 shows the variation in peak pressure with increasing vent size. As the vent area increases, the peak pressure caused by the combustion decreases. Figure 5.2.3.2-20 shows the variation in peak pressure with increasing steam concentration. As the steam concentration in the H_2-air-steam mixture increases, the peak pressure decreases.

The experiments performed at the Brookhaven National Laboratory (BNL) in the High-Temperature Combustion Facility (HTCF) showed that venting has a significant influence on both, the maximum flame speed and the transition to detonation. For a detailed description refer to Section 5.2.2.

The most comprehensive experimental program was conducted at the Battelle Model Containment ([5.77 – 5.81]). A view of this facility is given in Figure 5.2.3.2-21. More than 100 combustion

experiments were conducted in the BMC with the aim to study combustion under realistic severe accident conditions in a scaled-down volume. Tests are available from single-room arrangements with $40\ \mathrm{m}^3$ up to five-room selections with about $200\ \mathrm{m}^3$. In any case, a venting opening from the test section to the environment was included to restrict the combustion pressure rise to about 2 bar. The combustion phenomena studied in detail are ignition, slow combustion, acceleration, and jet ignition, as well as diluent impact (steam and CO_2) and obstacles. An example for the obstacle set-up is shown in Figure 5.2.3.2-22. Here, generic obstacles such as cylinders and rows of pipes with different blockage ratios were investigated apart from jets through openings of different diameters. In a simplified way the measured flame speed increases by a row of pipes in the flame path as illustrated in Figure 5.2.3.2-23. These data may be useful for model validation if larger obstacles or equipment are modelled explicitly by a code.

In order to look at scaling phenomena, the test facility DN-400 [5.82] was built. In this facility (Figure 5.2.3.2-24) that has only $1\ \mathrm{m}^3$ of volume, scaled identical obstacles were investigated and detailed measurements including turbulent fluctuations were conducted. The tests revealed a considerable scaling effect when the resulting flame speeds were compared with similar findings from the Battelle Model Containment, as shown in Figure 5.2.3.2-25. This strong effect of the test volume size on the combustion progress was identified to be mainly due to the much stronger wall effects and the missing buoyant influence in the early phase of combustion in the small facility and appeared to be challenging to applied combustion models.

A scaling to larger volume was achieved by using parts of the outdated PHDR [5.83] containment for combustion experiments (Figure 5.2.3.2-26). In this almost empty set of compartments with a volume of about $550\ \mathrm{m}^3$, tests with gas compositions typical of severe accidents including steam as a diluent were conducted. The data obtained can be used to validate combustion models in comparison with the experiments from the Battelle Model Containment.

Quite a different test facility has been operated in Japan. The NUPEC Large-scale Combustion Test Facility [5.84] is shown in Figure 5.2.3.2-27. With a volume of about $270\ \mathrm{m}^3$, it is rather big and is designed as a closed volume in contrast to the Battelle Model Containment and PHDR (vented combustion). With the numerous internal structures to represent large containment equipment such as steam generators and the connecting pipes between them, complex flame progress patterns can develop. This, together with the strong flame acceleration in the ring-like thick pipes (with internal orifices for additional flame acceleration), creates challenging situations to be simulated by combustion models. An example of possible flame branching following ignition near the bottom of one of the vertical cylinders is given in Figure 5.2.3.2-28. Very soon after ignition, the flame splits according to the available openings. Usually inside the horizontal ring-like pipes, a considerable increase of the flame speeds to several hundreds metres per second takes place coupled with local overpressures in the remainder of the test facility. As these last only short time and the test facility is completely closed the resulting long-term pressure build-up is dominated by the combustion in the main sphere. This is illustrated for different gas compositions in Figure 5.2.3.2-29.

The RUT Facility (Kurchatov Institute, Russia) was designed to investigate FA phenomena and the transition to detonations of various hydrogen-air-steam mixtures in a very large volume ($480\ \mathrm{m}^3$). It consists of a flame-acceleration section with periodic obstacles, followed by a "canyon". This facility is, therefore, very adequate for the scaling of experiments, performed in small-scale explosion tubes. The geometry of this test facility, together with the position of the instrumentation, is shown in Figure 5.2.3.2-30. For a description of representative experiments refer to Chapter 3 of this report.

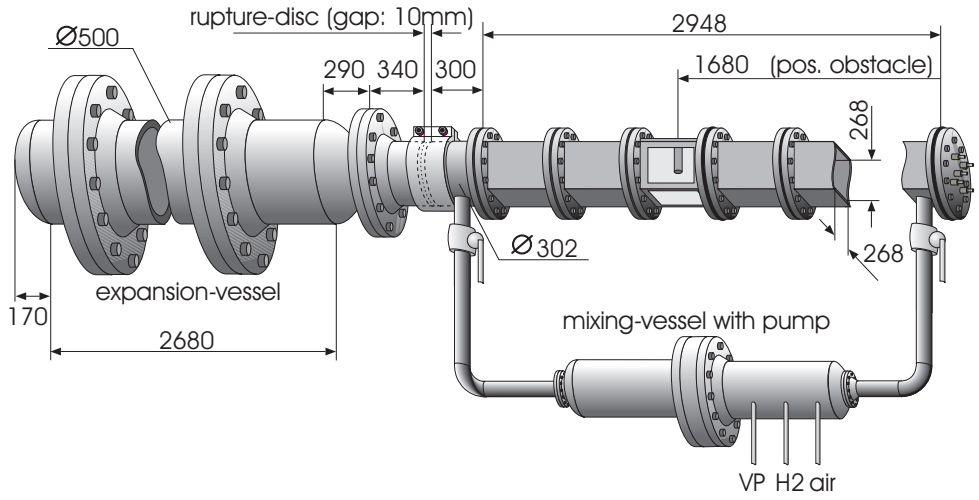

Figure 5.2.3.2-1 Geometry of the MuSCET Facility

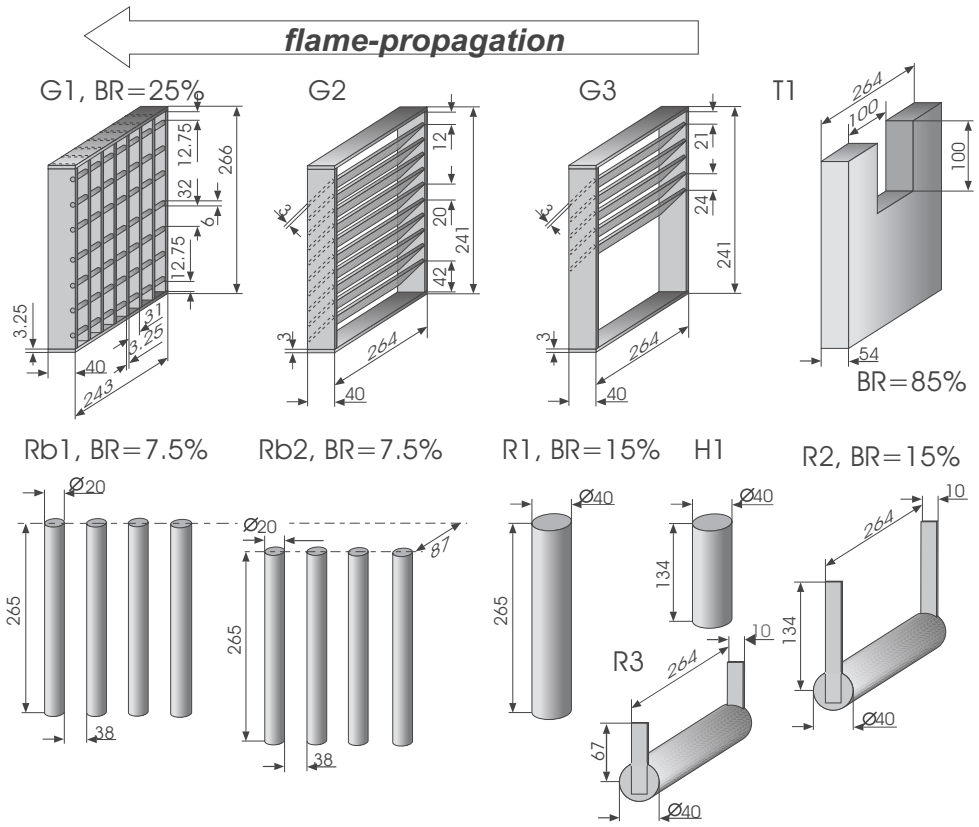

Figure 5.2.3.2-2 Containment typical obstacles investigated in the MuSCET Facility

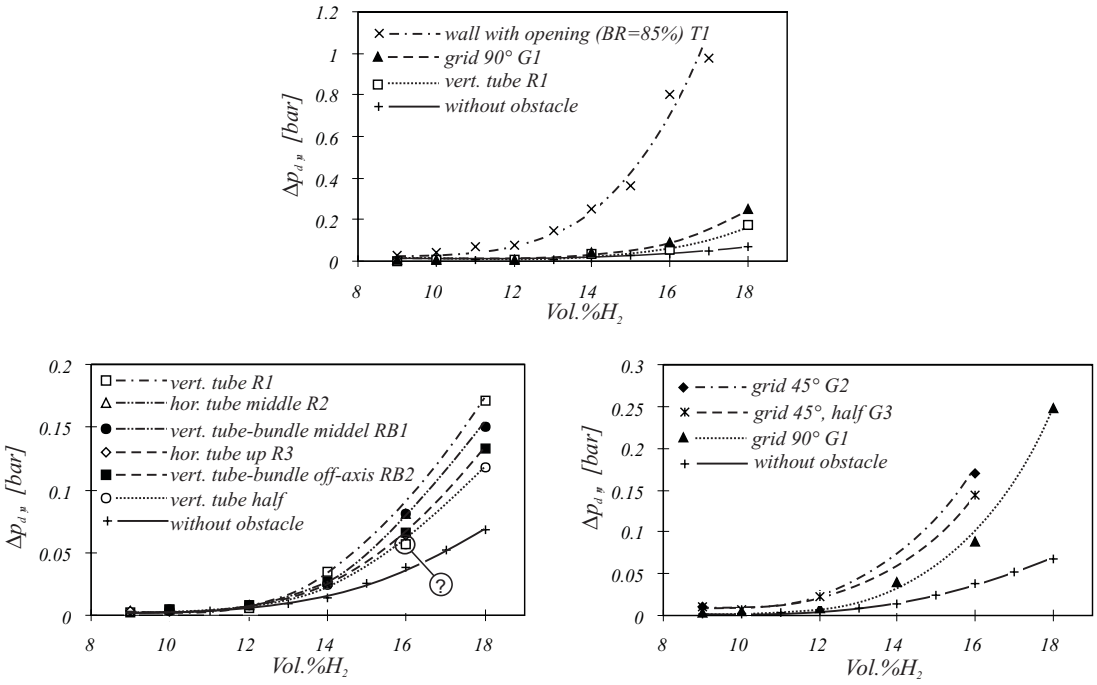

Figure 5.2.3.2-3 Maximum pressure rise for several obstacles of the MuSCET Facility

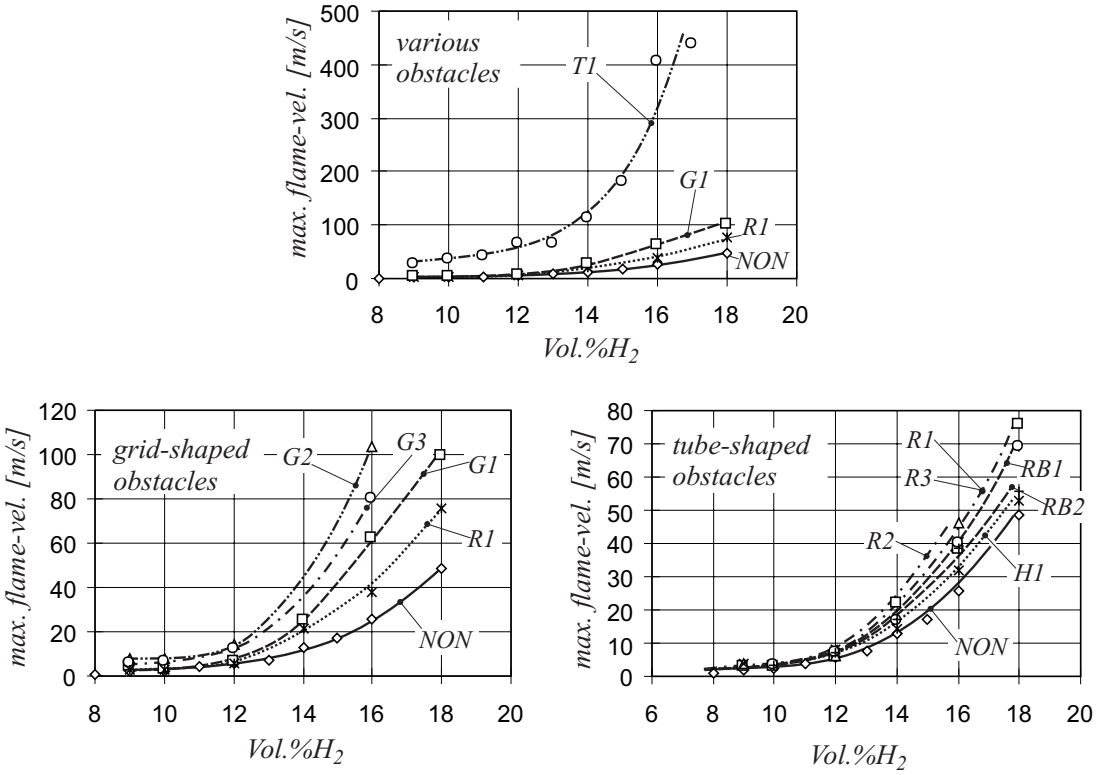

Figure 5.2.3.2-4 Maximum flame velocity behind various obstacles of the MuSCET Facility

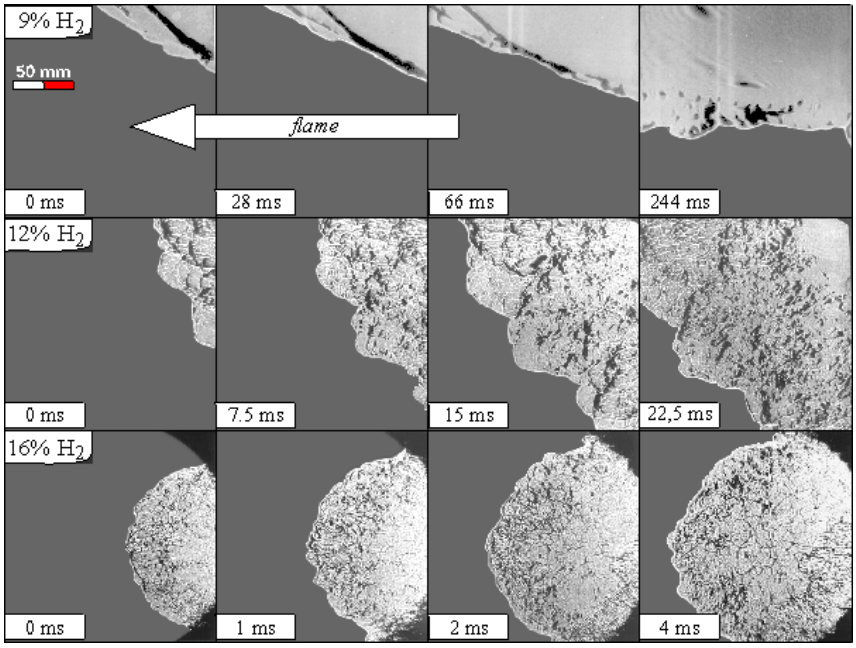

Figure 5.2.3.2-5 Schlieren images of propagating hydrogen-air flames without obstacles, MuSCET Facility

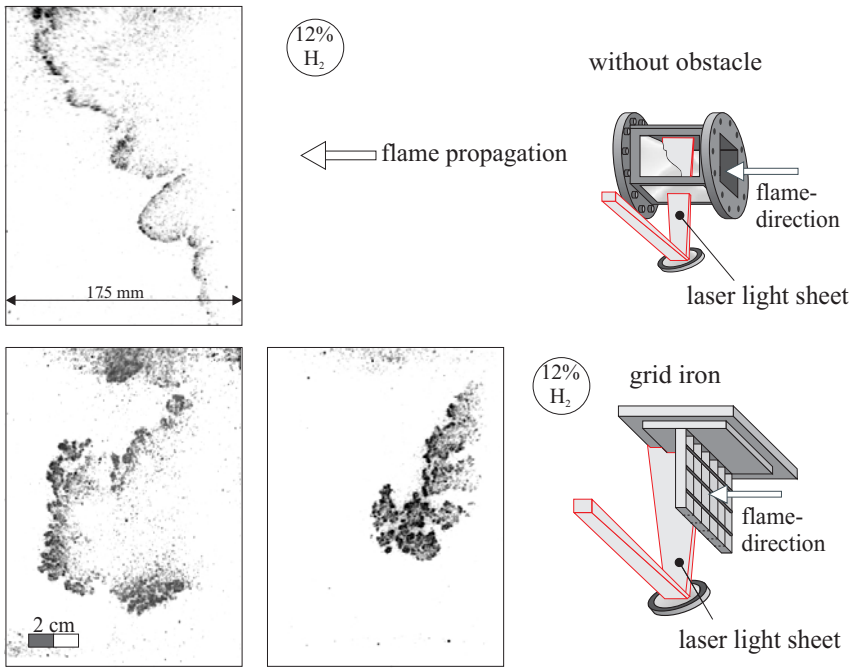

Figure 5.2.3.2-6 LIPF images of propagating hydrogen-air flames with and without being influenced by an obstacle, MuSCET Facility

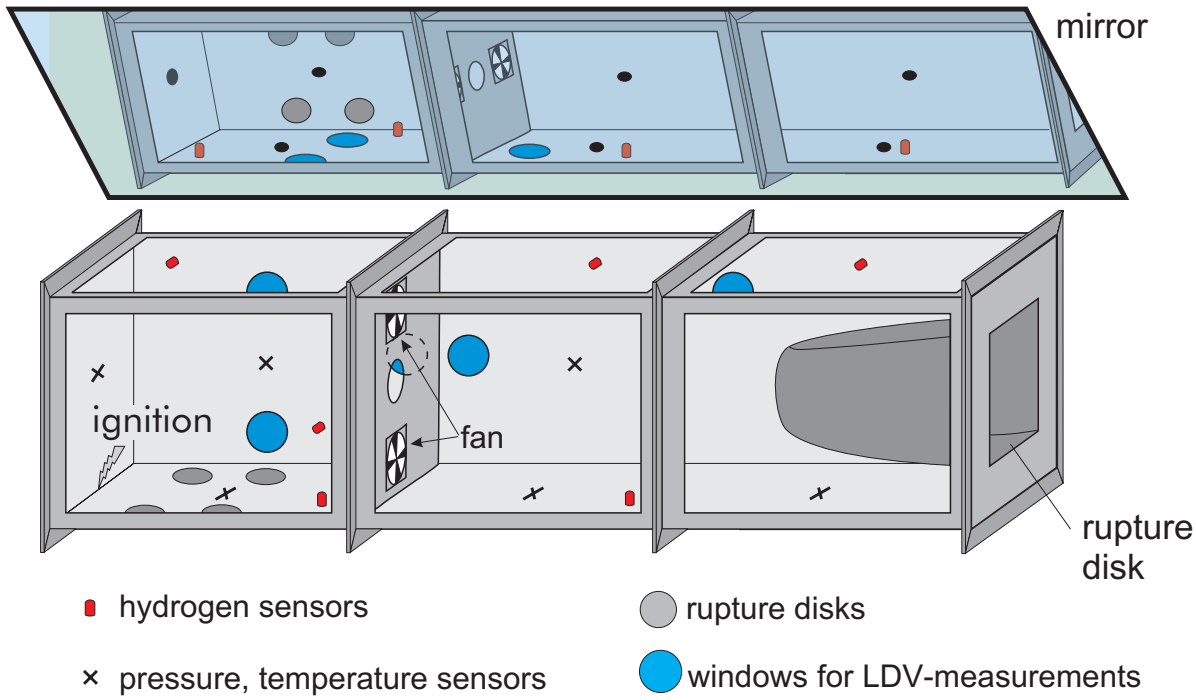

Figure 5.2.3.2-7 L.View Test Facility, University of Pisa

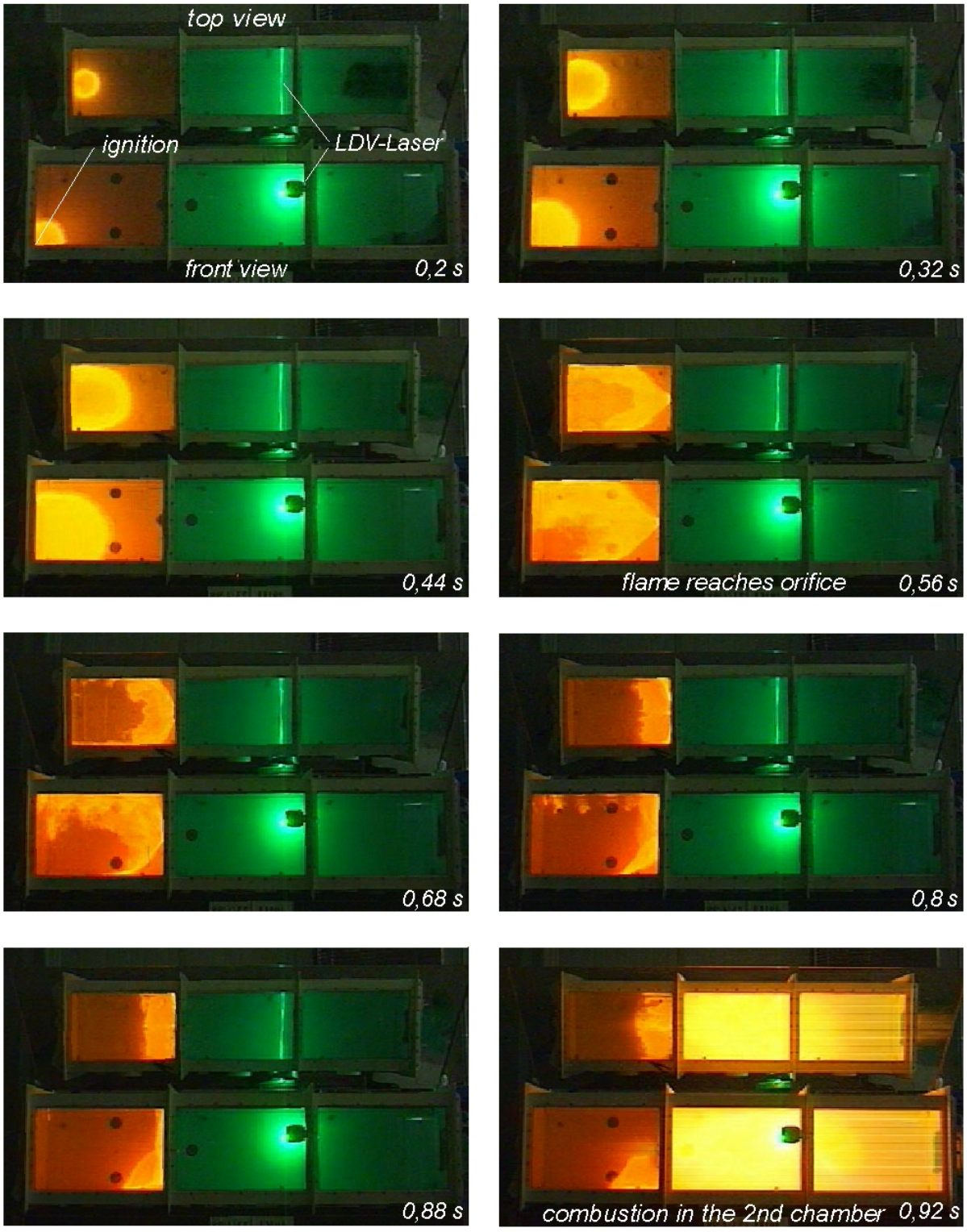

Figure 5.2.3.2-8 Example of a hydrogen combustion process in the L.VIEW Facility with a hydrogen concentration of 10.5 vol % and an orifice diameter of 70 mm

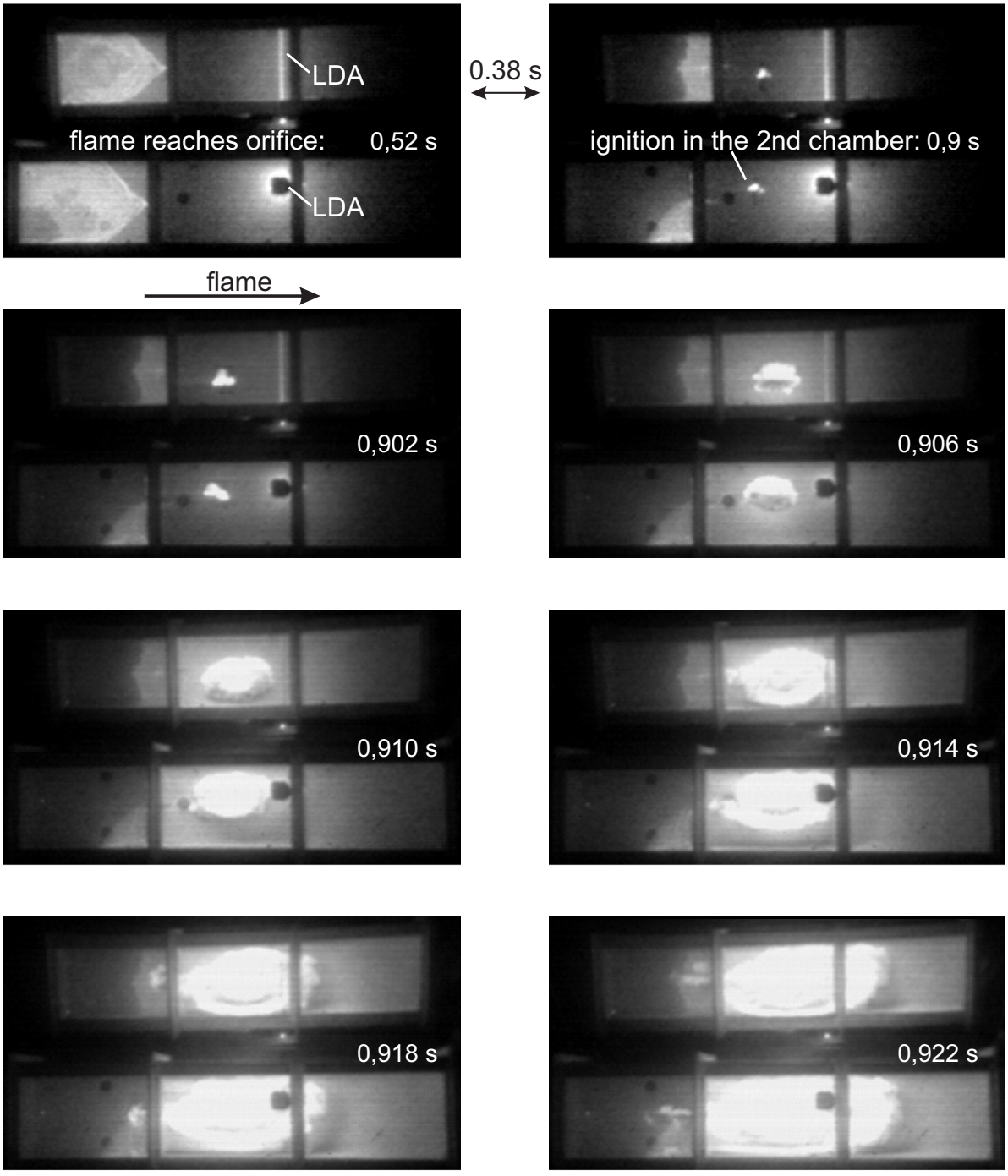

Figure 5.2.3.2-9 Ignition process of the test shown in Figure 5.2.3.2-8 with high temporal resolution

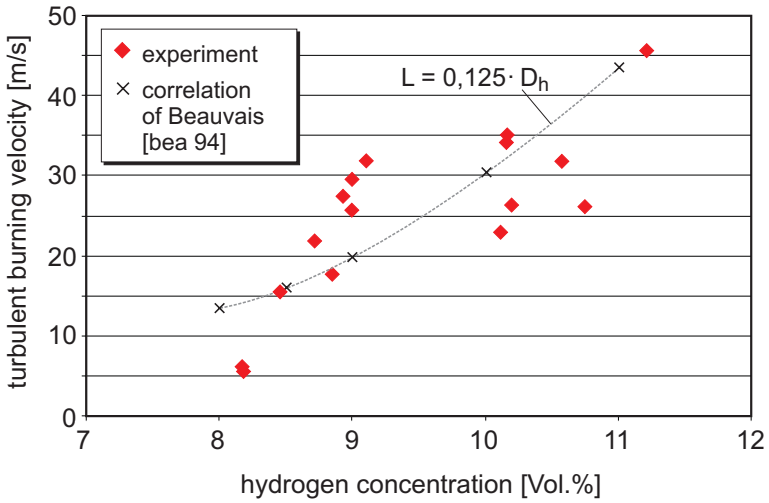

Figure 5.2.3.2-10 Calculated and measured turbulent burning velocity in the L.View Facility for direct ignition

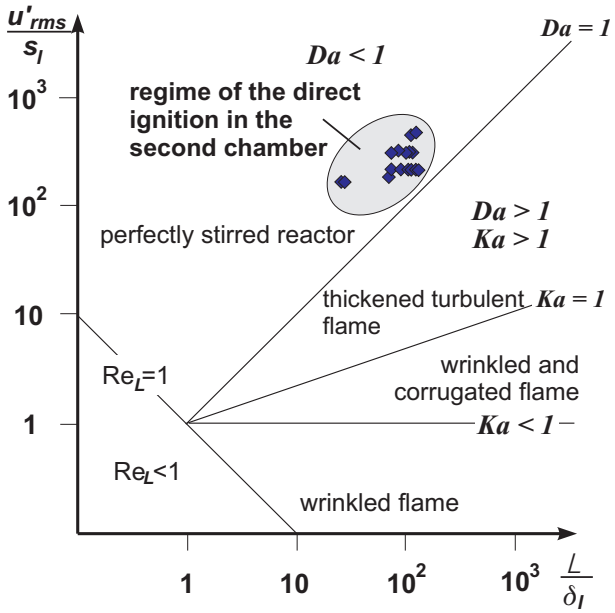

Figure 5.2.3.2-11 Regime of direct ignition in the second chamber

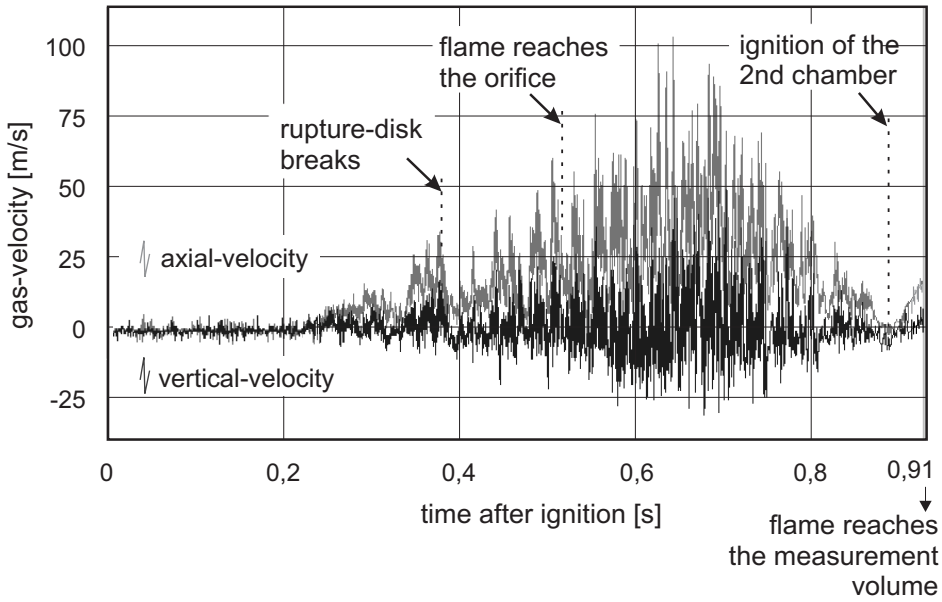

Figure 5.2.3.2-12 Flow velocity measured in the middle of the second chamber in the L.View Facility

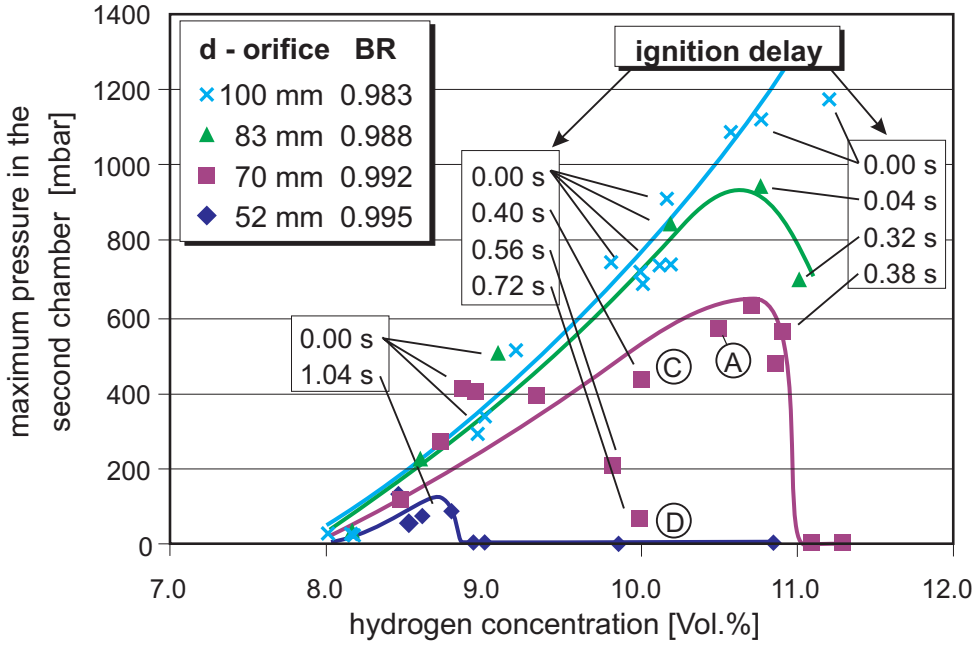

Figure 5.2.3.2-13 Maximum pressure in the second chamber in a dependence on ignition delay

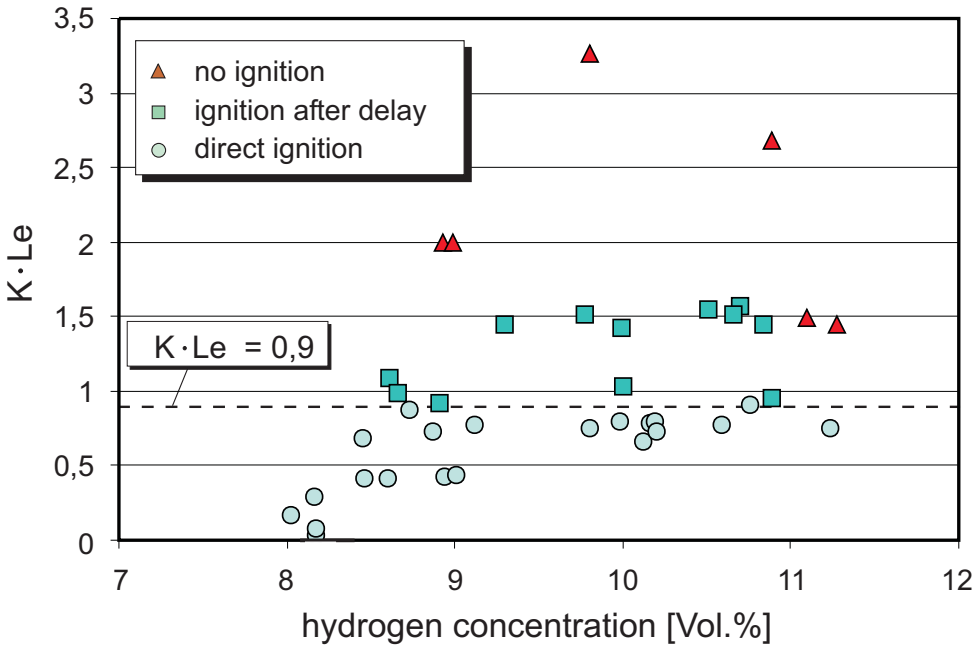

Figure 5.2.3.2-14 Quenching criterion for jet ignition

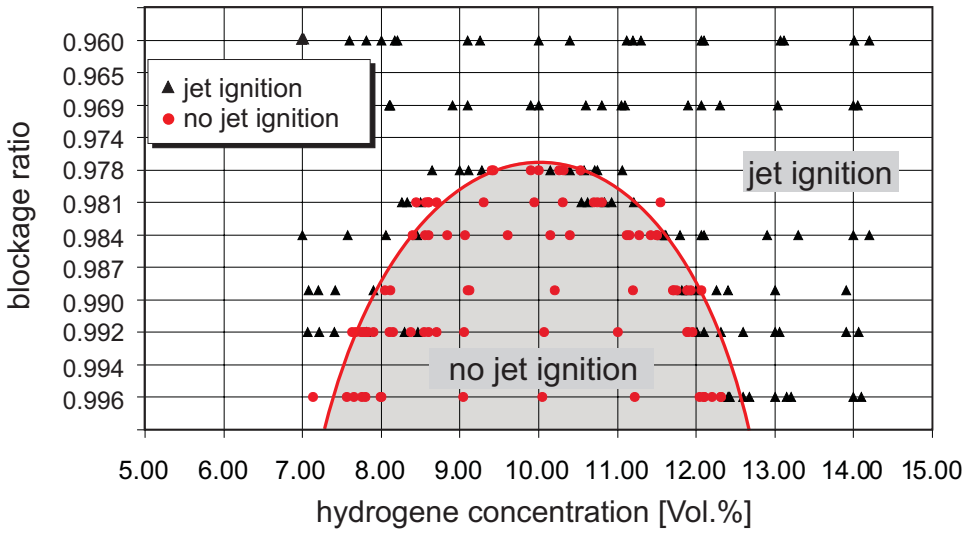

Figure 5.2.3.2-15 Flame-quenching as a function of blockage ratio, PuFlaG Facility

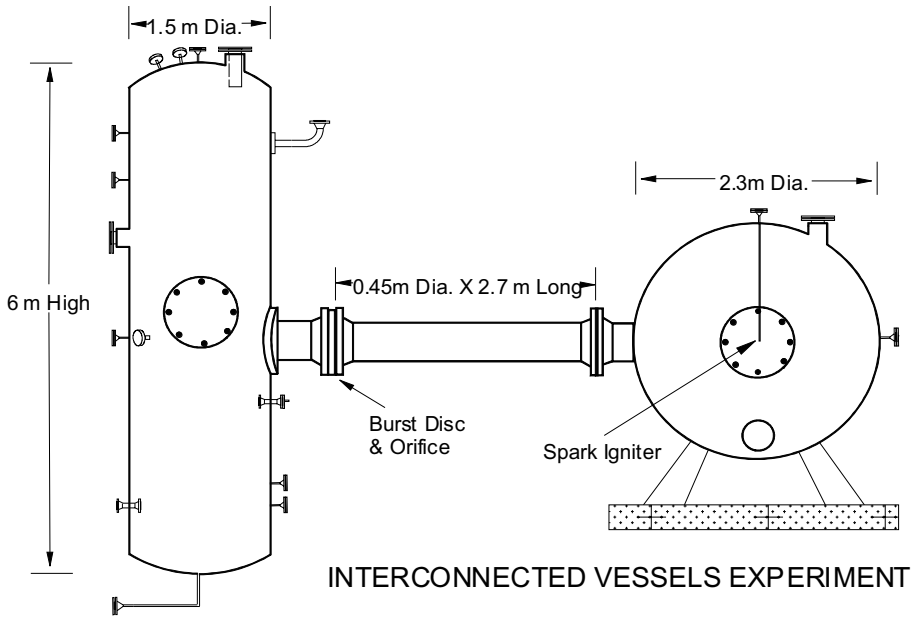

Figure 5.2.3.2-16 Schematic of the Large-scale Interconnected Vessels Facility showing burst disc holder and spark igniter locations, AECL's Whiteshell Laboratories

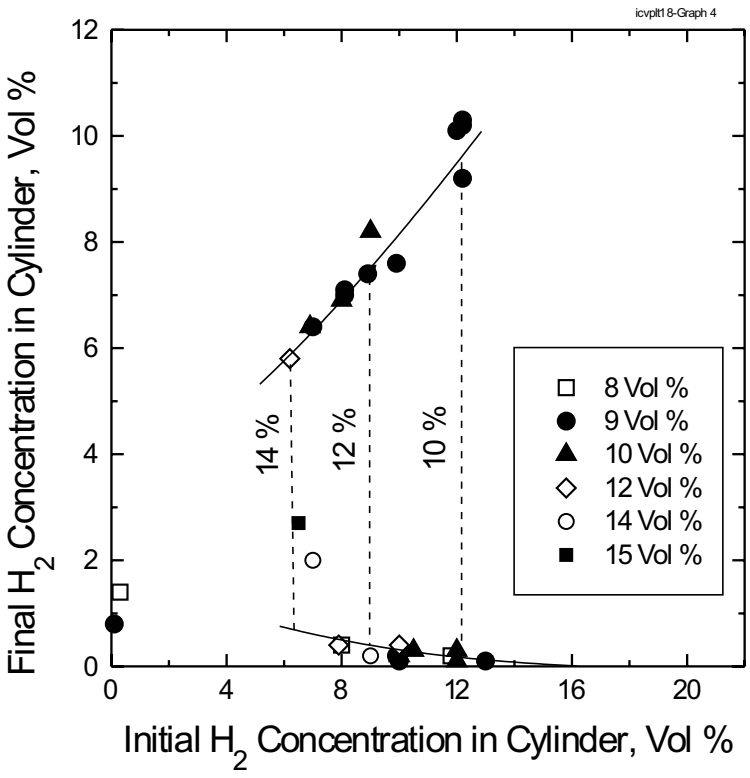

Figure 5.2.3.2-17 Final hydrogen concentration in cylinder versus initial hydrogen concentration in the cylinder for 8, 10, 12, and 14 vol % initial hydrogen concentration in the sphere with 15-cm orifice in the connecting pipe.

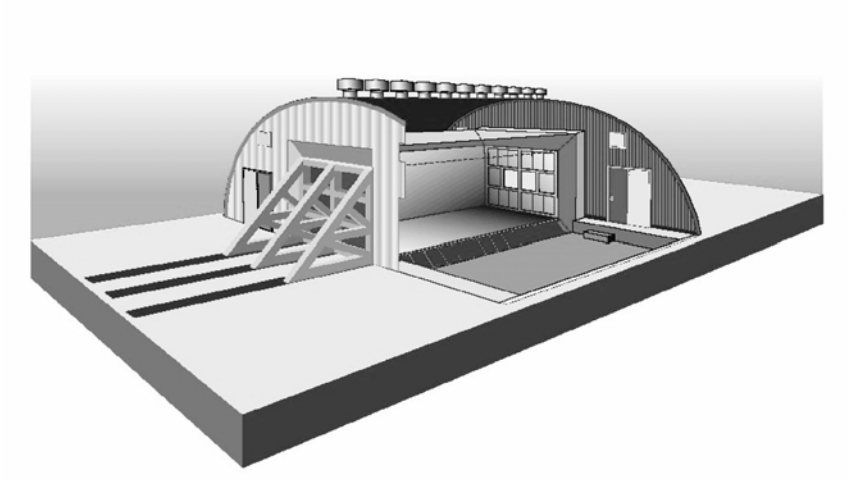

Figure 5.2.3.2-18 Cutaway schematic of the large-scale Vented Combustion Test Facility at theWhiteshell Laboratories, AECL

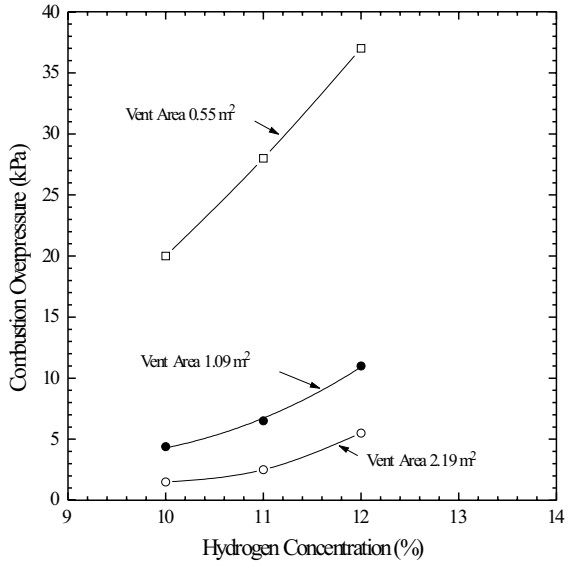

Figure 5.2.3.2-19 Variation of peak pressure as a function of hydrogen concentration for varying vent areas. Results of $120\ \mathrm{m}^3$ test chamber geometry at 25^oC

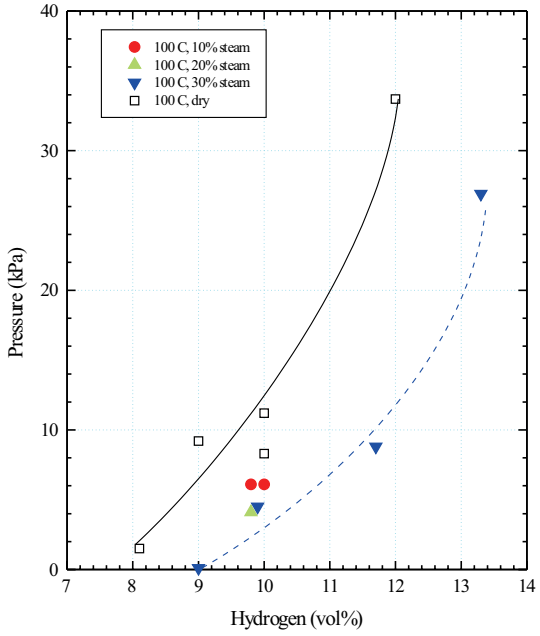

Figure 5.2.3.2-20 Variation of peak pressure as a function of hydrogen concentration for varying steam concentrations. Results of $120\ \mathrm{m}^3$ test chamber geometry, at 25^oC, with $0.55\ \mathrm{m}^2$ vent.

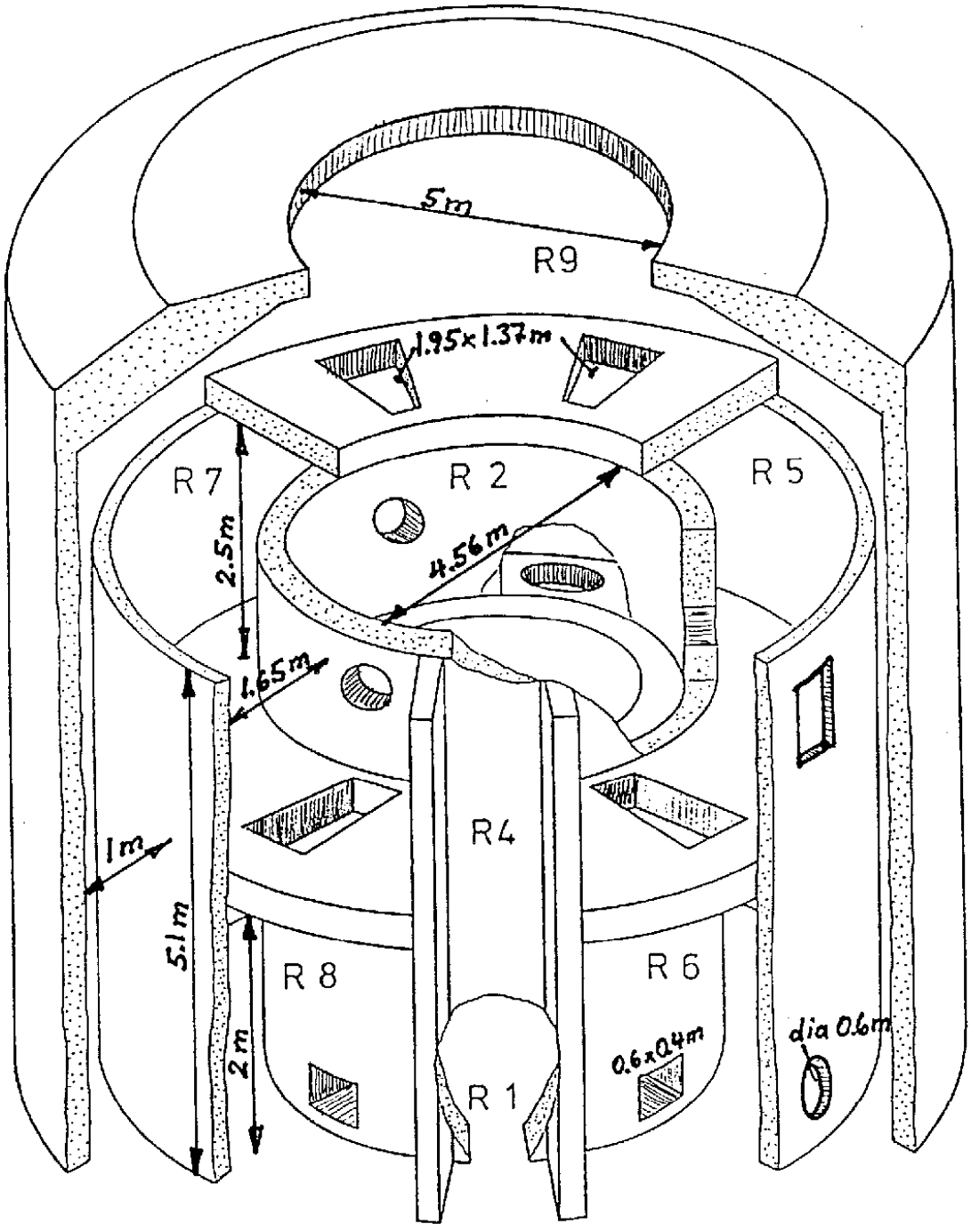

Figure 5.2.3.2-21 View of the Battelle Model Containment

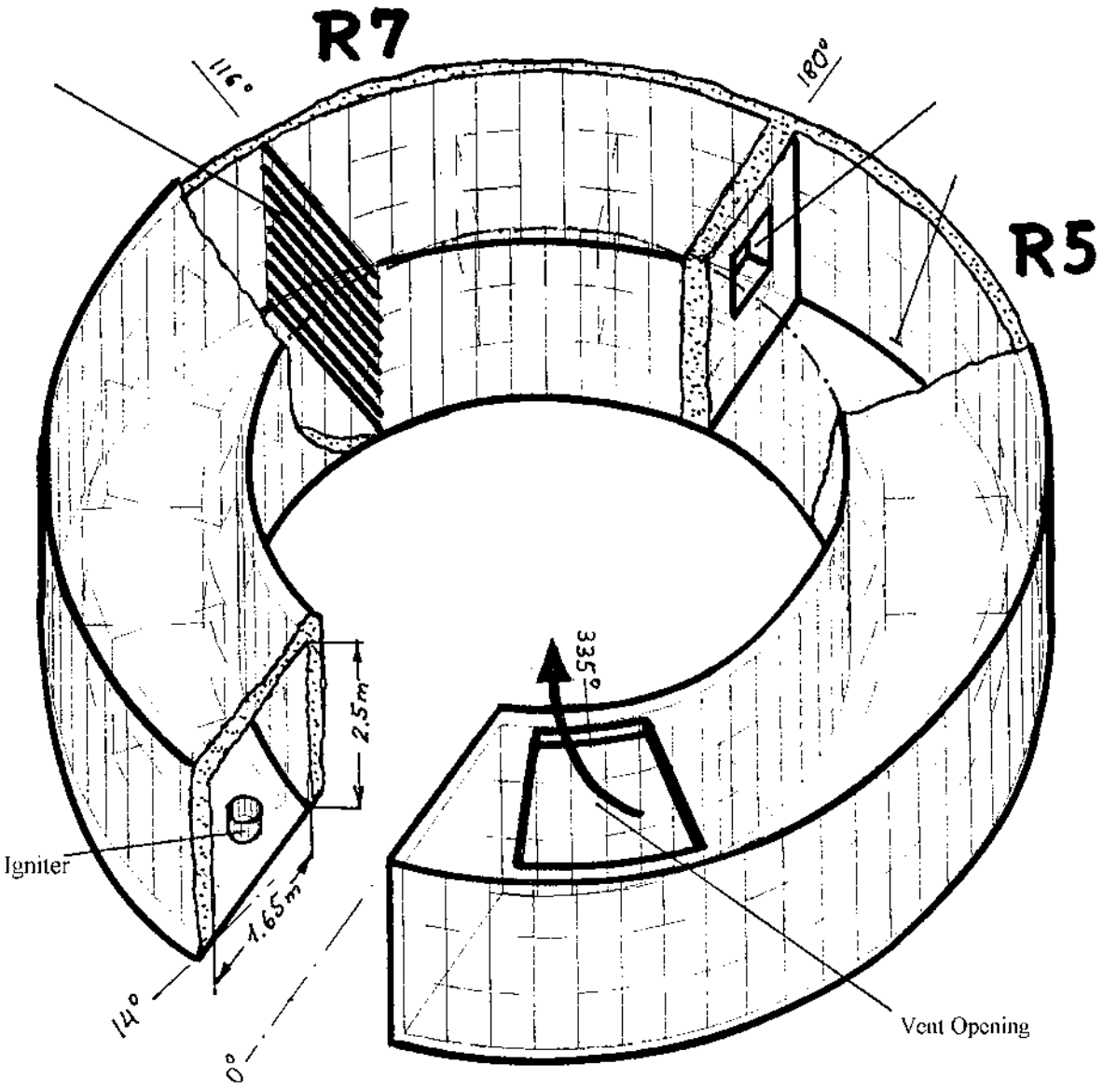

Figure 5.2.3.2-22 Two-compartment arrangement for the investigation of generic obstacles

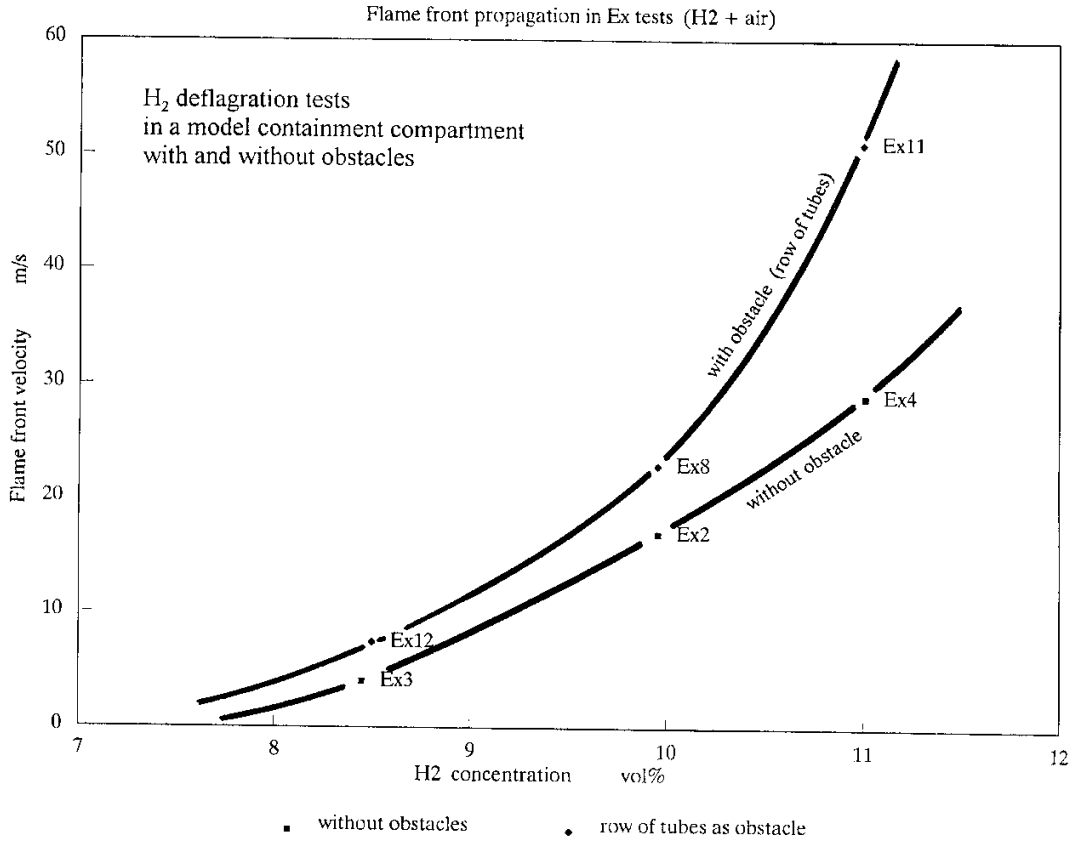

Figure 5.2.3.2-23 Impact of obstacles on the flame-front velocity in the Battelle Model Containment

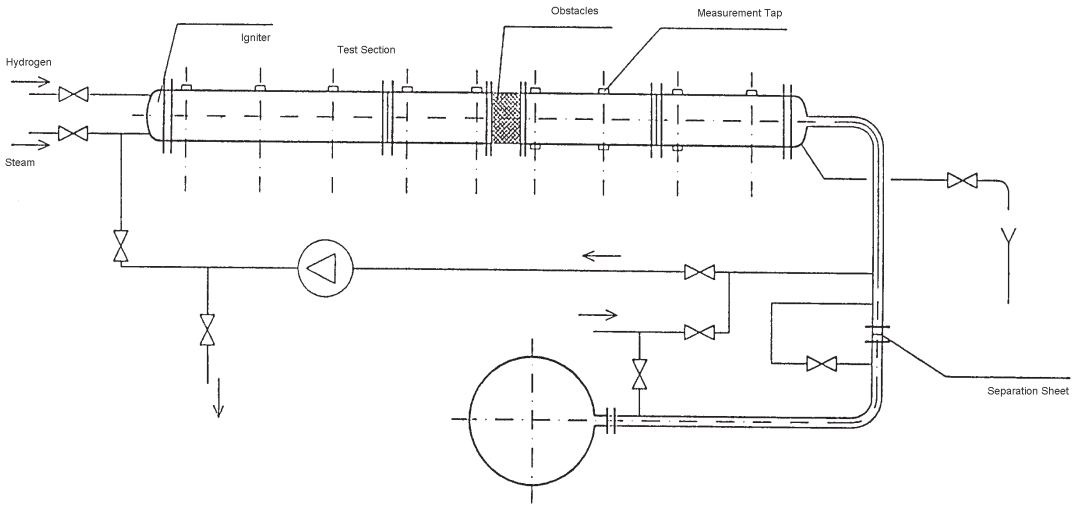

Figure 5.2.3.2-24 Test facility DN-400 for scaling from the Battelle Model Containment

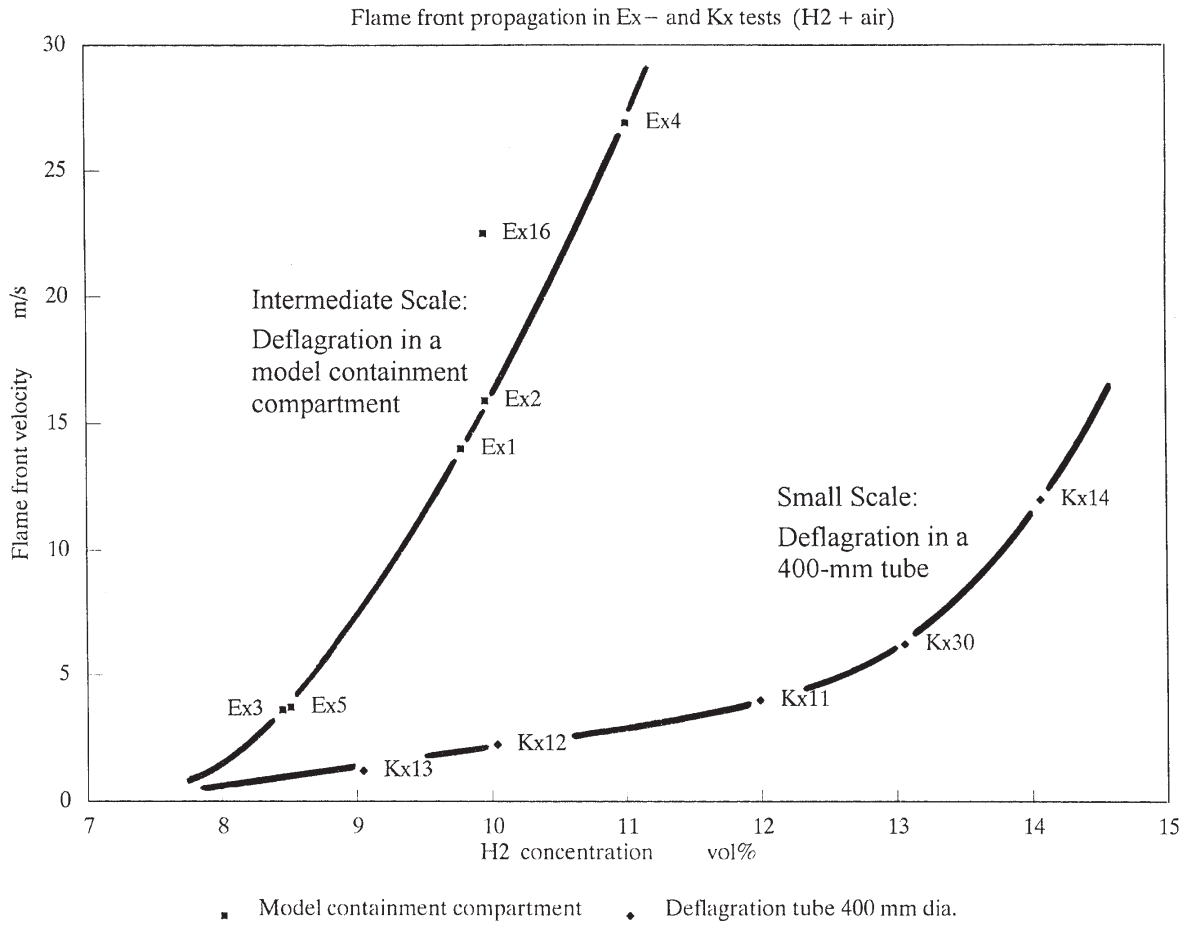

Figure 5.2.3.2-25 Impact of linear scale of the test facility on the flame propagation

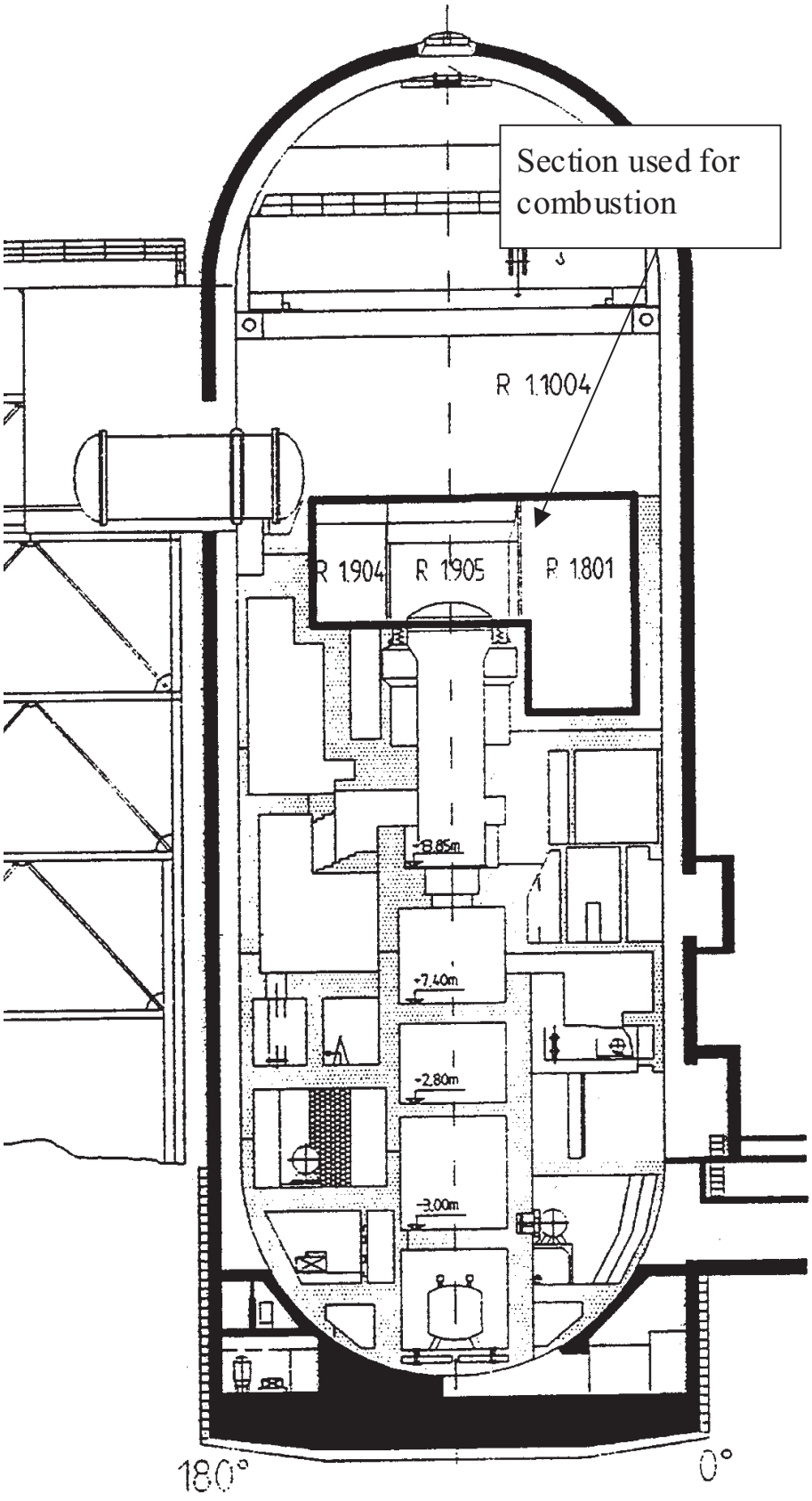

Figure 5.2.3.2-26 Hydrogen combustion experiments in the HDR

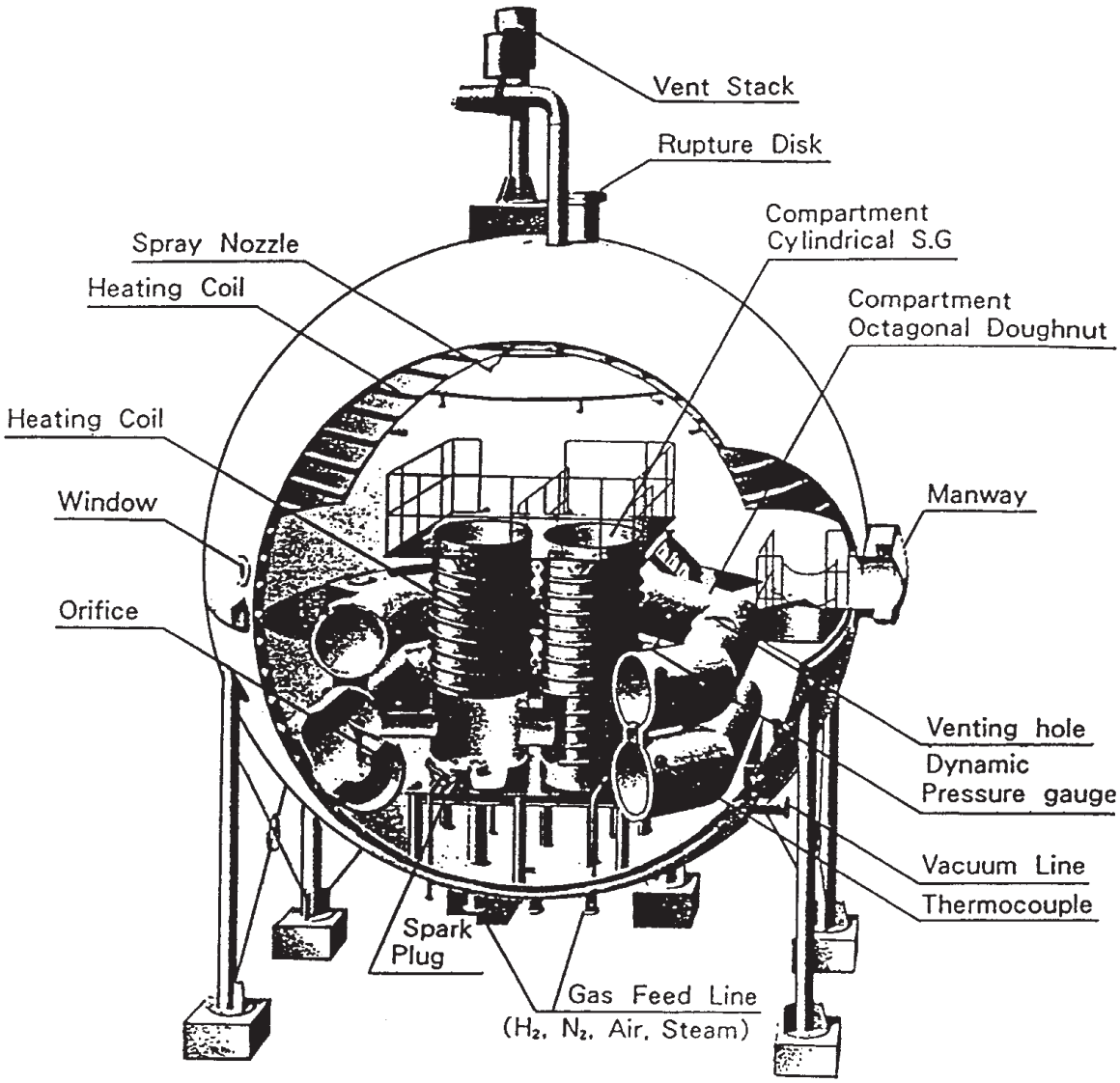

Figure 5.2.3.2-27 NUPEC's Large-Scale Combustion Test Facility

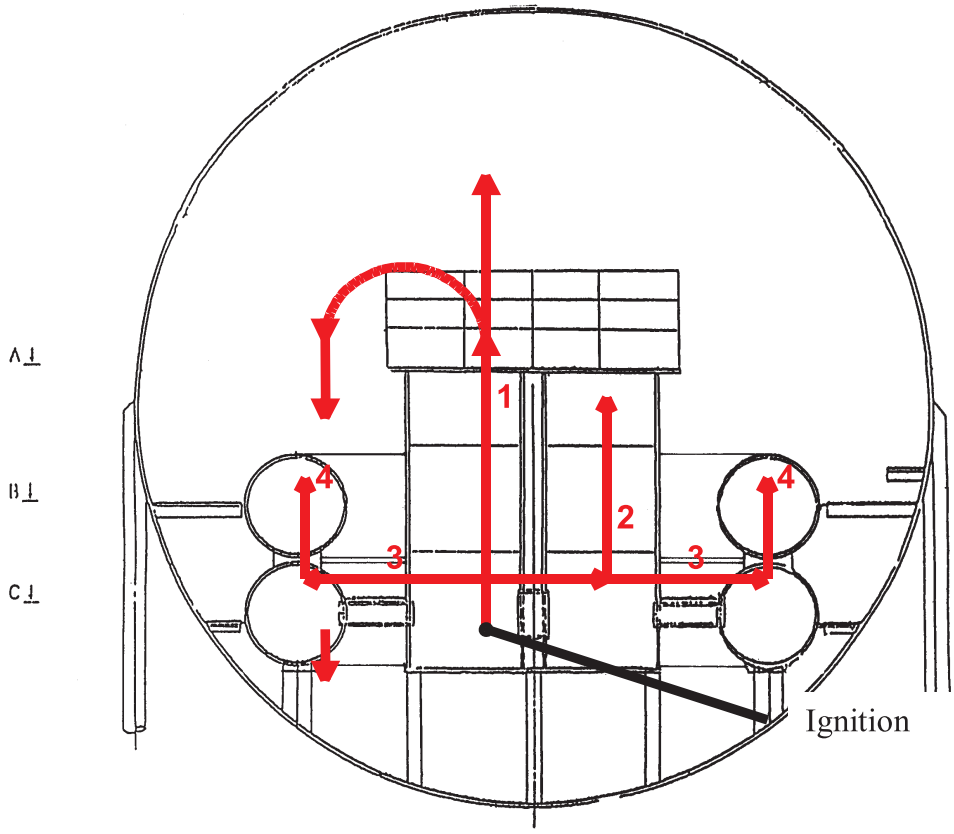

Figure 5.2.3.2-28 Principle flame branching for the steam generator, bottom ignition

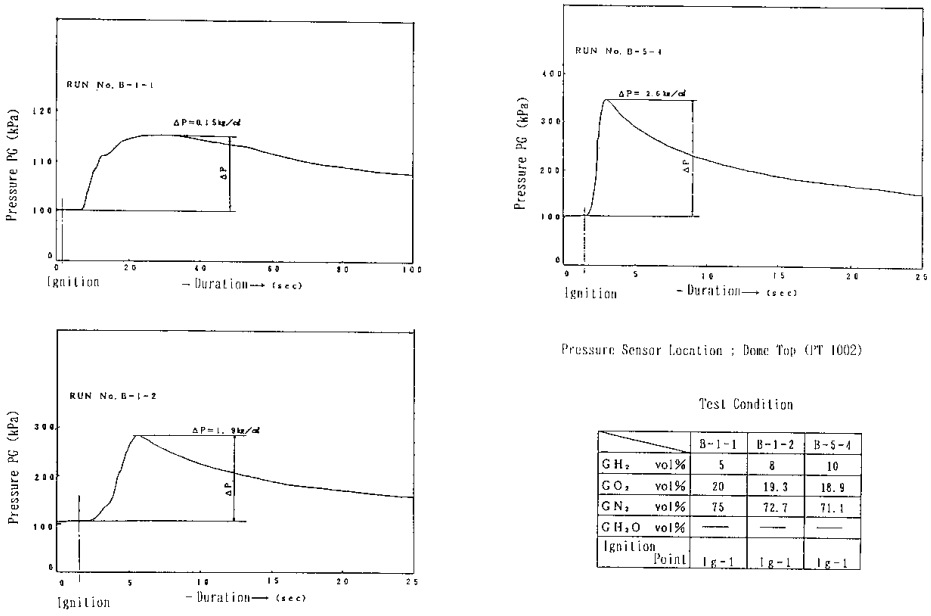

Figure 5.2.3.2-29 Pressure histories for different gas compositions

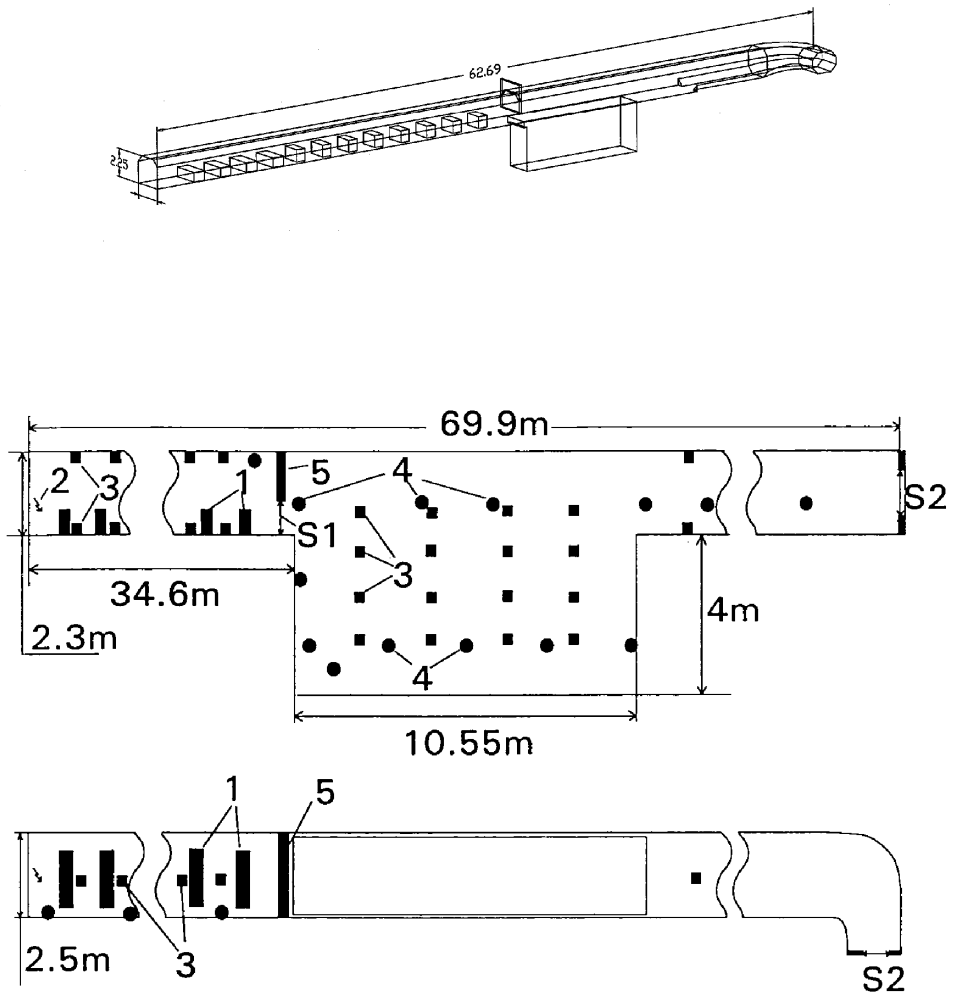

Figure 5.2.3.2-30 RUT Facility, Kurchatov Institute

5.3 Model Hierarchies Used in Practical Applications

5.3.1 Combustion in Containment System Codes (Lumped Parameter)[*]

5.3.1.1 Introduction

System codes are codes that are designed to describe the complexity of processes in a nuclear containment under accident conditions. The main physical phenomena of the multi-component multi-phase mixtures to model are

- releases of gases and water (steam), mixing of species;
- heat transfer, mainly heat losses to solid structures by convection and condensation;
- particle transport of water droplets, aerosols, and melt fragments; and
- chemical reactions, including fires and gas combustion.

These processes proceed in a more or less complex way (depending on the containment type and design and large geometry) over long time periods (typically in the order of days). Process times can be very different and can range from seconds for combustion to always-present for heat losses to structures.

In order to cover most or all of the processes mentioned, related code systems use a simplified mathematical approach. They subdivide a given geometry into zones, which can be linked to other zones by flow connections. Each zone may have sources or sinks of mass and energy. These codes can solve the following parameters:

- energy conservation of the system composed of zones. The kinetic energy transported by gas flows is very low and, therefore, not estimated.
- mass conservation in all zones. Mass changes caused by flows between zones are included.
- momentum balance between zones under the assumption that the momentum of a flow dissipates totally when entering a zone. This assumption is made because physical compartments of the containment and, hence, the model zones are usually large in volume ($100 \text{ to } 1000 \text{ m}^3$). With low speeds (1 to 10 m/s), it is unlikely that a flow continues through a zone. Therefore, momentum conservation in zones is not considered.

Apart from the standard lumped-parameter concept, the MELCOR code [5.85] (see Table 5.4.0-1) offers the possibility to solve for a momentum conservation. This feature is not included in the combustion model and will be discussed briefly.

A more complex combustion model – a flame-front combustion model – is implemented in the COCOSYS code [5.86] (see Table 5.4.0-1). The discussion of this model will also be used to illustrate the lumped-parameter concept in general.

[*] Contributed by Dr. M. Heitsch

Common to all lumped-parameter codes is that all nodes and flow connections have to be described individually. Therefore, models that have more than 200 to 250 nodes and more than 400 flow connections appear to be the upper limit of what a user can handle. The omission of the momentum conservation leads to a system of ordinary differential equations that can be solved implicitly and allows relatively large time steps.

5.3.1.2 The MELCOR Combustion Model

MELCOR is a fully integrated, engineering-level control volume computer code whose primary purpose is to model the progression of accidents in LWR NPPs. The relevant section of the user manual describes best the features of the combustion model [5.85]:

"The Burn (BUR) package models the combustion of gases in control volumes. These models consider the effects of burning on a global basis without modeling the actual reaction kinetics or tracking the actual flame front propagation. The models in the BUR package are based on the deflagration models in the HECTR 1.5 code. The only significant modifications made were to provide more direct user control of the models through the implementation of sensitivity coefficients and to include optional model parameters that are used to override the nominal parameters in control volumes in which direct containment heating (DCH) is occurring.

Deflagrations are ignited if the mole fraction composition in a control volume satisfies a form of LeChatelier's formula. Tests for sufficient H_2 and O_2 are performed, as well as an inerting test for the presence of excessive diluents (H_2O and CO_2). Deflagrations are propagated into adjoining control volumes after a user-specified fraction of the total burning time in the control volume has passed. Additional tests for the H_2 and CO mole fractions in those volumes need to be satisfied and a non-zero area for a gas flow path has to exist. There is, however, no test for checking valves.

The combustion rate is determined by the flame speed, the volume characteristic dimension, and the combustion completeness. The flame speed and combustion completeness can each be input as constant values, or they may be calculated from either user-specified control functions or the default HECTR correlations. The latter are derived from experimental data and depend on combustible and diluent gas concentrations.

For user convenience, the BUR package also prints messages to warn the user when the detonability criteria are satisfied in a control volume. However, only deflagrations are modeled; detonations are merely flagged and no other action is taken unless deflagration criteria are satisfied."

In summary, this combustion model adds sources of mass and energy to the respective control volumes but does not solve differential equations. For each control volume, a burning time is evaluated from the characteristic dimension (user input) and a flame speed (either user specified or calculated). These flame speeds may be uncertain.

The ignition limits checked include carbon monoxide and are adopted to mixtures in a containment under accident conditions.

5.3.1.3 The COCOSYS Combustion Model

By the very nature of MELCOR being a control volume code, it cannot simulate some aspects of combustion such as the following:

- The cold gas compression ahead of the reacting zone and hot gas expansion behind it are not modelled. Instead, a homogeneous mixture is used.
- Branching of a flame is not possible with this type of control volume code. Flame branching would only be possible with multiple nodes, properly defined. The potential difference introduced by this simplification is, in part, a function of analyst's nodalization of the problem.

In order to get a more predictable combustion model, a flame-front model according to Figure 5.3.1.3-1 has been implemented in COCOSYS. The model, named DECOR [5.87], [5.88], is characterized as follows:

- For those zones, which are subject to combustion, an unburned and a burned part are defined and are separated by a flame front.
- It is one-dimensional model with averaged conditions normal to the flame front.
- Combustion is possible in three predefined directions.
- Full pressure relief is assumed between the unburned and the burned parts on both sides of the flame front.

In principal, on both sides of the flame front, mass and energy balances are set up and the momentum exchange with other nodes, according to pressure and height differences, is calculated. Then both parts are linked together by the chemical reaction over the flame discontinuity. The chemical reaction inside the flame results in a displacement of the front, driven by a burning velocity derived from experiments.

The general lumped-parameter differential equations are first applied to both node parts linked by the flame, and then additional equations for the coupling between both are added. In an open thermodynamic system with a variable volume size, the following energy equation holds:

$$dQ = dU + dW \tag{5.3.1}$$

or with the definition of enthalpy ($I = U + pV$)

$$dQ = dI - pdV - vdp + pdV \text{ with } dW = pdV\ . \tag{5.3.2}$$

Time dependent, it writes

$$\frac{dQ}{dt} = \frac{dI}{dt} - V\frac{dp}{dt} = \frac{d(M_i)}{dt} - V\frac{dp}{dt}\ . \tag{5.3.3}$$

The code distinguishes between steam-saturated and steam-superheated conditions. The model derivation is similar; therefore, only the more common superheated situation is considered and presented. In a single node, we have ($k = 1..l$) species. Unlike the saturated conditions, no liquid water is available but

steam is included. To this node there are (j=1..q) entering flows and (j=1..p) leaving flows. The energy balance around the zone (or part of a zone in Figure 5.3.1.3-1) can be written as

$$\sum_{k=1}^{l}\left[\sum_{j=1}^{q} G_{kj}^{e} I_{kj}^{e} - \sum_{j=1}^{p} G_{kj}^{a} I_{kji}^{a}\right] + \frac{dQ^{e}}{dt} - \frac{dQ^{a}}{dt} = \sum_{k=1}^{l}\frac{d}{dt}(M_k I_k) - \sum_{k=1}^{l} V_k \frac{dp_k}{dt} \; . \tag{5.3.4}$$

On the left side of the equation we have the sum of the energy flows involving mass transport entering or leaving the node and of heat without mass transport entering or leaving the node. These flows lead to an increase of the inner energy expressed on the right side. The left side of Equation (5.3.4) shall be

$$H_1 = \sum_{k=1}^{l}\left[\sum_{j=1}^{q} G_{kj}^{e} I_{kj}^{e} - \sum_{j=1}^{p} G_{kj}^{a} I_{kji}^{a}\right] + \frac{dQ^{e}}{dt} - \frac{dQ^{a}}{dt} \tag{5.3.5}$$

and the right-most term can be modified to

$$\sum_{k=1}^{l} V_k \frac{dp_k}{dt} = V \sum_{k=1}^{l} \frac{dp_k(T, \mathrm{v}_k)}{dt} = V \sum_{k=1}^{l}\left[\left(\frac{\partial p_k}{\partial T}\right)_{\mathrm{v}_k} \frac{dT}{dt} + \left(\frac{\partial p_k}{\partial \mathrm{v}_k}\right) \frac{d\mathrm{v}_k}{dt}\right] \; . \tag{5.3.6}$$

The gradient of the enthalpy can be written as

$$\frac{dI_k(T, p_k)}{dt} = \left(\frac{\partial I_k}{\partial T}\right)_{p_k} \frac{dT}{dt} + \left(\frac{\partial I_k}{\partial p_k}\right)_{T} \frac{dp_k}{dt} \; , \tag{5.3.7}$$

and the specific volume

$$\frac{dv_k}{dt} = \frac{d\left(\frac{V}{m_k}\right)}{dt} = \frac{1}{M_k}\frac{dV}{dt} - \frac{V}{M_k^2}\frac{dM_k}{dt} \; . \tag{5.3.8}$$

Equations (5.3.6) to (5.3.8) merged into Equation (5.3.4) yield

$$\begin{aligned} H_1 = & \left\{\sum_{k=1}^{l} M_k \left[\left(\frac{\partial I_k}{dT}\right)_{p_k} + \left(\frac{\partial I_k}{\partial p_k}\right)_{T}\left(\frac{\partial p_k}{\partial T}\right)_{\mathrm{v}_k}\right] - V\left(\frac{\partial p_k}{dT}\right)_{\mathrm{v}_k}\right\}\frac{dT}{dt} \\ & + \sum_{k=1}^{l}\left\{I_k + \left[\frac{V}{M_k} - \left(\frac{\partial I_k}{\partial p_k}\right)_{T}\right]\left(\frac{\partial p_k}{\partial \mathrm{v}_k}\right)_{T}\frac{V}{M_k}\right\}\frac{dM_k}{dt} \\ & - \left[\sum_{k=1}^{l}\left(\frac{\partial I_k}{\partial p_k}\right)_{T}\left(\frac{\partial p_k}{\partial \mathrm{v}_k}\right)_{T} - \frac{V}{M_k}\left(\frac{\partial p_k}{\partial \mathrm{v}_k}\right)_{T}\right]\frac{dV}{dt} \; . \end{aligned} \tag{5.3.9}$$

Mass balances can be set up for $k = 1..l$ non-condensable species and steam entering ($j = 1..q$) or leaving ($j = 1..p$) the zone under consideration

$$\frac{dM_k}{dt} = \sum_{j=1}^{q} G_{K_j}^{e} - \sum_{j=1}^{p} G_{k_j}^{a} = G_k \; . \tag{5.3.10}$$

Mass flows between nodes are derived from a momentum balance. The standard equation of an incompressible flow is

$$\dot{G}_j = \frac{A_j}{I_j}\left[\left(p_{j_s} - p_{j_t}\right) + W_j - K_j G_j \mid G_j \mid\right] \tag{5.3.11}$$

where s indicates the source zone and t the target zone in case of a positive flow. The kinetic part is neglected. The static pressure head driving the flow in the simplest case is

$$w_j = \rho_j g\left(h_{j_s} - h_{j_t}\right) \; . \tag{5.3.12}$$

The density is averaged between both zones:

$$\rho_j = \frac{1}{2}\left(\rho_{j_s} + \rho_{j_t}\right). \tag{5.3.13}$$

The flow resistance is given by

$$K_j = \left(\zeta_0 + \zeta_A\right)\frac{1}{2\rho_j A_j^2}. \tag{5.3.14}$$

The form factor ζ_0 is user input and can be different for both flow directions. ζ_A is the loss coefficient of a pipe flow either in a laminar or in a turbulent flow regime that is decided by the code. After transformation of the preceding equations, a relation of the temperature gradient in the node can be found.

$$\frac{dT}{dt} = \frac{H_1 - H_2 - H_3 - H_5\frac{dV}{dt}}{H_4} \tag{5.3.15}$$

with Equation (5.3.5):

$$H_1 = \sum_{k=1}^{l}\left[\sum_{j=1}^{q} G_{kj}^{e} I_{kj}^{e} - \sum_{j=1}^{p} G_{kj}^{a} I_{kji}^{a}\right] + \frac{dQ^e}{dt} - \frac{dQ^a}{dt},$$

$$H_2 = \sum_{k=1}^{l} G_k I_k, \tag{5.3.16}$$

$$H_3 = \sum_{k=1}^{l}\left\{\left[\frac{V}{M_k} - \left(\frac{\partial I_k}{\partial p_k}\right)_T\right]\left(\frac{\partial p_k}{\partial \mathrm{v}_k}\right)_T \frac{V}{M_k}\right\} G_k, \tag{5.3.17}$$

$$H_4 = \sum_{k=1}^{l} M_k\left[\left(\frac{\partial I_k}{dT}\right)_{p_k} + \left(\frac{\partial I_k}{\partial p_k}\right)_T\left(\frac{\partial p_k}{\partial T}\right)_{\mathrm{v}_k}\right] - V\left(\frac{\partial p_k}{dT}\right)_{\mathrm{v}_k}, \tag{5.3.18}$$

$$H_5 = \sum_{k=1}^{l}\left[\left(\frac{\partial I_k}{\partial p_k}\right)_T - \frac{V}{M_k}\right]\left(\frac{\partial p_k}{\partial \mathrm{v}_k}\right)_T \tag{5.3.19}$$

Now with Equations (5.3.10), (5.3.11) and (5.3.15) mass and energy conservation in each node is available and can be applied to the combustion problem. Equation (5.3.15) contains the volume change over time as a free parameter. For two flame-front-coupled nodes (Figure 5.3.1.3-1), there is the following relation for the change in volume:

$$\left(\frac{dV}{dt}\right)^U = \left(\frac{dV}{dt}\right)^B. \tag{5.3.20}$$

The purpose of the deflagration model is primarily to describe combustion initiated by deliberate ignition, that means by ignition sources, which ignite a given mixture as early as possible. This allows one to assume full pressure relief on both sides of the flame and leads to

$$\left(\frac{dp}{dt}\right)^U = \left(\frac{dp}{dt}\right)^B. \tag{5.3.21}$$

Under superheated steam conditions (steam-saturated conditions are dealt with as well, but are not detailed here) the total pressure gradient can be written as

$$\left(\frac{dp}{dt}\right) = \sum_{k=1}^{l}\frac{dp_k}{dt} = \sum_{k=1}^{l}\left(\frac{\partial p_k}{\partial T}\right)_{\mathrm{v}_k}\frac{dT}{dt} + \left(\frac{\partial p_k}{\partial \mathrm{v}_k}\right)_T\frac{d\mathrm{v}_k}{dt}. \tag{5.3.22}$$

The specific volume can be expressed as

$$\frac{dv_k}{dt} = \frac{1}{M_k}\left(\frac{dV}{dt} - \frac{V}{M_k}\frac{dM_k}{dt}\right) . \tag{5.3.23}$$

Equation (5.3.23) integrated into Equation (5.3.22) yields

$$\frac{dp}{dt} = A\frac{dT}{dt} + B - C\frac{dV}{dt} \tag{5.3.24}$$

with

$$A = \sum_{k=1}^{l}\left(\frac{dp_k}{dT}\right)_{\mathrm{v}_k} \tag{5.3.25}$$

$$B = -V\sum_{k=1}^{l}\frac{G_k}{M_k^2}\left(\frac{\partial p_k}{\partial \mathrm{v}_k}\right)_T \tag{5.3.26}$$

$$C = -\sum_{k=1}^{l}\frac{1}{M_k}\left(\frac{\partial p_k}{\partial \mathrm{v}_k}\right)_T . \tag{5.3.27}$$

Equation (5.3.24) can be written down for the burned (B) and unburned (U) zone parts and together with Equation (5.3.15), (5.3.20) and (5.3.21) a system of three linear equations arises:

$$\begin{aligned} H_4^B\,\frac{dT^B}{dt} + H_5^B\,\frac{dV^B}{dt} &= H_1^B - H_2^B - H_3^B \\ H_4^U\,\frac{dT^U}{dt} - H_5^U\,\frac{dV^B}{dt} &= H_1^U - H_2^U - H_3^U \\ -A^B\,\frac{dT^B}{dt} + A^U\,\frac{dT^U}{dt} + \left(C^U + C^B\right)\frac{dV^B}{dt} &= B^B - B^U . \end{aligned} \tag{5.3.28}$$

This system of linear equations can be solved for the unknowns . The constants H_1 through H_5 and A, B, C on both sides of the flame front are known by the convective mass and energy exchange with other nodes and heat sources available. Which source terms the chemical reaction adds will be discussed next. Together with the mass balance equations for k species (Equation (5.3.10)), the flows between nodes (Equation (5.3.11)) and the equations from Equation (5.3.29) in case of combustion in a node or Equation (5.3.15) if no combustion is running, a coupled system of ordinary differential equations exists to describe the time-dependent behaviour of the total compartment model. COCOSYS automatically switches between Equation (5.3.15) and Equation (5.3.29) and re-organizes the Jacobi matrix if combustion in any zones starts or ends. The coupled system of equations is implicitly solved, thus allowing relatively large time steps. A more convenient quantity can be derived from the volume growth on the burned side:

$$\frac{dV^B}{dt} = \frac{dL_F}{dt}A_N\ n. \tag{5.3.29}$$

Equation (5.3.29) defines an average flame-front position from the growth of the volume on the burned side of the flame by multiplying with the cross-section of the node normal to the flame (see also Figure 5.3.1.3-2). The amount of volume burned per time is expressed as

$$\frac{dV^{BR}}{dt} = SfA_N . \tag{5.3.30}$$

S is the actual burning velocity (laminar or turbulent) according to local conditions ahead of the flame. f is a stretching factor which takes care of the folding and stretching of the flame and is related to the normal cross-section. The factor f also absorbs phenomena of the physics not included in the model and general uncertainties; these need to be determined from experiments. The burning velocity is correlated from experiments. So far, most of the application of the combustion model has been done with a correlation from Reference [5.89]. It reads

$$\frac{S_T}{S_L} = \left[1 + B\left(\frac{\mathrm{u}'}{S_L}\right)^2\right]^{1/2} + \left[1 - exp\left(\frac{-u'}{S_L}\right)\right]\frac{(\varepsilon - 1)}{\sqrt{3}},\ \varepsilon = \frac{\rho^U}{\rho^B},\ B = 16\ . \tag{5.3.31}$$

Other options for this correlation can be found in Reference [5.87]. The chemical reactions are modelled as simplified one-step reactions. They include the reaction

$$2H_2 + O_2 \rightarrow 2H_2O + 119.8MJ\ \ and\ \ 2CO + O_2 \rightarrow 2CO_2 + 10.1MJ\ . \tag{5.3.32}$$

Source terms caused by combustion can be found in the equations of the zone parts on both sides of the flame for mass and energy. They are summarized for the hydrogen reaction in Table 5.3.1.3-1.

The specification of the source terms includes the possibility of incomplete combustion ($M^R_{H_2}$), which was observed during many experiments and is dependent on the hydrogen mole fraction ($< 10\%$) available as correlation. Further modules, necessary to run the model presented, are

- The deflagration limits in all zones of the containment model must be constantly checked to either start or stop combustion. During a running combustion that is due to the ongoing flow exchange processes, the limits may no longer be fulfilled and combustion stops.
- The combustion model allows a more realistic flame branching into other zones if the flame front crosses open flow connections. This is illustrated in Figure 5.3.1.3-3. This figure depicts a representation with two burning axes and shows that additional input to characterize the connections between zones is now necessary. A flame can only propagate, if the flame front comes close to the respective connection.
- The folding of a flame and local pressure differences usually lead to a somewhat earlier flame propagation to another zone than the flame-front position would allow. An empiric mechanism is built in to accomplish this.

Table 5.3.1.3-1 Source terms with the combustion of hydrogen

	Mass per Time	Energy per Time
	Zone Part B (Burned Side)	
Contribution to (Species k)	$\sum_{j=1}^{q} G_{k_j}^{e}$, Entering the zone part	$\sum_{j=1}^{q} G_{k_j}^{e} i_{k_j}^{e}$
Hydrogen ($C_{Mol} = 7.936$)	$\frac{dV^{BR}}{dt} / V^{U} \left\{ M_{H_2}^{U} - min\left[M_{O_2}^{U}, C_{Mol}\left(M_{H_2}^{U} - M_{H_2}^{R} \right) \right] / C_{Mol} \right\}$	$\frac{dV^{BR}}{dt} / V^{U} M_{H_2}^{U} I_{H_2}^{U}$
Oxygen	$\frac{dV^{BR}}{dt} / V^{U} \mathrm{x} \left\{ M_{O_2}^{U} - min\left[M_{O_2}^{U}, C_{Mol}\left(M_{H_2}^{U} - M_{H_2}^{R} \right) \right] \right\}$	$\frac{dV^{BR}}{dt} / V^{U} M_{O_2}^{U} I_{O_2}^{U}$
Steam	$\frac{dV^{BR}}{dt} / V^{U} \left\{ M_{D}^{U} + \frac{1 + C_{Mol}}{C_{Mol}} \times min\left[M_{O_2}^{U}, C_{Mol}\left(M_{H_2}^{U} - M_{H_2}^{R} \right) \right] \right\}$	$\frac{dV^{BR}}{dt} / V^{U} M_{D}^{U} I_{D}^{U}$
Other species	$\frac{dV^{BR}}{dt} / V^{U} M_{k}^{U}$	$\frac{dV^{BR}}{dt} / V^{U} M_{k}^{U} I_{k}^{U}$
		$\frac{dV^{BR}}{dt} \left(\frac{Q_{com}}{V^{U}} \right) \left(M_{H_2}^{U} - M_{H_2}^{R} \right)$
	Zone Part U (Unburned Side)	
Contribution to (Species k)	$\sum_{j=1}^{p} G_{k_j}^{a}$, leaving the zone part	$\sum_{j=1}^{p} G_{k_j}^{a} I_{k_j}^{a}$
Hydrogen	$\frac{dV^{BR}}{dt} / V^{U} M_{H_2}^{U}$	$\frac{dV^{BR}}{dt} / V^{U} M_{H_2}^{U} I_{H_2}^{U}$
Oxygen	$\frac{dV^{BR}}{dt} / V^{U} M_{O_2}^{U}$	$\frac{dV^{BR}}{dt} / V^{U} M_{O_2}^{U} I_{O_2}^{U}$
Steam	$\frac{dV^{BR}}{dt} / V^{U} M_{D}^{U}$	$\frac{dV^{BR}}{dt} / V^{U} M_{D}^{U} I_{D}^{U}$
Other species	$\frac{dV^{BR}}{dt} / V^{U} M_{k}^{U}$	$\frac{dV^{BR}}{dt} / V^{U} M_{k}^{U} I_{k}^{U}$

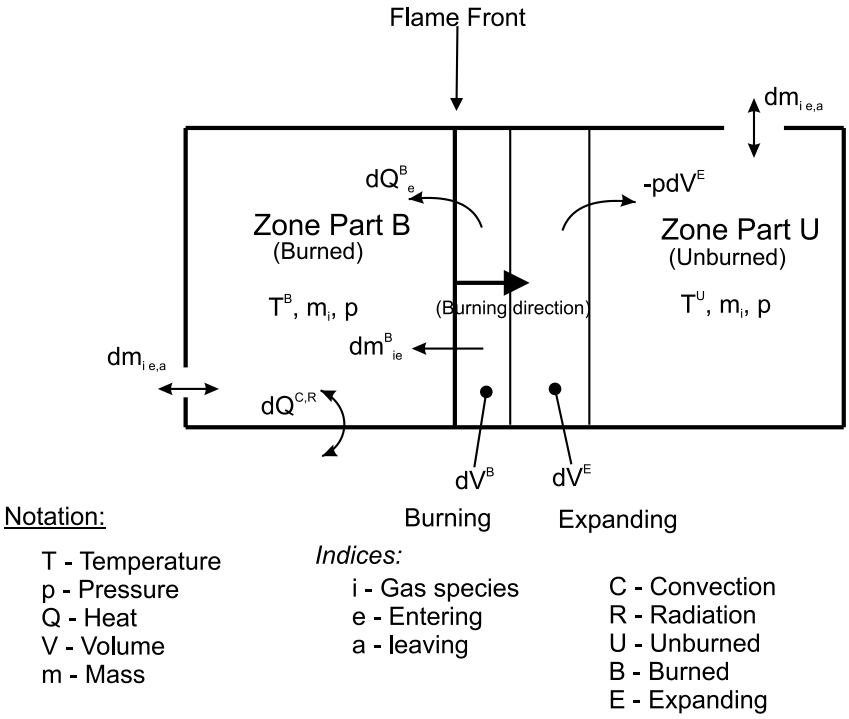

Figure 5.3.1.3-1 Outline of the flame-front model of COCOSYS (DECOR)

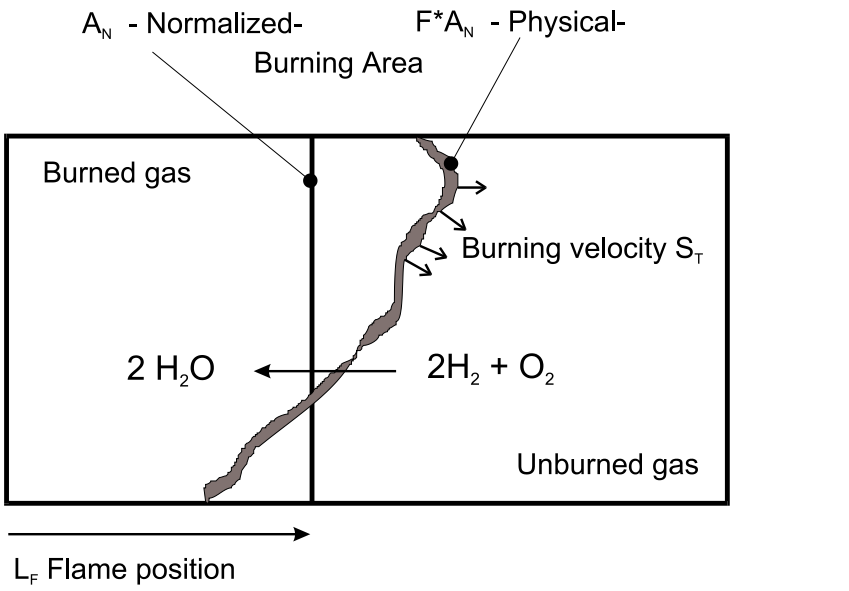

$S_T * f * A_N + dVE/dt = A_N * dL_F/dt$

Combustion + Expansion = Total displacement of the flame

Figure 5.3.1.3-2 Flame-front definition and burning velocity

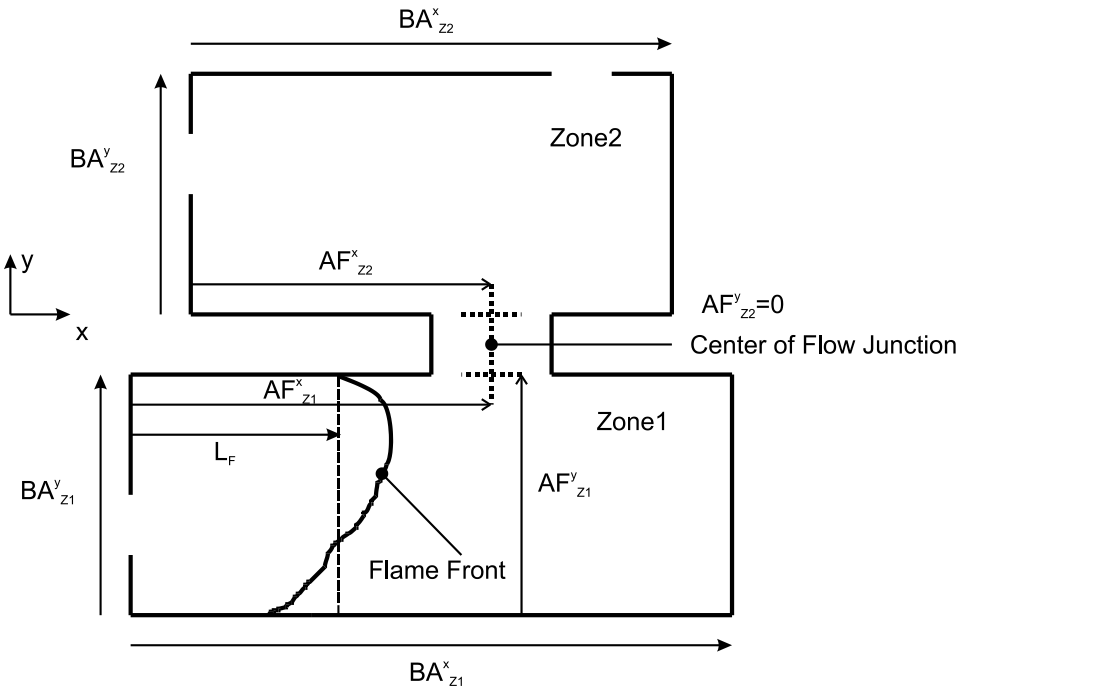

Figure 5.3.1.3-3 Flame branching and burning axes

5.3.1.4 Examples of application

Two applications to experiments illustrate the use of the described combustion model. The first is an experiment conducted at the L.VIEW Test Facility (Figure 5.2.3.2-7). It was conducted using 10.5% of hydrogen in air homogeneously premixed in both compartments. The COCOSYS nodalization can be very simple because the flame fronts moves through the zones, and their subdivision is not important (Figure 5.3.1.4-1). Combustion starts slowly in compartment R1, reaches the circular connection to R2, undergoes strong acceleration in this orifice and burns much faster in R2. Combustion in R2 is approximately 10 times faster than in R1 and ends long before combustion in R1 is completed. This also leads to a short time backflow from R2 to R1 because of the pressure distribution $(p_{R1} > p_{R2})$ and an intensification of the combustion in R1. These effects can well be modelled by the flame-front model DECOR, as can be seen from Figure 5.3.1.4-2. The considerable acceleration through the orifice between R1 and R2 can also be seen from Figure 5.3.1.4-3. The flame-front position versus time in R1 increases much slower than in R2.

The second example is a simulation of complex deflagration in the NUPEC's Large-scale Combustion Test Facility in Japan (Figure 5.2.3.2-27). This test facility permits a number of flame paths and therefore intensive flame branching, as illustrated in Figure 5.2.3.2-28. One test with 10.5% of hydrogen and 30% of steam in the initial mixture (B-2-6) has been analyzed with DECOR [5.90]. The resulting pressure versus time as a comparison between measurement and analysis is depicted in Figure 5.3.1.4-4. According to the fact that the test facility is closed and completely filled with a burnable mixture, dynamic pressure peaks in several locations are superimposed by a constant pressure increase all over the facility.

The one-dimensional combustion model needs the derivation of the flame-stretching factor Equation (5.3.30) from experiments. For this purpose, throughout the validation process of the model, several combustion modes were defined and then stretching factors were determined. The code decides at the beginning of a combustion in a zone, which mode should be applied by checking local mole fractions and the history of the preceding combustion in neighbouring zones. Figure 5.3.1.4-5 gives a summary of the combustion modes available in the code and the values used for the NUPEC tests. The flame-stretching factors depend on the progress of the flame (expressed in the figure by the dimensionless factor x/d) and accelerate the flame depending on their curvature.

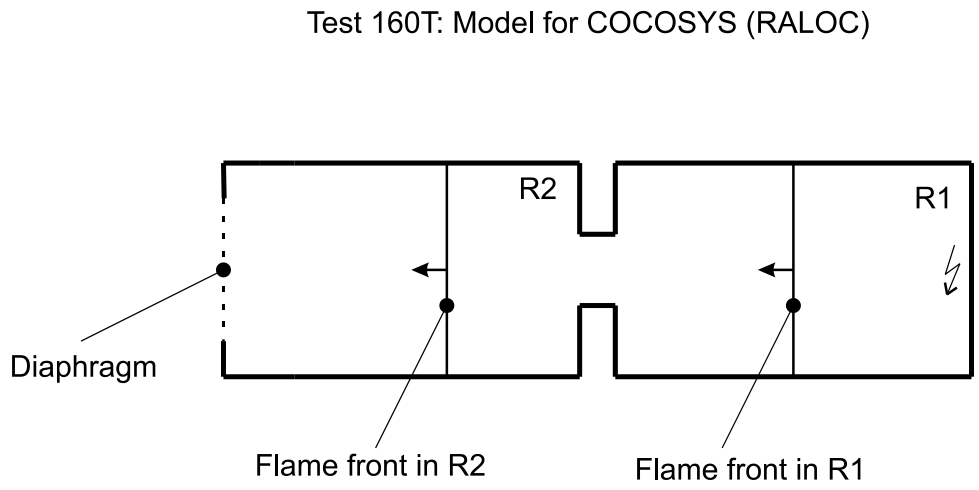

Figure 5.3.1.4-1 Nodalization scheme for the L.VIEW test 160T

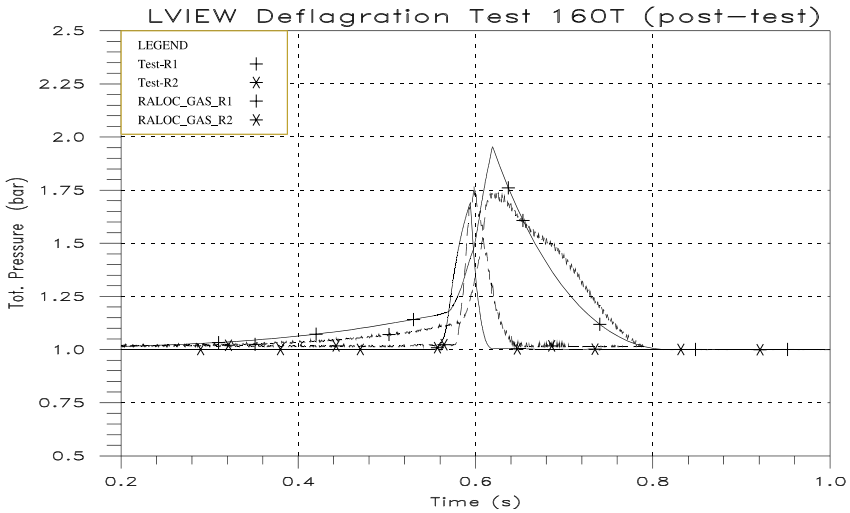

Figure 5.3.1.4-2 Pressure history in the 2 compartments of the L.VIEW test facility with initial conditions of 10.5% hydrogen in air (test values are dotted)

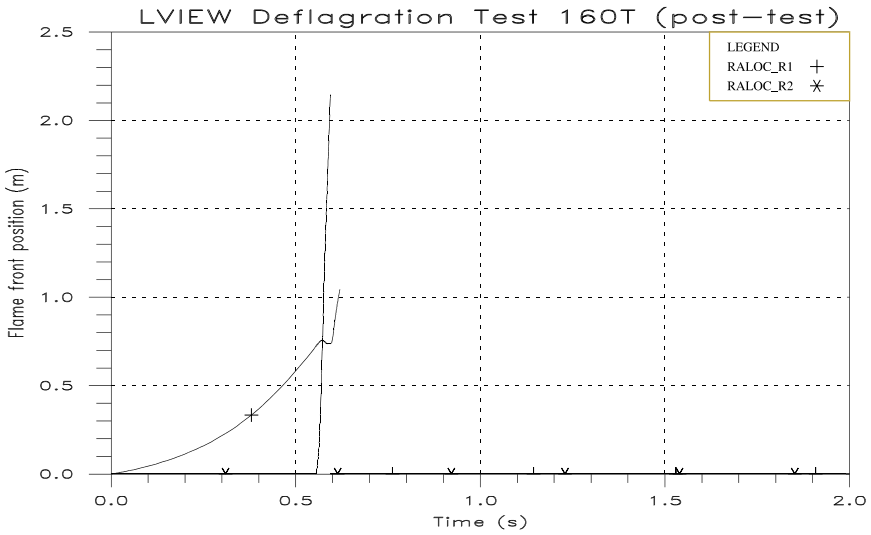

Figure 5.3.1.4-3 Progress of the flame fronts in both test compartments

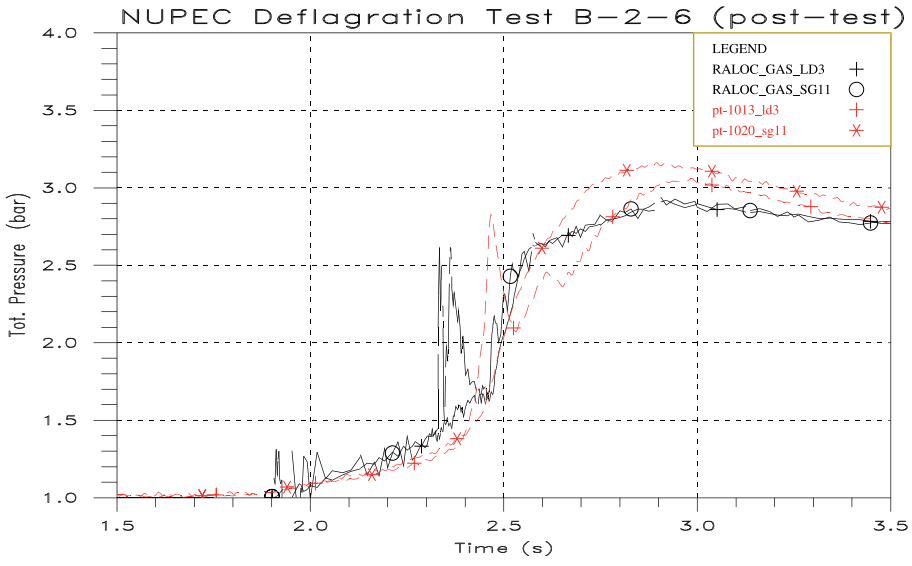

Figure 5.3.1.4-4 Comparison of the pressure buildup of experiment B-2-6 to the COCOSYS simulation

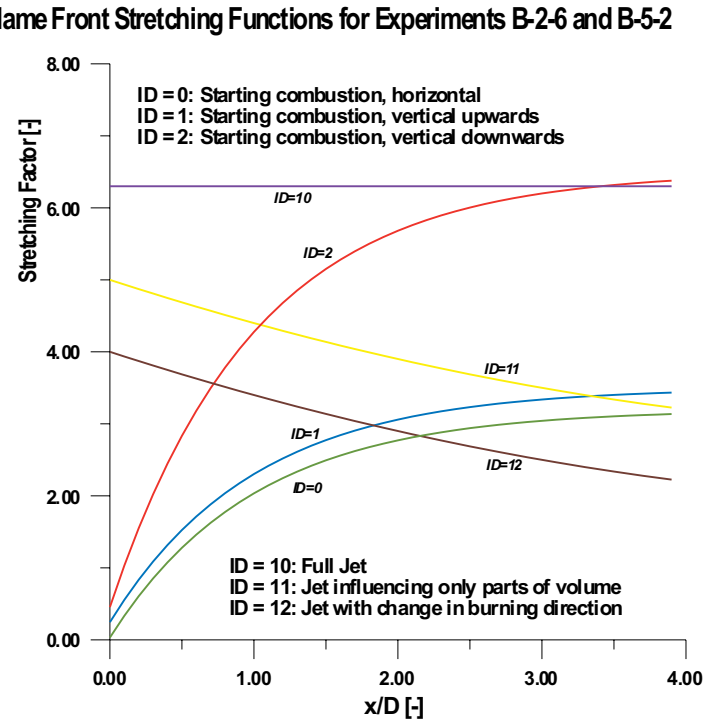

Figure 5.3.1.4-5 Stretching factors for six different combustion modes applicable to the NUPEC large-scale combustion tests (x is the current flame position in a zone, and D is the hydraulic diameter)

5.3.1.5 Coupling to CFD combustion codes

Instead of using the built-in combustion model DECOR in COCOSYS, an interface has been developed to include an external CFD combustion code. By this action, it is expected that the increased capabilities of CFD combustion modelling can be made available to long-term system codes. The interface is characterized by the following features:

- The codes to be involved were developed independently and should retain their individual structure. This eases later inclusion of modified code versions or other codes.
- A message paradigm (PVM - Parallel Virtual Machine [5.91]) is used to provide online data transport between the codes. Additional modules in the codes are needed to send and receive data.
- With respect to a nuclear safety application, the lumped-parameter code is considered as the basic code that runs all the time. If combustible conditions are detected anywhere in the spatial model, the CFD combustion code with actual initial conditions is activated and starts providing combustion data.
- The computational grids of the areas in question have to be created before the coupled run and are not subject to data exchange. They must be consistent.
- The COCOSYS combustion model is only partially used. It gets combustion rates from the CFD code and sends back actual boundary conditions. The combustion rates find access into the source

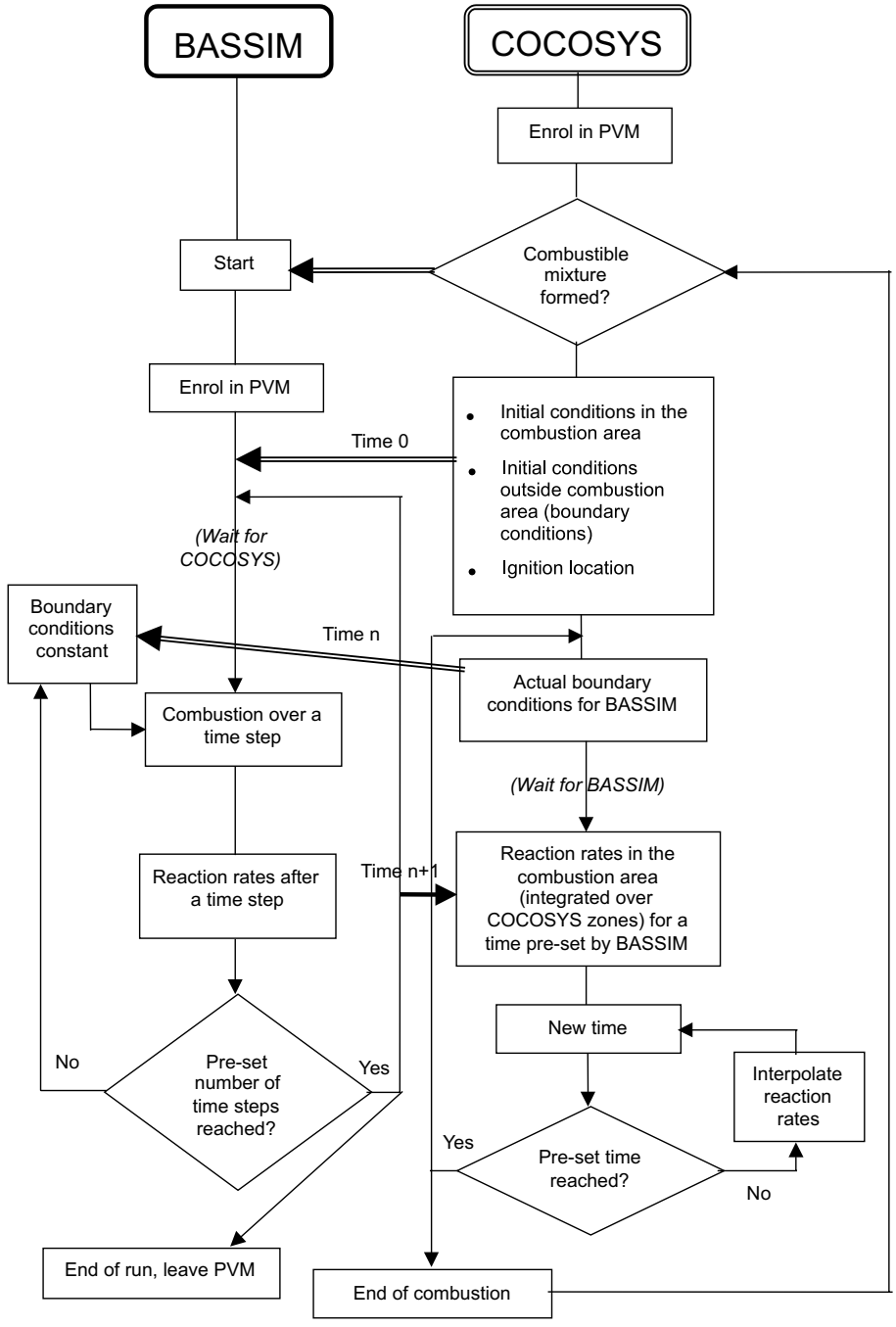

Figure 5.3.1.5-1 Outline of data exchange between a CFD code (here, BASSIM) and the lumped-parameter environment COCOSYS

terms of DECOR (see Table 5.3.1.3-1). It is expected, that the CFD combustion code models only a section of the total system; therefore, it needs the actual conditions at the boundaries.

This type of coupling has been implemented in the CFD combustion code BASSIM and COCOSYS. The principle data flow between these codes is outlined in Figure 5.3.1.5-1. COCOSYS has the general control and spawns also BASSIM as a child process when combustible mixtures have been detected. It is possible to have several child processes, which means there is combustion at different isolated locations. During combustion, the CFD code gets the time control because it is easier to synchronize both codes by steering the lumped-parameter code accordingly. Pressure, temperature, and concentrations in zones surrounding the combustion area (boundary conditions) are held constant during a CFD time step.

Computing times of the CFD code are approximately 10 times higher than for the lumped-parameter code. This code is therefore often in a wait cycle. A different data flow is also available for a coupling when solely gas mixing is of interest.

5.3.1.6 Limitations of combustion models in lumped-parameter codes

Limitations of the lumped-parameter concept in terms of combustion are as follows:

- They cannot provide detailed flow field predictions. All processes that mainly depend on these may be restricted in their results. These can be high-momentum gas-mixing phenomena, combustion, particle flows, and others.
- Therefore, lumped-parameter combustion models are only applicable to slow combustion (FA and DDT criteria not fulfilled) with flame speeds not exceeding $200 \text{ to } 300$ m/s. Whether this is fulfilled may be hard to decide prior to running a simulation. Special care should be taken during the validation process of the model to fix the application limits.
- Combustion as a very fast- and short-term process cannot be described in many details. It is worthwhile simulating combustion with a lumped-parameter code, whenever the impact within a large system like a containment is of interest and to get a first idea of the pressure increase and energy input.

However, there are also merits of the use of lumped-parameter codes in containment accident analyses:

- They are widely used to describe relevant physical processes expected to occur during severe accidents.
- They reflect the interactions between the different processes and are well-suited to perform parameter investigations to identify the impact of uncertainties. This applies mainly to phenomena not fully understood and modelled because the inherent uncertainties do not either justify or even enable the high effort of more detailed (CFD) models.
- They can run over the necessary process times (several days) with the available computer resources.
- Many years of user experience and experimental validation have been spent to get mature code tools.

As a result, a coupling between the simpler lumped-parameter concept and complex CFD codes appears to be very promising. The interface can be arranged that all slow, long-term processes are included in the standard lumped-parameter models and all fast and flow-dependent phenomena into CFD models. The two groups of models have then to communicate online to provide the necessary data exchange (see above).

5.3.2 Combustion in Hybrid CFD/LP-Codes[*]

5.3.2.1 The TONUS code [5.92]

There are two different types of safety analysis codes: (i) multi-compartment lumped-parameter codes such as CONTAIN [5.93], JERICHO [5.94], MAAP [5.95] or RALOC [5.96] and (ii) general-purpose multi-dimensional field codes, such as GASFLOW/HMS [5.97] and GOTHIC/WGOTHIC [5.98] (see Table 5.4.0-1). The advantages of type (i) codes relative to type (ii) codes are simplicity and fast processing; the disadvantages are its limitations for inherently multi-dimensional and unsteady events. The idea of the IPSN TONUS code development is to combine the two modelling approaches in a single system so as to leave the user with the option of either way of modelling. The TONUS code consists of the following features:

- A lumped-parameter model for distribution and slow combustion, comparable with that in JERICHO. Bulk and wall condensation, wall heat transfer and spray models are available, and simplified models for hydrogen combustion using flame velocity correlations are implemented.
- A semi-implicit finite-element low-Mach-number scheme for distribution and slow combustion using the standard zero-Mach-number combustion model [5.99], [5.92]. Turbulence is modelled by the Favre-averaged Navier-Stokes equations and a $k - \varepsilon$ model including buoyancy and weak compressibility effects. Transport equations are discretized by a second-order finite-element method for arbitrary Reynolds number. Both single-step Arrhenius kinetics for laminar and an eddy breakup model for turbulent combustion are available.
- An explicit finite-volume fully compressible scheme for up-to-now detonation simulations. The reactive Euler equations are solved using a second-order upwind finite volume formulation on unstructured grids. Source terms are handled by "operator-splitting" ([5.100], [5.101]).

5.3.2.2 Code construction and structure

The TONUS code is built using the CASTEM 2000 [5.102] system, and its user data manipulating language is called GIBIANE to achieve the flexibility and modularity required in modelling the complex reactor system at hand. The object-oriented structure of this system allows us to build, in a limited amount of time, versatile tools for computing complex flow situations. In particular, CASTEM 2000 encapsulates algorithms in generic data/operation sequences called "procedures", which present to the user a simplified interface with only a limited number of parameters to define. Thus TONUS consists of a set of procedures dedicated to containment modelling.

[*] Contributed by E. Studer

5.3.2.3 Combustion modelling in the lumped-parameter approach

The TONUS lumped-parameter combustion model is derived from work performed for French PSA level 2. This first model has been developed in order to have an estimation of the maximum flame velocity reached in real containment geometry. In this stand-alone model described in Figure 5.3.2.3-1, the following hypotheses have been made:

- Containment geometry is described by interconnected parallelepipedic control volumes for which pressure, temperature, and mixture compositions, that is, the thermalhydraulic conditions are know before ignition (conditions in the unburned gas are not modified during the calculation).
- Combustion in a control volume only depends on the thermalhydraulic conditions described above and on combustion processes in the previously burnt volume (upstream conditions). Acoustics-induced preconditioning of gases far in front of the flame is modelled here by an approximate increase of turbulence intensity u'.

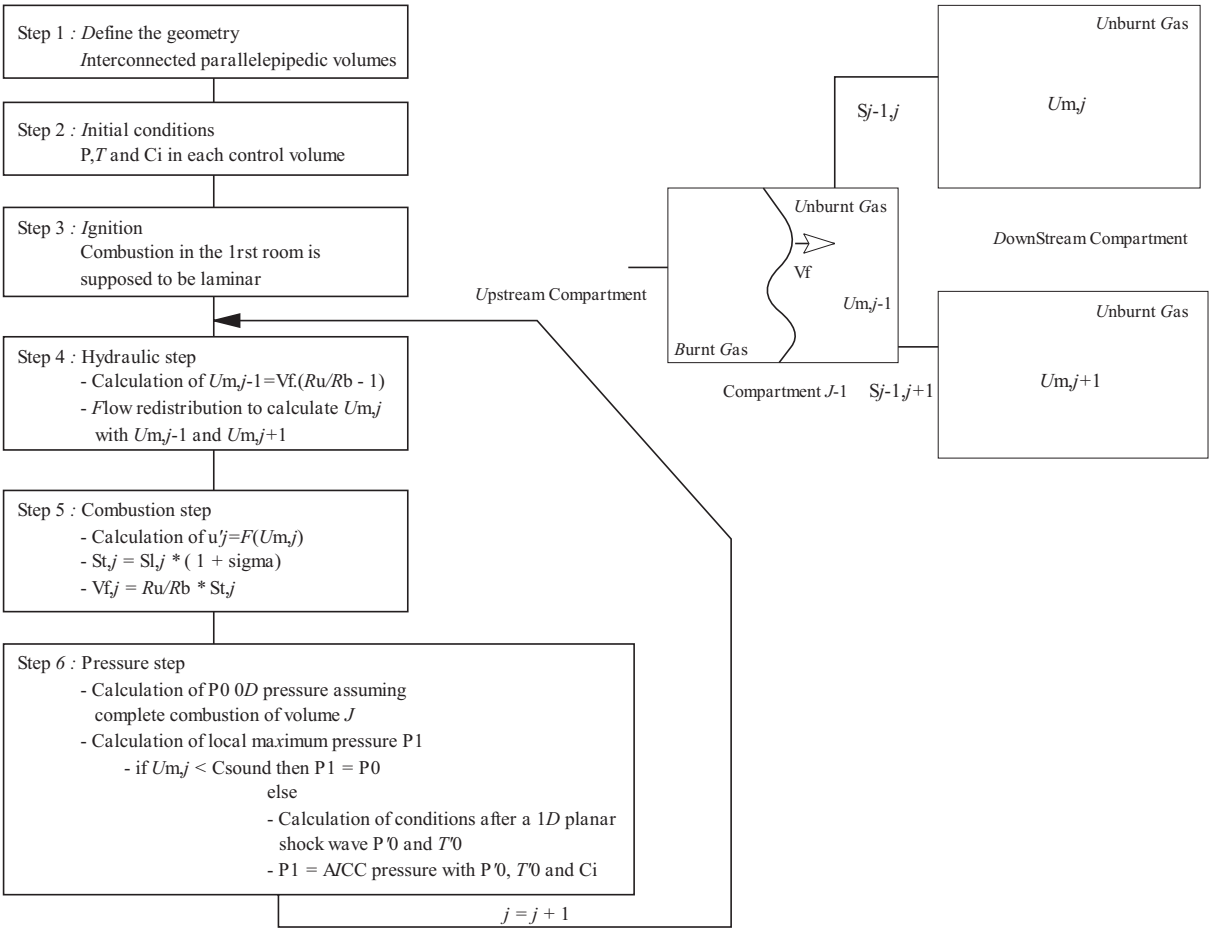

Figure 5.3.2.3-1 Flow chart of the simplified probabilistic safety analysis (PSA) level 2 combustion model

With these preliminaries, the description of combustion is essentially reduced to determining the passage of a turbulent flame speed S_T over the characteristic length L of the control volume, [5.103]. Passage of

flames between control volumes is determined on the basis of additional propagation conditions based on the Shapiro diagram.

Turbulent velocity correlation. Many authors have proposed correlations for turbulent combustion [5.104 – 5.108]. Parameters are mainly laminar flame velocity S_L, expansion ratio ρ_u/ρ_b, the root-mean-square (RMS) fluctuation velocity u', the turbulence integral length scale and adjusted constants. These laws are derived from experimental and theoretical considerations. Three turbulent combustion correlations were compared for a given mixture composition and with different level of turbulence (via u'). Hydrogen-air mixtures at room temperature and pressure were chosen. Explosion tube diameter is supposed to be 6.6 cm with a blockage ratio of 30%. Characteristics of the mixtures are given in Table 5.3.2.3-1 and the results are summarized in Figure 5.3.2.3-2. In the present study, Peters correlation has been chosen:

$$\frac{S_T}{S_L} = 1 + \bar{\sigma} \tag{5.3.33}$$

$$\bar{\sigma}^2 + 0.39\frac{l}{l_F}\ \bar{\sigma} - 0.78\frac{u' \cdot l}{S_L \cdot l_F} = 0 \tag{5.3.34}$$

with S_L: laminar flame velocity (m/s), u': RMS fluctuation velocity (m/s), l: turbulence integral length scale (m), and l_F laminar flame thickness (m).

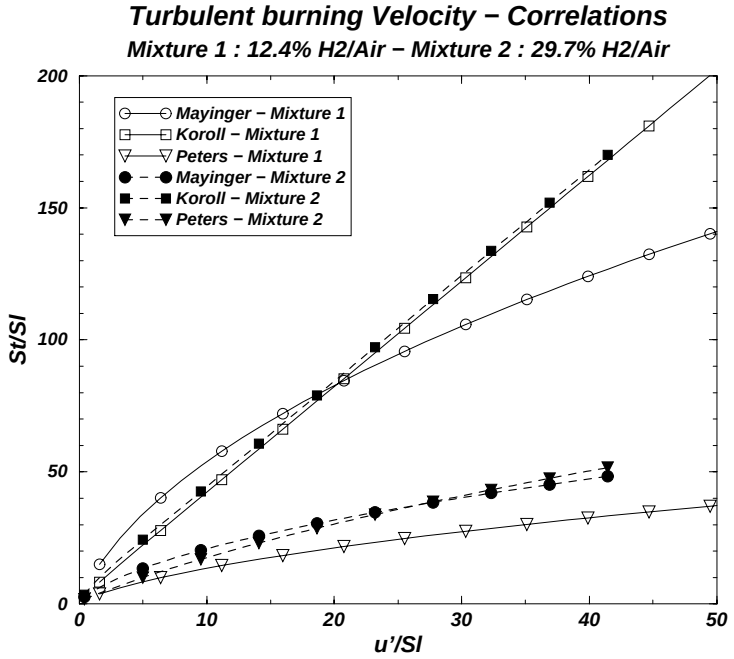

Figure 5.3.2.3-2 Comparison of turbulent flame velocity correlation

It should be emphasized that considerable uncertainties exist even after a turbulent velocity correlation has been selected. Typically, these correlations appear in the form of non-dimensional ratios of S_T/u', so that precise evaluation of S_T still requires an accurate assessment of the turbulent intensity u'.

RMS fluctuation velocity u'. Unfortunately, there is only a minor database for these estimates. In this work, we have used results from the Russian RUT Facility to determine the missing parameters. The

Table 5.3.2.3-1 Mixture characteristics

Characteristics	Mixture 1	Mixture 2
Hydrogen vol %	12.4	29.7
Laminar flame velocity (m/s)	0.62	2.41
Laminar flame thickness (m)	$1.2\ 10^{-4}$	$3.1\ 10^{-5}$
Turbulence integral length scale (m)	$6.4\ 10^{-3}$	$6.4\ 10^{-3}$

RUT Facility has a characteristic geometrical size similar to inner rooms in a real containment, and this model is mainly devoted to a pressure-water reactor (PWR) with pre-stressed concrete containment vessel. The turbulence intensity is defined as a fraction of the fluid velocity U_m.

Validation. The first step concerning validation of this simplified combustion model is verification on selected RUT large-scale turbulent combustion results. As an example, Figure 5.3.2.3-3 gives the flame position versus time calculated in the first channel of the RUT Facility with the model on RUT stm7 test. Blockage ratio is about 30%, and the mixture composition is 17.5 vol % hydrogen diluted by 25.7 vol % of steam at about 100^oC (well-mixed initial conditions).

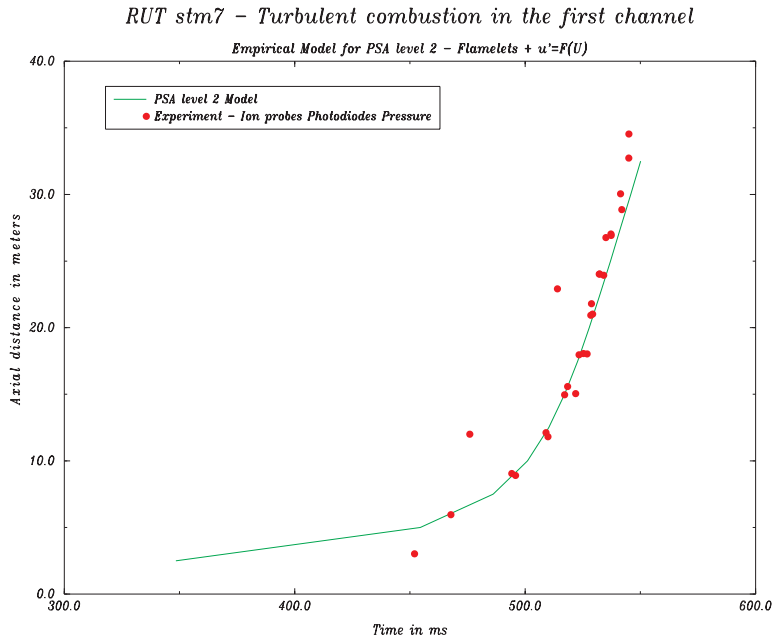

Figure 5.3.2.3-3 Verification of the simplified combustion model.

Other tests such as FLAME experiments were calculated and also some small-scale experiments were performed at AECL (Figure 5.3.2.3-4). Developed correlations give good results if the blockage is between 0.3 and 0.6 and if the ratio between tube diameter and obstacle spacing is between 1 and 2.

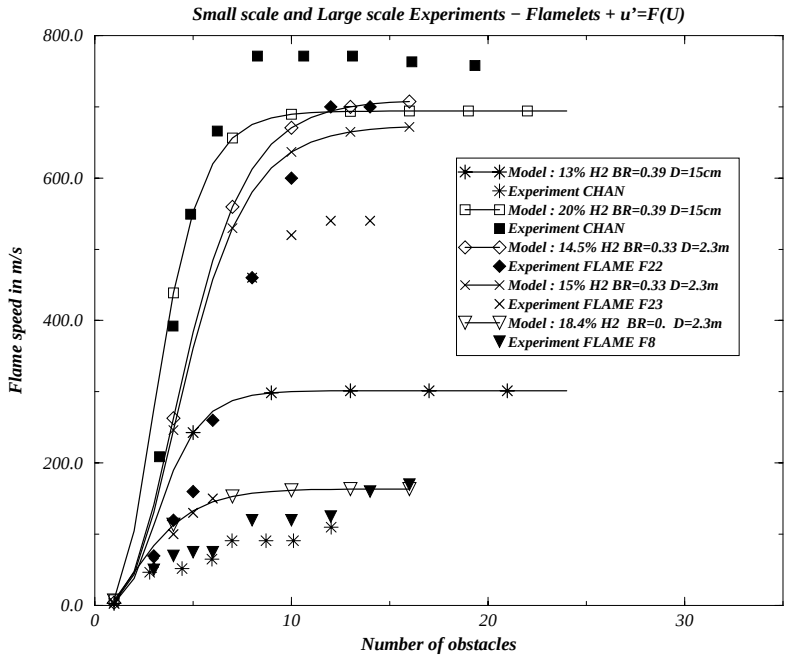

Figure 5.3.2.3-4 Validation against experimental data from AECL [5.109] and from the FLAME facility [5.110]

Effect of mixture gradients has also been computed using an experiment performed in Russia [5.43]. The tube diameter is 17 cm, and, a hydrogen gradient in air has been created via hydrogen diffusion (19.5 vol % near the ignition point and 4.5 vol % at the end of the tube). Results show a good agreement with the experiment and the quenching point is well predicted (Figure 5.3.2.3-5).

Other large-scale verifications were performed regarding the NUPEC large-scale combustion experiments [5.111]. Tests number B1-2 and B1-3 have been simulated (8 vol % and 15 vol % of hydrogen in dry air at initial room pressure and temperature). These verification tests show a good behaviour of our very simplified combustion model in terms of flame-front propagation (Figure 5.3.2.3-6.) and also pressure transient (Figure 5.3.2.3-7). Some additional work is needed to validate the correlation for the turbulent velocity correlation u' in case of small tube diameter. Some preliminary investigations show a large influence of the definition of the turbulent integral length scale.

The model described above was implemented in the TONUS lumped-parameter code only for slow flame regime. In this implementation, the turbulent flame velocity, described above, is calculated in each downstream control volume using the turbulence intensity u' constructed with the junction velocity between the two connected volumes (once at the ignition time). Modifications regarding leading shock wave were not implemented because of the restrictions of lumped-parameter equations (low Mach-number hypothesis). Validation studies of slow flame regime are in progress in the NUPEC large-scale experiments (B1-2 test: 8 vol % in dry air).

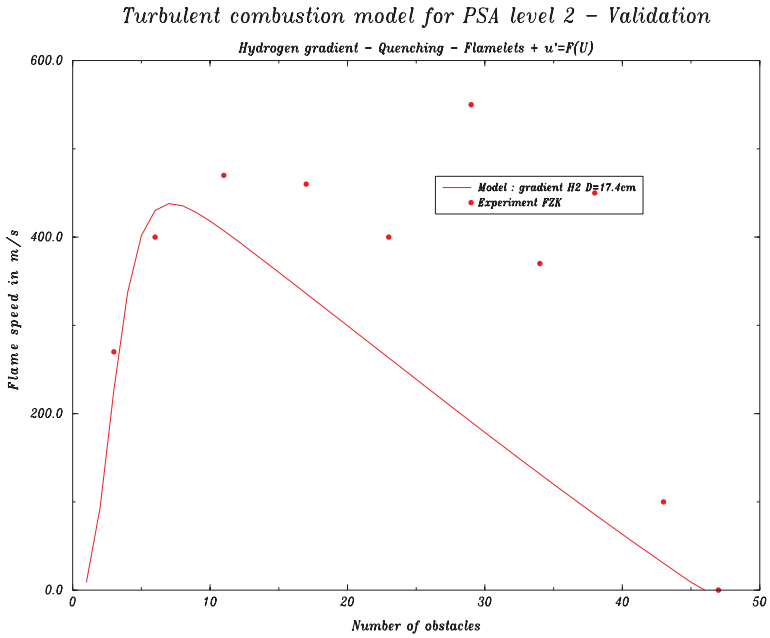

Figure 5.3.2.3-5 Verification of simplified combustion model – Effect of hydrogen gradient

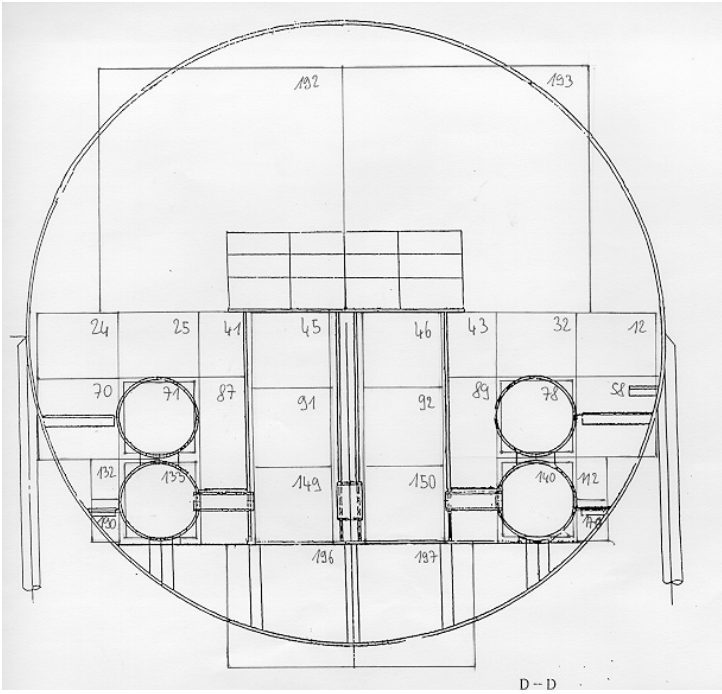

Figure 5.3.2.3-6 Flame arrival time in seconds (experiment B1-2 calculation)

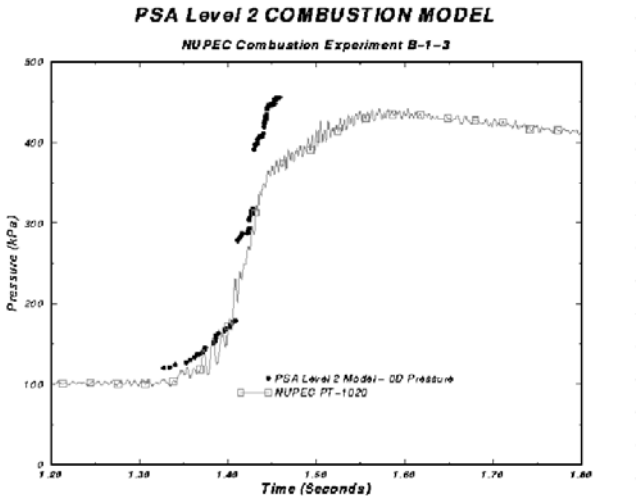

Figure 5.3.2.3-7 Pressure transient – comparison between calculation and experimental results (lumped-parameter pressure P0)

5.3.2.4 Multi-dimensional combustion simulation

Multi-dimensional combustion simulations using the TONUS environment are work that is in progress. An illustration of the TONUS low Mach-number flow solver and eddy breakup turbulent combustion model validation is given in Figures 5.3.2.4-1 and 5.3.2.4-2 [5.112]. This test corresponds to a turbulent combustion in the FZK tube (12 m long, 350 mm diameter). The blockage ratio is 0.3, and the mixture is 10 vol % of hydrogen at room conditions. Verifications are also available for the fully compressible flow solver in the same final report. Others validation and verification studies are not yet available.

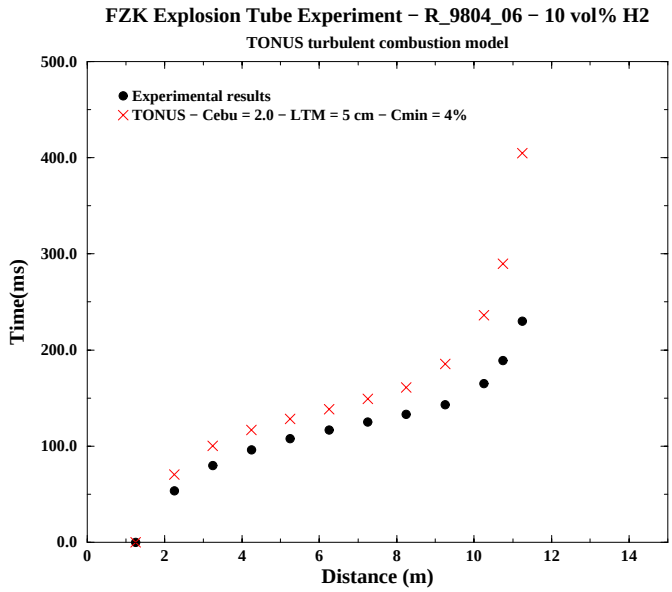

Figure 5.3.2.4-1 Flame position, TONUS calculation

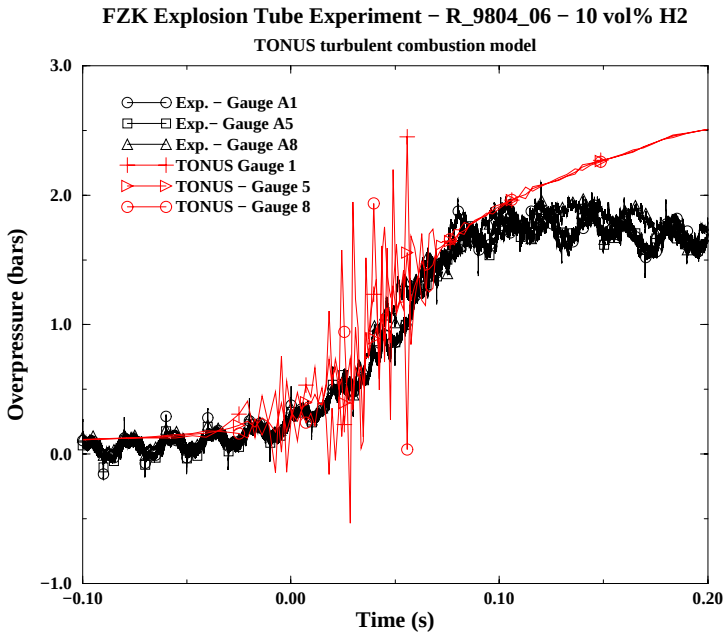

Figure 5.3.2.4-2 Overpressure, TONUS calculation

5.3.2.5 Current implementation of DDT criteria in TONUS

The following two necessary conditions to create a detonation from a fast turbulent flame are currently favoured as DDT criteria implemented in the TONUS code:

Criterion 1. (Data compiled at the Kurchatov Institute in Moscow [5.113]) According to a review of international data related to the onset of DDT and specific experiments conducted at the RUT Facility, this criterion is related to the mixture explosion sensitivity. The DDT condition requires a characteristic system size D to be larger than 7 times the corresponding detonation cell size λ. The length scale D depends on the geometry involved (e.g., in large volumes it should be the size of the room or the size of an hydrogen cloud; in channel geometries, it should be the height or the distance between obstacles).

Criterion 2. (Data compiled at AECL and FZK experiments, [5.109]) A minimum turbulent deflagration velocity, characterized by the lead shock Mach number, appears to be required to create DDT. The proposition by AECL is $Ma > 1.5$ for a limited range of mixtures. More generally, FZK proposes $Ma = f(H_2)$ for general hydrogen concentrations and with an empirical fitted function f(.). This approach is supported by the RUT Facility experiments. This criterion is related to an older approach based on the minimum running distance. These two necessary conditions will be used to create a single condition for the onset of a detonation in the TONUS code. The methodology is first to compute where criterion 1 is reached before ignition of the mixture and then, during combustion, to evaluate the location where criterion 2 is reached. DDT is likely to occur wherever both criteria are met simultaneously. To calculate the 2 criteria, the follwing data are needed in the lumped-parameter and in the multi-dimensional approach:

Detonation cell size evaluation. Different alternatives have been considered: (i) computation of induction lengths from a Zeldovic-von Neumann-Döring (ZND) model and correlation to cell size following

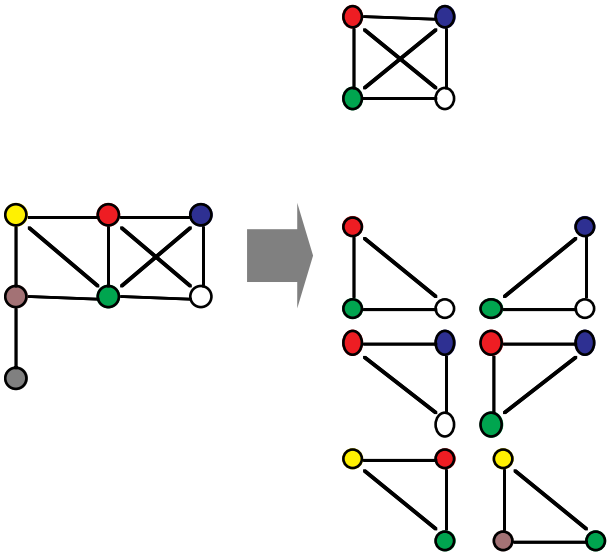

Figure 5.3.2.5-1 Extraction of a sub-graph representing the relevant connected control volumes in a lumped-parameter approach for DDT criteria evaluation

Reference [5.114], and (ii) polynomial interpolation between experimental data. Because the first option requires an expensive detailed chemistry model, we employed the second option for the first implementation. An Arrhenius law ($= A \cdot exp(-E_a/R \cdot T)$ was chosen as an approximate formula, and the free parameters A, E_a/R were fitted on experimental results available in the open literature [5.115 – 5.117] (For details see the final report [5.118]).

Local Mach-number evaluation. Computation of the local sound speeds is straightforward in both the lumped-parameter and multi-dimensional approaches. While the latter also provides the characteristic flow velocity as a field variable, an ad hoc approximation must be invoked in the former. We have chosen to assess the fluid velocity in a cell by the atmospheric junction velocity. Others choices should be examined during applications.

Geometrical size D. The geometrical size D is a characteristic length of a reactive mixture cloud, and in well-mixed conditions it corresponds to the room size. In the calculations, it has been chosen to use the detonation cell size variable to determine the size of the cloud. According to minimum and maximum system dimensions, isovalues of detonation cell sizes have been chosen by the user. In groups of cells in which the detonation cell size is smaller, the Nth isovalues are determined. Using these subgrids, the geometrical size D can be estimated as the smallest distance between the barycentre and border, volume over border area etc. There are still open questions on this subject to determine the right geometrical dimension. Sensitivity studies should be performed for each possible choice. In the lumped-parameter approach, when a cloud has been identified (detonation cell size lower than the Nth isovalue) a graph is constructed and then, we have to extract all the complete graphs with a dimension greater than 3 (all possible connections). An example is given in Figure 5.3.2.5-1. A revised methodology will be implemented according to the conclusions of this report especially concerning the geometrical characteristic length size D. Regarding lumped-parameter approach, a proposal is given in Chapter 6.

5.3.3 Combustion in CFD Codes Using the Eddy Dissipation/ Eddy Breakup Concept (EDC/EBU)[*]

5.3.3.1 Introduction

This section presents an example for turbulent combustion simulation using an eddy dissipation concept, as described in Chapter 4.3, by means of the COM3D code (see Table 5.4.0-1). This code was selected for this purpose because of its current active application to full-scale 3D reactor containment problems (2 million cells). The development of the COM3D code was started at the Kurchatov Institute [5.119] and was continued at FZK ([5.120], [5.121]). The sections that follow describe the code models and their validation by experimental results on different scales.

5.3.3.2 Code Description

The structure, the essential components, and the underlying physical models of the COM3D code are shown in Figure 5.3.3.2-1, and the models equations are summarized in Figures 5.3.3.2-2 and 5.3.3.2-3.

- The gas dynamic model includes the Favre-averaged conservation laws of total mass, momentum, energy, and species mass.
- The turbulence modelling offers the choice between two different treatments
  - standard $k - \varepsilon$, and
  - RNG $k - \varepsilon$ [5.122] (renormalization group theory)

  The RNG model, compared with the standard $k - \varepsilon$-model, provides more accurate predictions for flows with rapid distortions and large eddys.
- The thermodynamic model distinguishes four gas components (H_2, O_2, N_2, H_2O).
- The chemistry model describes the reaction rate with medium and high turbulence intensity. This allows one to treat thickened turbulent flames ($Da > 1$) and a quasi-homogeneous reaction regime ($Da < 1$). If the chemical reaction is the faster step, the rate is governed by the turbulent dissipation or the decay of eddies (eddy dissipation model). Otherwise, a corresponding Arrhenius equation is used to model the chemical reaction rate.
- To solve these equations numerically, a TVD [5.123] (total variation diminishing) procedure is used. The equations are solved on a 3D Eulerian carthesian grid.

It is crucial to verify the different models implemented in the COM3D code in a systematic step-by-step procedure. Different individual models were tested on increasingly complex problems.

[*] Contributed by Dr. W. Breitung

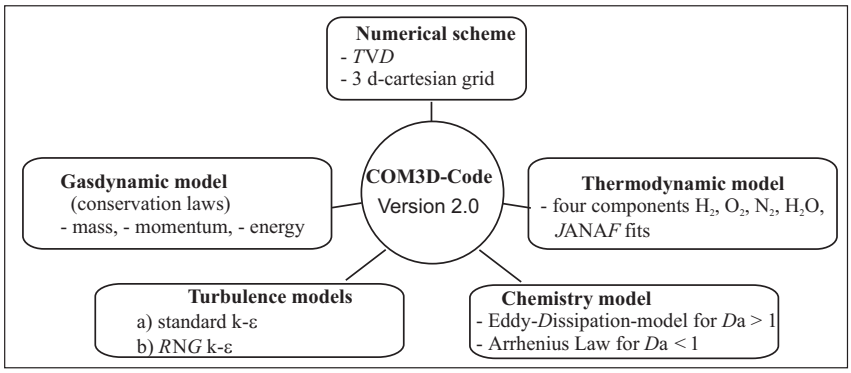

Figure 5.3.3.2-1 Structure and models of the COM3D code

Hydrodynamic equations

The set of conservation laws for mass, momentum, energy and species reads as

$$(\rho)_t + (\rho u_j)_{x_j} = 0,$$

$$(\rho u_j)_t + (\rho u_i u_j)_{x_j} = \rho g_i - p_{x_i} + M_{ij,x_j}, \quad i = 1,2,3$$

$$(\rho e)_t + ((\rho e + p)u_j)_{x_j} =$$

$$\rho g_j u_j + u_i M_{ij,x_j} + (\frac{\mu_{tur}}{C_h}(e - \frac{1}{2}u_i u_i + \frac{p}{\rho})_{x_j})_{x_j} + B + \rho\epsilon,$$

$$(\rho f_\alpha)_t + (\rho f_\alpha u_j)_{x_j} = \overline{\dot{w}}_\alpha + (\frac{\mu_{tur}}{C_{f_\alpha}} f_{\alpha,x_j})_{x_j},$$

here

$$e = \sum_{\alpha=1}^{N} \frac{f_\alpha}{\mu_\alpha}\left(h_\alpha + \Delta h_\alpha^0 - RT\right) + \frac{1}{2}u_j u_j, \quad f_\alpha = \frac{\rho_\alpha}{\rho},$$

$$M_{ij} = -\frac{2}{3}\delta_{ij}(\rho k + \mu_{tur} u_{r,x_r}) + \mu_{tur}(u_{i,x_j} + u_{j,x_i}).$$

Closure of the equation depends on the knowledge of the following variables: μ_{tur}, k, ε, (theory of turbulence) and $\overline{w}_\alpha$ (combustion model).

Figure 5.3.3.2-2 Hydrodynamic equations of the COM3D code

Figure 5.3.3.2-3 Standard $k-\varepsilon$, $RNG-k-\varepsilon$, and reaction model, as implemented in the COM3D code

5.3.3.3 Code validation

The forward facing step problem. The supersonic flow through a 2D duct with a forward-facing step was analyzed. This numerical test problem has been investigated by many authors using various codes and different numerical methods. The correct solution is well-known. This high-velocity problem provides a good test for both the ability of the COM3D code to solve the Euler equations numerically and for the correctness of the thermodynamic data (JANAF-fits). Figure 5.3.3.3-1 shows a corresponding result. The calculated stagnation pressure, angle of bow shock, shear layer position, and downstream shock pattern are in good correspondence with the known numerical solutions. The total variation diminishing (TVD) scheme used in the COM3D code preserves shock fronts very well.

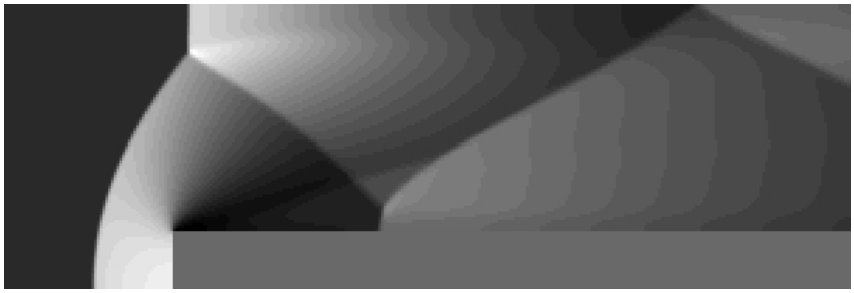

Figure 5.3.3.3-1 COM3D verification on a hydrodynamic test problem. Supersonic flow through a duct containing a forward-facing step: N_2**,** $M = 3$**,** $p_0 = 1$ **bar,** $T_0 = 298$ **K. The computational grid is** 100×300 **cells. Good agreement is observed with the known solutions.**

He-air turbulence test. The 12-m FZK tube was used for inert tests in a shock tube mode. The tube is divided by a membrane in two parts (Figure 5.3.3.3-2). The 3-m-long section can be pressurized, and the bursting of the membrane creates a shock wave travelling into the adjacent low-pressure section (e.g., at 1 bar), which contains circular orifices as obstacles. The velocity and pressure amplitude of the shock wave decrease by partial reflection and turbulence generation. Then, the measured pressure signals at different locations can be compared with numerical simulations based on different turbulence models. This allows the verification of the turbulence models under inert conditions, without disturbances by a combustion process. Using three different levels of turbulence modelling – without turbulence, with $k - \varepsilon$, with RNG $k - \varepsilon$ – the experiment on turbulence generation and dissipation in inert He-air was simulated with COM3D. An uniform 3D cartesian grid with 1-cm mesh spacing, which results in a total of 390 000, cells, was used for the calculation. Figure 5.3.3.3-3 compares a measured pressure signals with the COM3D calculations without turbulence model and the RNG $k - \varepsilon$ model. The calculation without the turbulence model shows considerable deviations from the measured pressure data. Including a $k - \varepsilon$ or RNG $k - \varepsilon$ model provides a better agreement with the experiment. The calculation matches the measured pressure associated with the incoming wave very well. The differences between the $k - \varepsilon$ and RNG $k - \varepsilon$ models were only minor; thus $k - \varepsilon$ appears sufficient for the investigated problem.

Reactive flow tests in different scales. The 12-m tube was modified to allow turbulent combustion tests on a medium scale (Figure 5.3.3.3-4). In the whole tube, equally spaced ring-shaped obstacles are installed to block a certain ratio of the flow path. The eddy break up combustion model of the COM3D code contains a reaction rate constant c_f, which must be obtained empirically from experimental results. A large series of calculations for turbulent combustion experiments with different H_2 concentrations and blockage ratios confirmed a value of $c_f = 6 \pm 1$ for a great variety of experiments. A comparison between measured and calculated pressure is displayed in Figure 5.3.3.3-5 for a test with 15% H_2 and

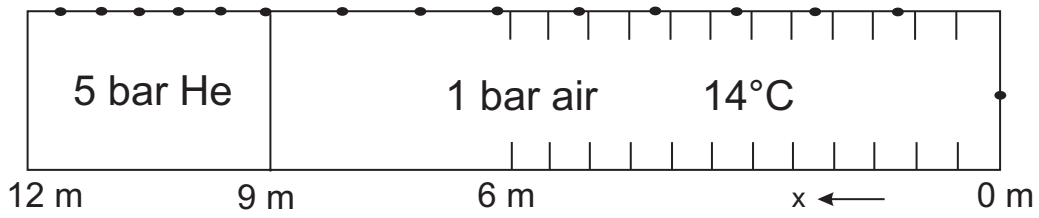

Figure 5.3.3.3-2 Shock tube configuration of FZK 12-m tube

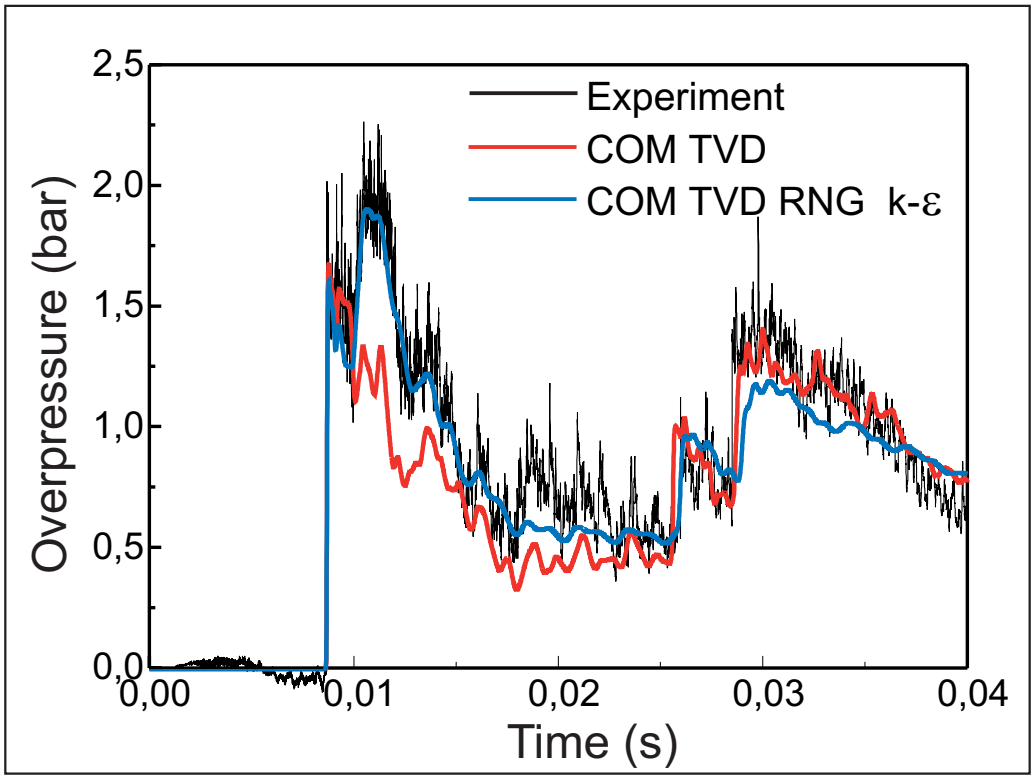

Figure 5.3.3.3-3 Comparison between measured and calculated pressure in inert shock tube test ($x = 4.25$ m)

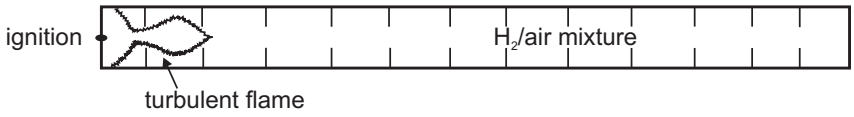

Figure 5.3.3.3-4 Schematic view of 12-m FZK tube equipped with obstacles

30% blockage ratio. It shows good agreement with the data for the integral combustion development and local pressure loads [5.124].

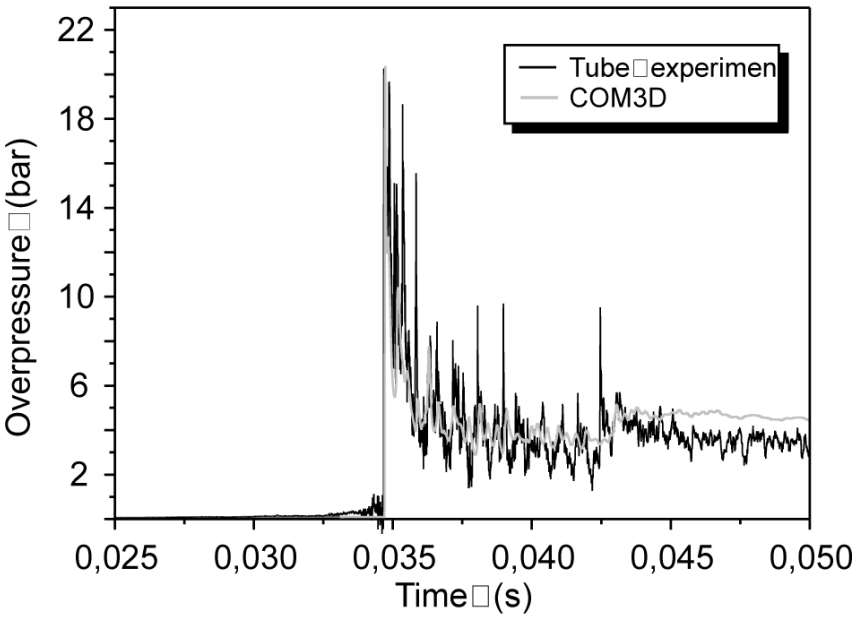

Figure 5.3.3.3-5 Comparison of calculated and measured pressure signals for tube experiments

Large-scale experiments performed in the RUT Facility [5.125] yielded further data for confirmation of the combustion model. The RUT Facility is depicted in Figure 5.2.3.2-30 . The whole facility has a lenght of about 60 m and a cross-section area of $5.25\ \mathrm{m}^2$ in the channel part. Figure 5.3.3.3-6 shows as an example the good agreement between measured and calculated data. A c_f-value of 6 was used as in the medium-scale calculation. All major peaks in the experimental data can be identified in the calculation, showing that the simulation captures properly the essential wave propagation phenomena in the complex 3D enclosure.

Conclusions. Using the COM3D code as an example, this section showed the major steps necessary for the development of a verified CFD program for reactive flow. A 3D code was developed for simulating fast turbulent combustion in H_2-air-steam mixtures. The exploited models (numerical, gas dynamic, thermodynamic, turbulence, chemical kinetics) were validated on medium and large test problems and experiments. The COM3D code may be considered as a verified tool for sufficiently accurate simulations of fast turbulence combustion on a full reactor scale. An example of a reactor application will be given in Chapter 6.

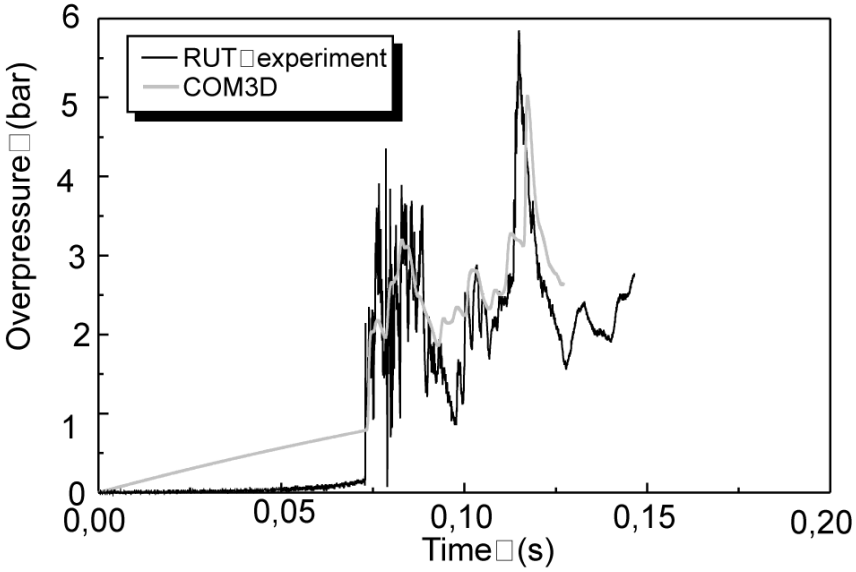

Figure 5.3.3.3-6 Comparison of calculated and measured pressure signals for RUT Facility experiment

5.3.4 Application of the eddy breakup model to a complex geometry[*]

The NUPEC Large-scale Test Facility (Figure 5.2.3.2-27) offers interesting features to be used for combustion model validation. It was built to be similar in design to a nuclear containment, and it models the major components of a nuclear containment in its interior. These components are hollow and are open for gas flow and flame passage but act also as obstacles for flows around them.

For CFX-4.2 ([5.126], see Table 5.4.0-1) a block structured grid was created, with the aim to include all relevant components. Figure 5.3.4-1 shows a view of the inner of the sphere and reveals the two steam generator cylinders surrounded by two ring-like pipes (“doughnuts”). Figure 5.3.4-2 shows a view of the outer shell cut off. This picture shows that all inner parts of the test facility are interconnected by small pipes. From the cylinders, two pipes enable flows to the lower doughnuts. After a circular turn of 90^o, two pipes branch the flow to the upper doughnuts. From there, again after a 90^o turn, connections to the outer sphere exist.

The grid consists currently of about 52 000 cells, and this number can be considered as a minimum. Respective investigations have not yet been conducted to characterize the influence of the combustion process. Figure 5.3.4-3 gives two examples of the grid related to internals of the test facility. On the right side of Figure 5.3.4-3 the upper part of the upper doughnut has been removed. This reveals that in the doughnuts additional orifices are installed in order to provoke continued flame acceleration.

The combustion model used is the eddy breakup approach with Damköhler cut-off to model flame quenching. The reaction then rate reads as follows:

$$R = -\rho \frac{\varepsilon}{k} \, C_R C_A M_{lim} \tag{5.3.35}$$

[*] Contributed by Dr. M. Heitsch

with

$$C_R = 23.6 \left(\frac{\mu\varepsilon}{\rho k^2} \right)^{\frac{1}{4}}, \tag{5.3.36}$$

$$C_a = 1.0 \; if \; D \geq D_{ie}$$
$$C_a = 0.0 \; if \; D < D_{ie} \; . \tag{5.3.37}$$

D_{ie} is a threshold Damköhler number below which the chemical reaction is suppressed to simulate local quenching.

$$M_{lim} = min \left(m_F, \frac{m_O}{I}, B\frac{m_P}{1+I} \right) \; . \tag{5.3.38}$$

The m_F, m_O, and m_P are the mass fractions of fuel, oxidizer, and products respectively. The stoichiometric coefficient of the chemical reaction is denoted by i. The Damköhler number is defined by the following form:

$$D = \frac{\tau_t}{\tau_{CH}} \tag{5.3.39}$$

with the turbulent time scale defined as

$$\tau_t = \frac{k}{\varepsilon} \tag{5.3.40}$$

and the chemical induction time (after Schott and Kinsey [5.127]) given by

$$\tau_{CH} = A_{CH} e^{\frac{T_A}{T}} \left(\rho m_F\right)^a \left(\rho m_O\right)^b \; . \tag{5.3.41}$$

A_{CH} is a constant, T_A an activation temperature, and a and b are exponents for the fuel and oxygen density respectively. The constants from Equations (5.3.37), (5.3.38) and (5.3.41) are distinct for the hydrogen-oxygen reaction but depend also on the scale of the test facility. In Reference [5.128] detailed investigations on different scales and test facilities were conducted to fix the constants. With this support, the following constants are set:

$$D_{ie} = 5, A_{CH} = 2.25 * 10^{-11}, T_A = 9132, a = 0, b = -1, B = 1 \; . \tag{5.3.42}$$

Test B-2-6 from the NUPEC experimental program has been simulated. The same deflagration experiment has also been analyzed, as described in Reference [5.90]. The initial mixture is composed of 10.5% hydrogen, 12.5% oxygen, 30% steam, and the rest is nitrogen. Ignition takes place in the left steam generator close to the bottom, and the combustion progress is most of the time asymmetric. First, a flame expands upwards through the steam generator cylinder into the outer sphere of the test facility. Very soon, the flame front also branches through the available connection pipes into the outer lower doughnuts. In Figure 5.3.4-4 at two different times, the progress of the deflagration is shown. Shaded contours of temperature are used to illustrate the flame propagation. The upper part (at 0.9 s) spots the moment when on the left side of the test facility the lower doughnut is reached, and in the right steam generator cylinder the flame progressed less . Later, at 1.305 s (lower part of the figure), hot gases tend to leave from the upper doughnut into the sphere. This means, that (invisible in the figure) through the available connection pipes the upper doughnut is already reached by a flame. However, in the lower doughnut, combustion has not reached the right section because no elevated temperatures can be seen there.

Figure 5.3.4-5 is a comparison of the pressure history in the left steam generator and in the upper doughnut, a comparison of measured values with simulated values. In the early phase, the modelled combustion

is faster than the measured combustion. This is why the laminar initial phase has not been modelled and from the beginning a full turbulent combustion is assumed. Later, the simulation overestimates the buildup of total pressure in the test facility. This may be true to the complete consumption of all the fuel, what is inherently involved in the eddy breakup model by default. Radiative losses from the hot steam may also play a certain role and may lower the pressure but have not yet been included. It should be stressed that the presented simulation intentionally did not modify basic model constants in order to get a better agreement with measured data. Instead, this analysis demonstrates the capabilities of the combustion model and its implementation in the CFX model available for a blind simulation,for example, in a nuclear containment.

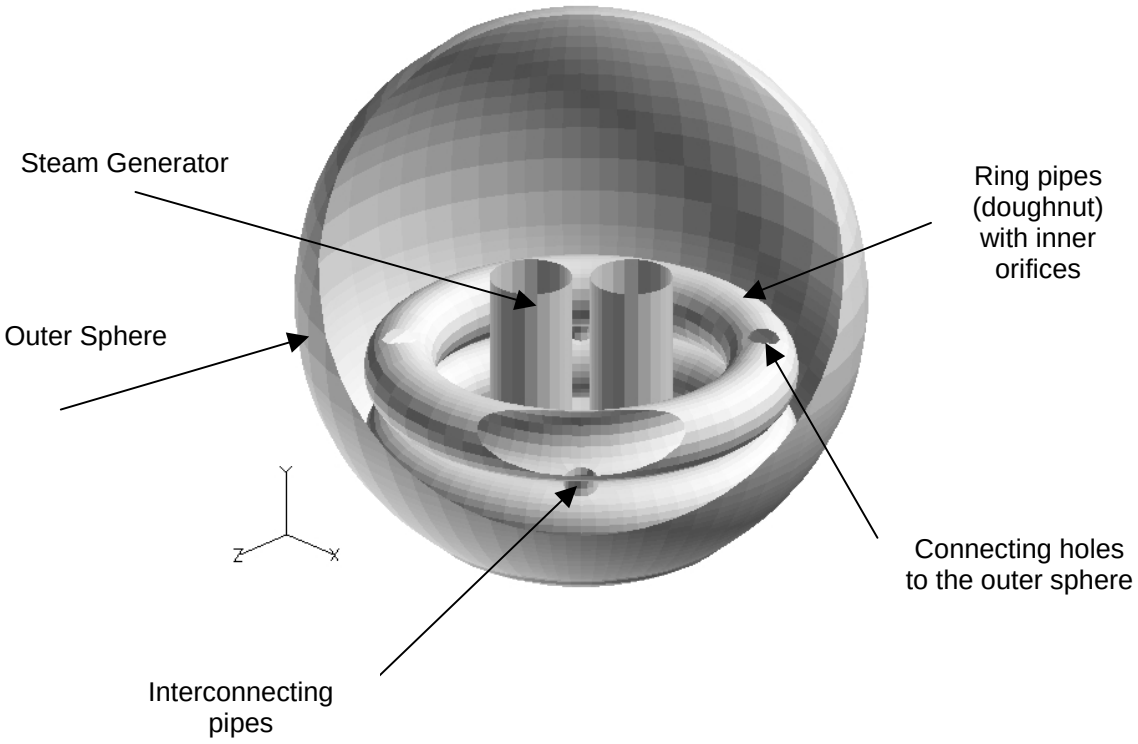

Figure 5.3.4-1 Cutaway view through the CFX model of the NUPEC Large-scale Test Facility

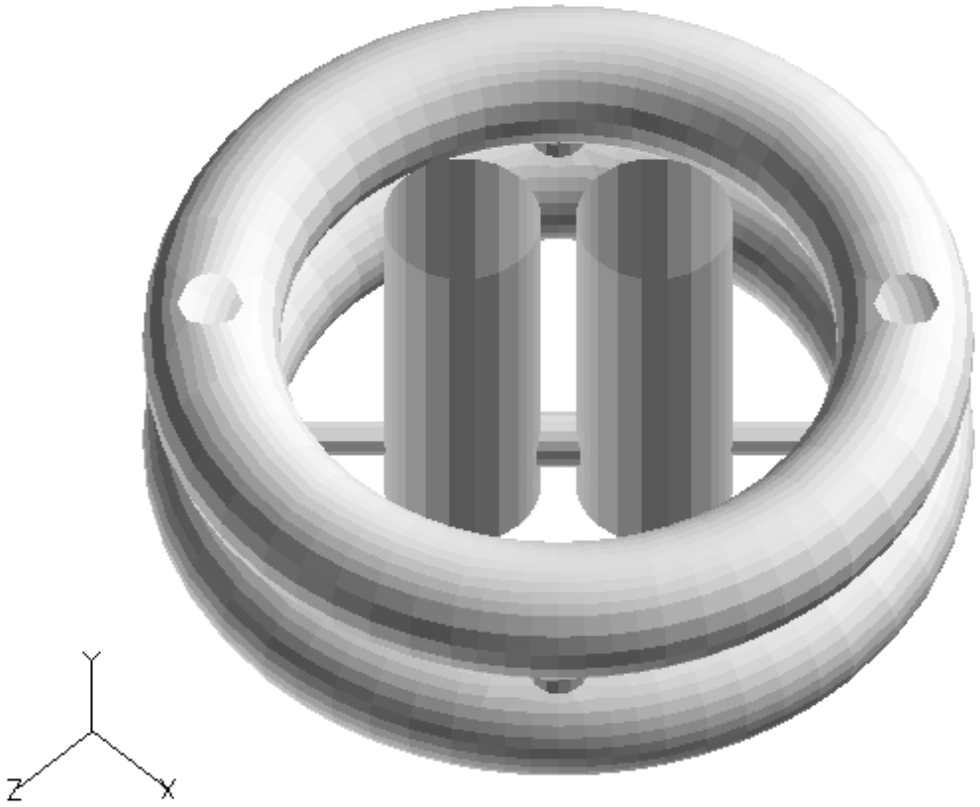

Figure 5.3.4-2 Perspective view of the modelled internals with interconnecting pipes

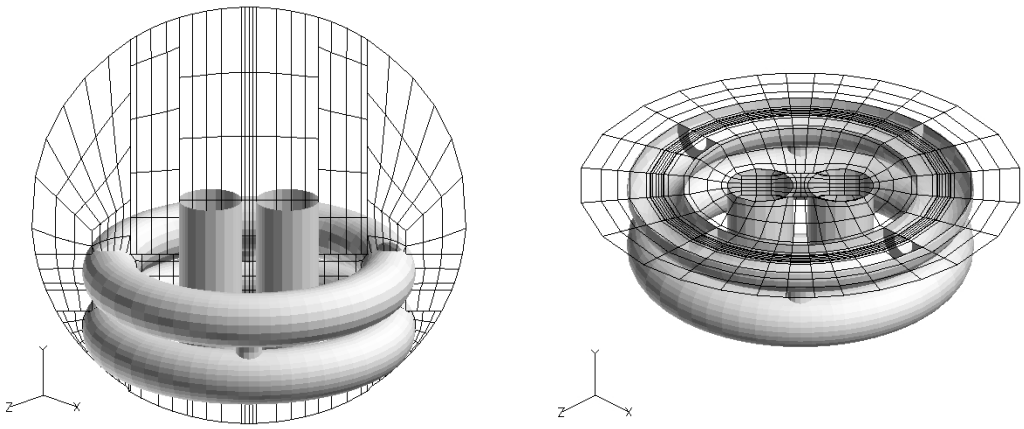

Figure 5.3.4-3 Examples of the grid used

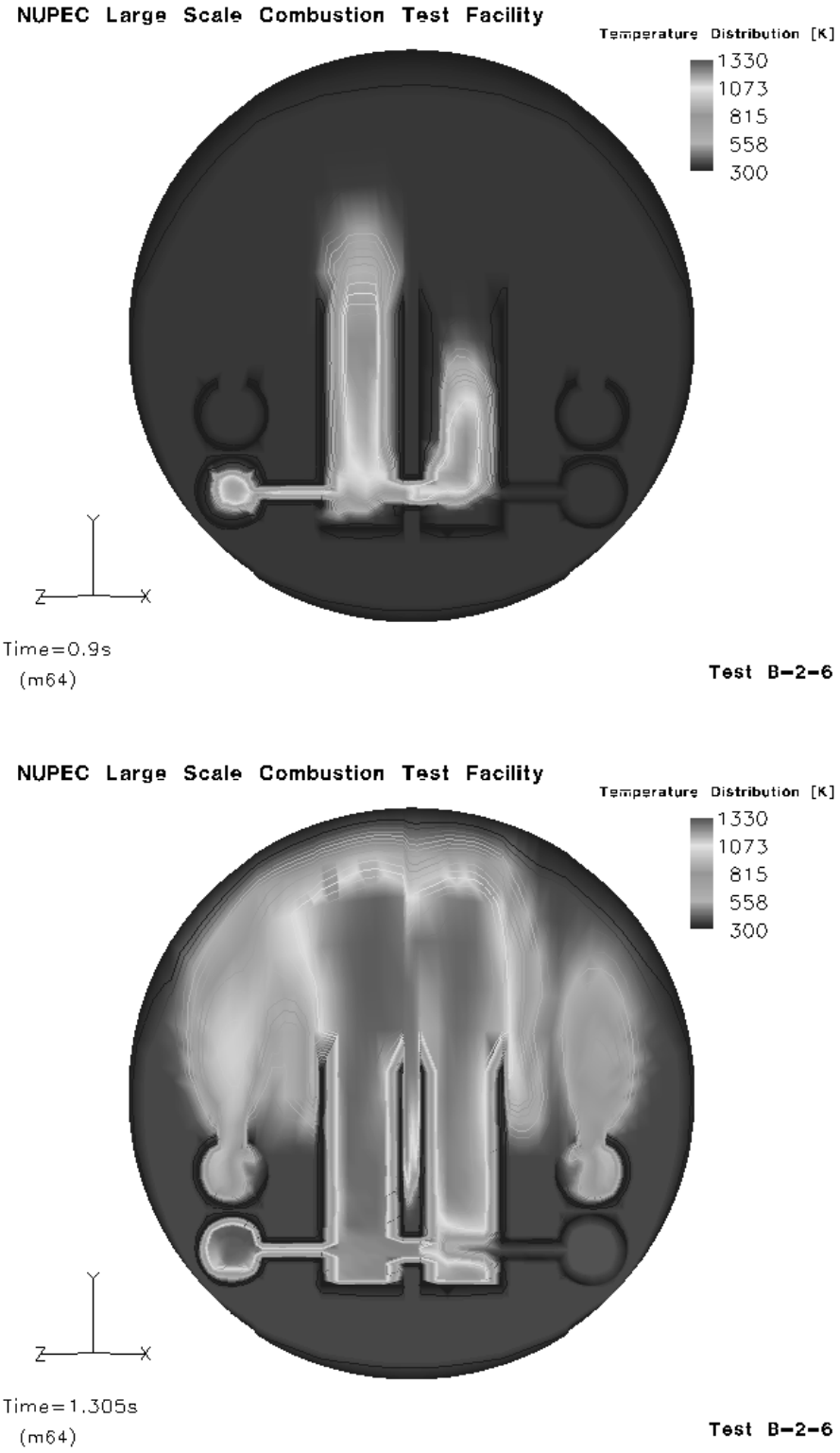

Figure 5.3.4-4 Shaded contours of temperature to characterize the flame progress at two different times

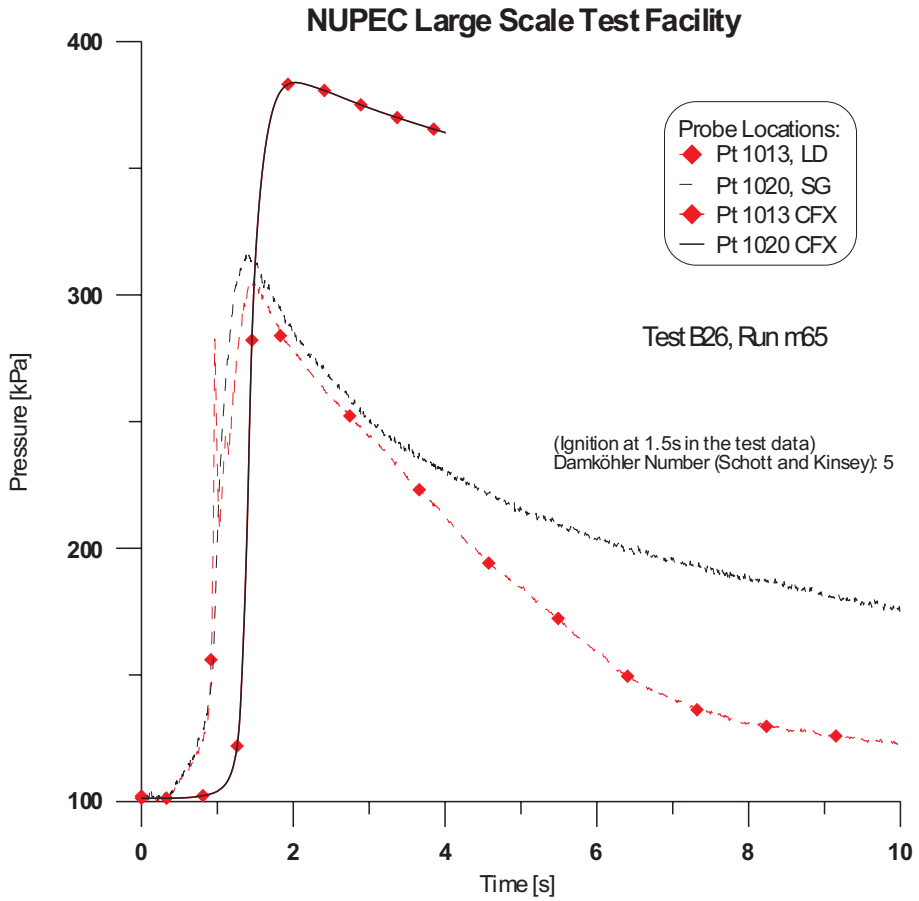

Figure 5.3.4-5 Pressure increase as comparison between measurement (dotted) and simulation

5.3.5 Combustion in CFD Codes Using a Probability Density Function (PDF)[*]

5.3.5.1 Introduction

A calculation method for combustion systems of interest comprises a number of essential components. These include the conservation equations, numerical solution methods, turbulence models, and combustion models. In order to focus the attention on the development of a model for the premixed hydrogen-air combustion process, it is convenient to implement the model into a commercial CFD code. The present contribution describes the implementation of a PDF combustion model into the commercial codes CFX and CFX-TASCflow from AEA Technology plc. (see Table 5.4.0-1). The basic development of the reported model is described by Durst and Mayinger [5.129] and Durst [5.130, 5.131], and follows along the lines of Pope [5.132], Bray [5.133] and Borghi [5.134].

The main assumption of the model is that the thermodynamic state of the system can be related to one single progress variable

$$c = \frac{Y_{H_2O}}{Y_{H_2O,\infty}} \,, \tag{5.3.43}$$

taken to be the mass fraction of water as the reaction product, normalized by the final water mass fraction

[*] Contributed by A. Eder

at the end of the combustion reaction. Further, it is assumed that the chemical rections are in equilibrium, which leads to deterministic relations between the mass fractions of the involved species. The chemical conversion rates of the involved species can generally be expressed depending on the thermodynamic state and composition of the involved mixture and an Arrhenius-type rate factor.

Together with the former of the above assumptions, which relates any thermodynamic quantity to the reaction progress, the latter assumption enables us to relate the chemical conversion rates of the individual species to the reaction progress c. The production rate of c itself is defined correspondingly to Equation (5.3.43):

$$w_c = \frac{w_{H_2O}}{Y_{H_2O,\infty}} \, , \tag{5.3.44}$$

with w_{H_2O} as the chemical production rate of water is treated in the same way. The resulting balance equation for the reaction progress variable reads

$$\frac{\partial}{\partial t}(\rho c) + \frac{\partial}{\partial x_i}(\rho u_i c) = \frac{\partial}{\partial x_i}\left(\Gamma_{H_2O}\frac{\partial c}{\partial x_i}\right) + w_c(c) \, . \tag{5.3.45}$$

The chemical closure problem arises from the well-known difficulty of resolving the length and time scales involved in a turbulent flow with the spatial resolution of the numerical grid and appropriate time steps, resulting from limitations both in computer memory and calculation time. Consequently, turbulent flows in engineering applications are treated by suitably averaging the corresponding balance equations (time–/Reynolds–, ensemble–, density-weighted/Favre-averages). In the above balance equation for the reaction progress, this leaves us with an average of the reaction rate, which, because of the high non-linearity of the exact term (involving an exponential function in the Arrhenius rate factor), cannot be expressed in terms of the average of the reaction progress, i.e.,

$$\overline{w}_c(c) \neq w_c(\overline{c}) \, . \tag{5.3.46}$$

In fact, as many authors point out, this approach can lead to errors of several orders of magnitude. Therefore, the turbulent reaction rate $\overline{w}_c$ must be accounted for by an appropriate turbulent combustion model.

The approach reported in the present contribution is based on a relation known from experimental investigations. If the instantaneous values of a turbulently fluctuating quantity φ and the corresponding probability density function (PDF) $P(\varphi)$ can be determined, then the mean value can be calculated as

$$\overline{\varphi} = \int_{-\infty}^{+\infty} \varphi P(\varphi) \, d\varphi \, . \tag{5.3.47}$$

In our case of the turbulent reaction rate this leads to

$$\overline{w}_c(\mathbf{x}, t) = \int_0^1 w_c(c) P(c; \mathbf{x}, t) \, dc \, , \tag{5.3.48}$$

where we have extended the dependencies in order to indicate that we are intererested in solutions in the whole calculation domain rather than only at one single measuring location. Contrary to the situation of an experiment where both the expressions that are integrated result from measurements, we are left with the task of still having to relate the second term to the (mean) flow. The present contribution simply assumes a generic shape for $P(c)$ with specific shapes constituted by not too many parameters, which,

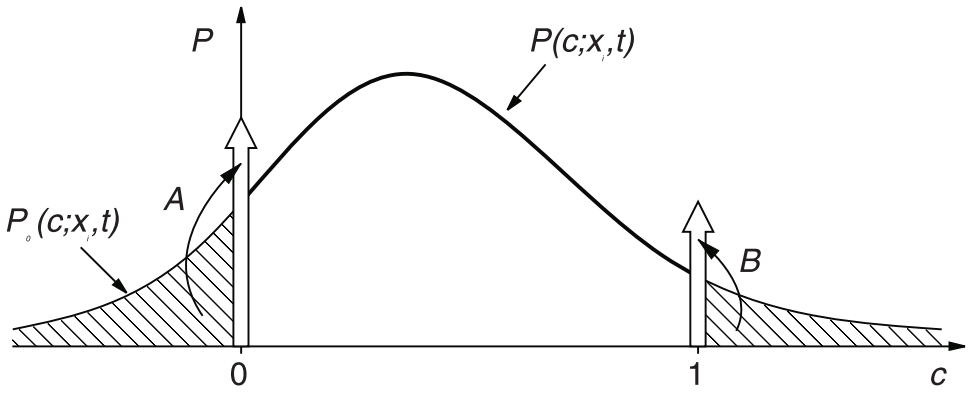

Figure 5.3.5.1-1 Gaussian PDF clipped to $0 \leq c \leq 1$

in turn, can be determined from the flow field. As, in general, these parameters will vary with the flow field, this gives $P(c; \mathbf{x}, t)$. The mean value can then be determined by numerically equating the above integral. Similar to Lockwood and Naguib (cf. [5.135]), we chose a Gaussian distribution for the shape of the PDF, clipped to the region of definiton of the progress variable (Figure 5.3.5.1-1), in order for the PDF to meet the required normalization condition

$$\int_1^0 P(c)\, dc = 1 \,. \tag{5.3.49}$$

A Gaussian distribution is given by

$$P(c) = \frac{1}{\sigma\sqrt{2\pi}} e^{-\frac{1}{2}\left(\frac{c-\mu}{\sigma}\right)^2} , \tag{5.3.50}$$

with the two parameters μ and σ determining the specific shape. The relation to the mean flow is achieved by taking into account that the first and second (central) moments of the distribution of the reaction progress c; that is, mean $\overline{c}$ and variance $\overline{c'^2}$ are defined in connection with the PDF:

$$\overline{c} = \int cP(c)\, dc \tag{5.3.51}$$

and

$$\overline{c'^2} = \int (c - \overline{c})^2 P(c)\, dc \,. \tag{5.3.52}$$

Provided that, in addition to the mean reaction progress $\overline{c}(\mathbf{x}, t)$, which is one of the flow variables anyway, $\overline{c'^2}(\mathbf{x}, t)$ is also known from the solution of the flow field; the two equations above determine μ and σ appropriately, so that $P(c; \mathbf{x}, t)$, required in Equation (5.3.48), is defined. Therefore, the solution of an additional balance equation for $\overline{c'^2}$ is required. This equation can be derived from the balance equations for c and $\overline{c}$.

In order to speed up the calculation procedure, the combustion model makes use of the fact that the region of definition of c is restricted between 0 and 1 and that $\overline{c'^2}$ is bounded, too:

$$0 \leq \overline{c'^2} \leq \overline{c}(1 - \overline{c}) \,. \tag{5.3.53}$$

Therefore, $P(c;\mathbf{x},t)$ can be tabulated as $P(c;\overline{c},\overline{c'^2})$ beforehand, so that the calculation of $P(c)$ during the flow solution is replaced by a simple lookup table procedure.

Regarding the instantaneous reaction rate $w_c(c)$ we have, so far, deliberately remained vague, as it leads us to some demanding difficulties regarding the combustion model. Our first assumption was that one reaction progress variable is sufficient to adequately describe the state of the reaction. Consequently, we can take into account no more than one chemical reaction. We are therefore talking about what in chemical reaction kinetics is known as a one-step global reaction scheme.

The implied difficulties arise as we try to find quantitative data for reaction parameters required in the Arrhenius rate factor such as activation energies and frequency factors. A global reaction scheme can only serve as an approximation of, in fact, a far more complex reaction scheme involving maybe hundreds of elementary reaction steps. Only few contributions in the literature actually state values for these parameters by fitting the results of a calculation with a one-step scheme to some experimental or numerical set-up of greater complexity. Naturally, the results found in this way are not only influenced by the chosen reaction scheme and initial conditions as would be required in our case, but also by varying boundary conditions and even the type of combustion, i.e., premixed versus diffusion flames.

We have, therefore, chosen to determine $w_c(c)$ from the simulation of a simple model flame (one-dimensional, laminar, adiabtic, propagating freely at steady state) taking into account detailed chemical kinetics. For such set-ups, programs such as PREMIX (Kee et al. [5.136]) from the CHEMKIN (Kee et al. [5.137]) suite of codes or INSFLA (c.f. Maas [5.138], Maas and Warnatz [5.139]) exist. These codes account for finite rate chemical kinetics and exact molecular transport mechanisms. Starting from a initialization, the profiles of all involved species over the flame front can be calculated for a flame, propagating in a premixed H_2 in air mixture. From this result the required information regarding w_c can be extracted for discrete water mass fractions, relating w_c to c to give $w_c(c)$.

5.3.5.2 Code validation

Test geometry. The applied PDF combustion model has been validated with measurements performed in explosion tubes of different scale. In this section, an exemplary code validation for a round explosion tube, closed at both ends – ··PHD-Tube, Technische Universität München·· ([5.41,5.71,5.112,5.140 – 5.142]), inner diameter 66 mm, length 6.5 m – is shown. This tube is filled with turbulence-promoting obstacles over a length of 3 m, starting from the ignition spot (round obstacles with a blockage ratio of 60% and a spacing of 185 mm, $l/d \approx 2.8$), in order to accelerate the flame rapidly. The mesh for the explosion tube used by the numerical simulation is based on a block-structured topology. Figure 5.3.5.2-1 shows the mesh of the explosion tube, used for this test calculation. This mesh consists of about 6700 control volumes. In order to avoid degenerated cells in the centre of the tube, a butterfly topology has been used; that is, a H-grid topology in the centre of the mesh is connected to a surrounded O-grid topology (see Figure 5.3.5.2-1). Because of the symmetry of the investigated problem only one half of the tube is considered. A further reduction is not possible because bouyancy effects have to be taken into account for the investigated combustion regime (13 vol % H_2). In the region where the mixture is ignited, the grid is refined. Since the obstacles are placed only in the first half of the tube, a coarser grid resolution is used behind the last obstacle.

Boundary conditions and initialization. At the walls, slip conditions are defined for the momentum equation. The use of slip boundary conditions is valid in the considered combustion processes because the expansion flow passing through the obstacles placed in the tubes dominates the turbulence production.

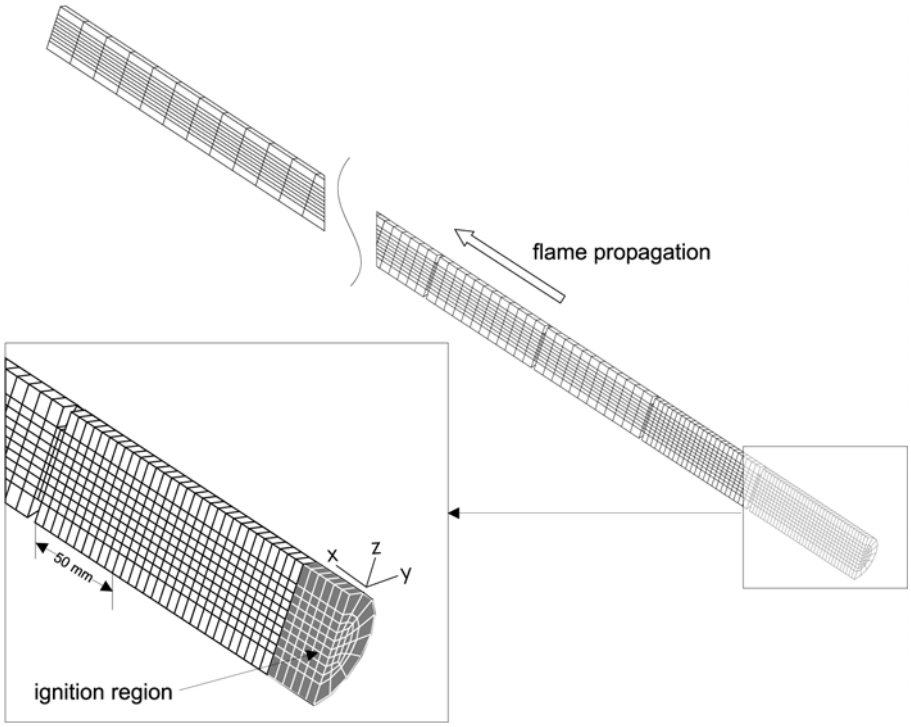

Figure 5.3.5.2-1 Mesh for the PHD tube

Therefore, shear stress at the walls serving as a turbulence promotor can be neglected. Concerning the energy equation, an adiabatic boundary condition is set. Test calculations revealed that the use of a constant ambient wall temperature, which is suggested by Ardey [5.56], has no significant influence on the combustion simulation.

It is often suggested that when combustion simulations in closed facilities are being done that an ignition model be used (e.g. [5.130]) in order to get a good approximation of the startup process, and to overcome the problem of the initialization of an existing flame front and the flow field involved. Further in the verification process and the comparison with experimental data, the ignition process has been found to be insignificant for the investigated geometries. For the initialization of the combustion process, a preburnt area in the ignition region (see Figure 5.3.5.2-1) is defined. In this region the value for the reaction process is set to $\tilde{c} = 1.0$ (fully burnt) and the temperature to the corresponding value.

Numerical control. In principle, the time resolution should be chosen in a way that it is possible to resolve the occuring pressure waves. With respect to the grid resolution, the time step should be of the magnitude

$$\Delta t < \frac{\Delta x}{a_0}\,, \tag{5.3.54}$$

where a_0 is the speed of sound in front of the flame (unburnt gas). In combustion simulations pressure waves occur, which possibly propagate much faster than the speed of sound a_0. The time step has to be adjusted to take into account the expected propagation speed of the pressure wave and the flame front. This is an absolute necessity if the numerical solution of the flow field is calculated explicitly for reasons of the stability of the solution process. In the case of an implicitly calculated flow field, the time step can be set higher with the consequence that pressure waves are not clearly resolved. In the performed

combustion simulations, the time step has been chosen to be $\Delta t = 2 \cdot 10^{-5}$s.

Comparison of calculation and experiment. A comparison between the flame propagation measured in the experiments and the calculation revealed a significant difference, which is shown in Figure 5.3.5.2-3. The calculated flame speed is considerably slower compared with the measurement. The difference can be explained by the flame propagation: The maximum measured flame speed is of the magnitude of 600 m/s. By the fact that this is a supersonic propagation related to the initial mixture, a direct interaction of the flame front and the induced pressure wave is taking place. In the case of the 13 vol % H_2 in air combustion process in the explosion tube, it was observed that after the ignition process and the passing of the first obstacles, the flame front is coupled to the pressure wave because of the strong acceleration of the flame in this region. In Figure 5.3.5.2-2 the described coupling is shown at a position of $x = 2.25$ m. After passing the last obstacle, the flame decelerates and a decoupling of the pressure wave occurs. This behaviour can be seen in the lower picture of Figure 5.3.5.2-2 where the flame front and the pressure distribution are shown over time at the position $x = 4.25$ m, which is located in the second half of the tube.

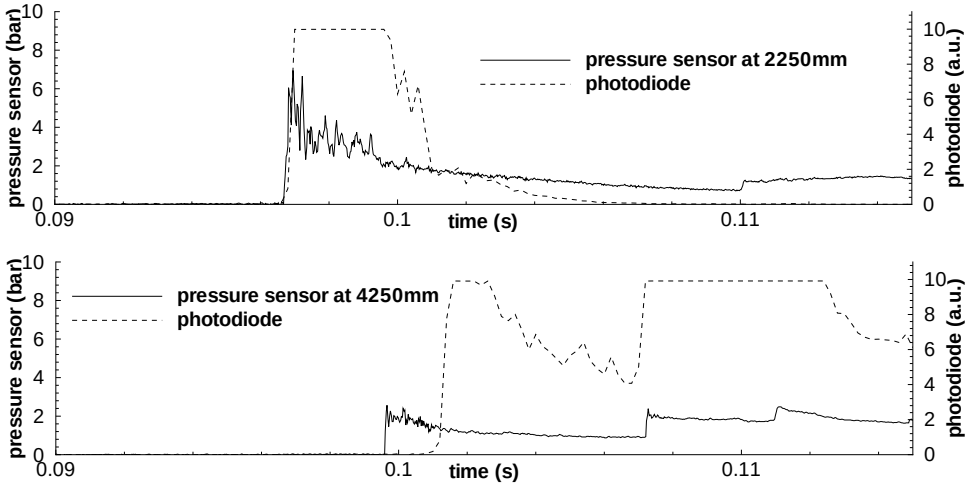

Figure 5.3.5.2-2 Flame-front and pressure-wave interaction in the PHD-tube (13 vol % H_2 in air combustion process)

The coupling of the flame front and the pressure wave has the consequence that the flame is burning into a mixture with a thermodynamic state, which is different from the initial conditions of $T_0 = 293.0$ K and $p_0 \approx 1$ atm. In this case the combustion takes place in an area that is due to the compressing effect of the shock wave characterized by a higher pressure and enthalpy level, which causes significant higher reaction rates. For the initialization with a higher pressure and enthalpy level, a pressure of $p_0 = 6$ bar and a temperature of $T_0 = 488$ K have been chosen. The pressure level is extracted from the measurements and the temperature is calculated by assuming an isentropic change of the thermodynamic state. This leads to an increase of the reaction rate in the range of about an order of magnitude. It has to be emphasized that the change of the reaction rate $w_{H_2O}(c)$ has of course a strong influence on the PDF reaction rates.

Because the consideration of changes of the enthalpy and pressure level during one calculation is not yet implemented in the presented PDF model, the following approach is applied: In order to improve the numerical simulation in the part of the tube where the flame is accelerated to its maximum speed, the

calculation is performed with a PDF reaction rate based on the actually occuring pressure and temperature level. It has to be emphasized that the definition of these levels is a very rough approximation but is appropriate enough to prove the assumptions. Of course, this strategy will lead to an overestimation of the reaction rate during the startup process and the end of the combustion process but will be a good approximation if the flame front is coupled to the pressure wave.

In Figure 5.3.5.2-3 the calculated flame propagation based on the modified PDF reaction rates is shown. It can be seen that within the startup process the flame speed is overestimated. This originates on the one hand because of the initialization and on the other hand because of the earlier described overestimation of the reaction rate in this region. Comparing the region from 1 m to 3 m distance from the ignition point, a good agreement between the calculation and the experiment can be seen. The maximum flame speed is well predicted with the calculation. In this region, the assumption of the coupling of the flame front and the pressure wave is valid. After passing the last obstacle (at $x = 3$ m) the calculated PDF reaction rate overestimates the real reaction rate and, therefore, the flame speed is not predicted accurately. The simulation was performed up to the time when the flame front reached the end of the tube.

For the comparison of the pressure distribution over the time of the calculation and the experiment, the position $x = 2.25$ m is chosen. As can be seen in Figure 5.3.5.2-4 the pressure level and distribution behind the maximum peak is well predicted. But the calculation is not able to predict the maximum pressure peak because the chosen resolution in time (time step size of $\Delta t = 2 \cdot 10^{-5}$ s) and space ($\Delta x \approx 0.04$ m) is not accurate enough.

In Figure 5.3.5.2-5 the flame front and the concerning turbulence field are depicted in the range of 2.5 m $\leq x \leq 3.0$ m of the PHD tube during the combustion process. It can be seen that because of the propagation of the flame front with a velocity faster than the speed of sound of the initial mixture, the turbulence field is induced together with the arrival of the flame front.

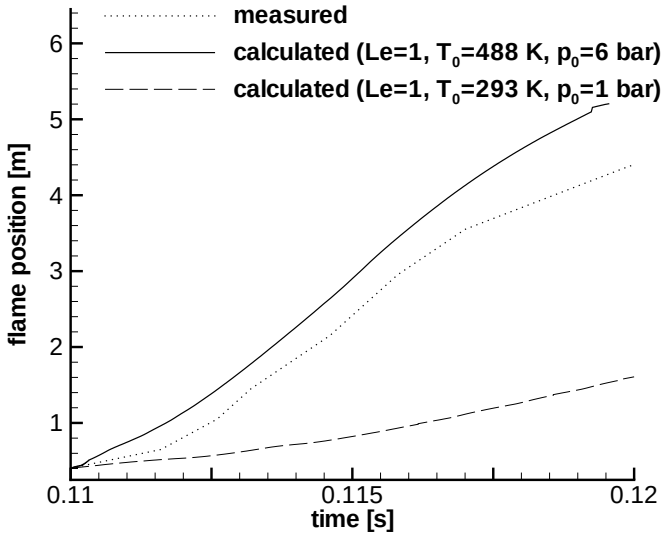

Figure 5.3.5.2-3 Comparison of experimentally determined data with numerical calculations of the flame propagation in the PHD tube for a 13 vol%-H_2 in air mixture

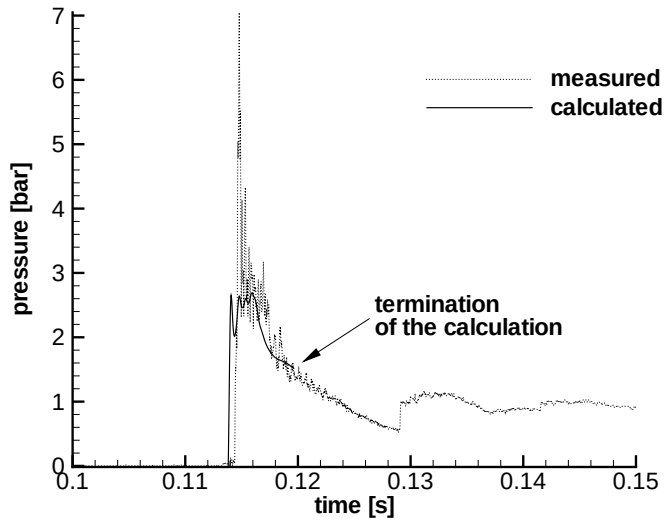

Figure 5.3.5.2-4 Comparison of the pressure distribution between experiment and calculation

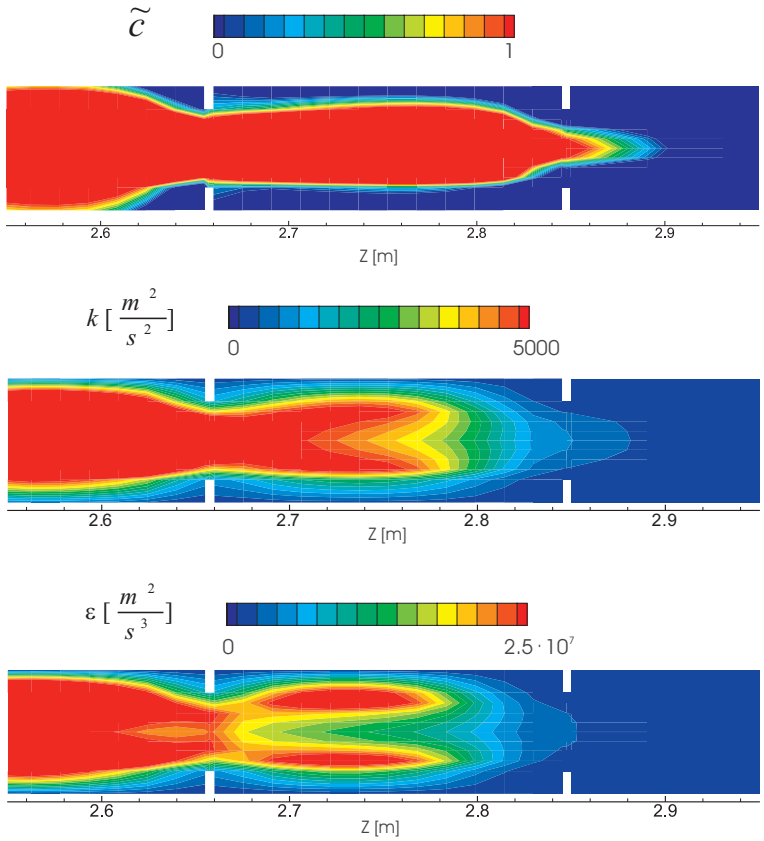

Figure 5.3.5.2-5 Flame-front and the turbulence field during the combustion process in the PHD tube (13 vol % H_2 in air)

5.3.6 Model Clusters with Specialized Tools for Specific Tasks[*]

5.3.6.1 High-performance computing capabilities

Numerical simulations of reacting flows in complex geometries (e.g., associated with hot jet ignition, flame acceleration, or explosion phenomena) have shown that significant computer resources are necessary, to resolve different time and length scales of the physical processes involved [5.143 – 5.146]. Therefore, new versions of reactive Navier-Stokes and Euler flow solvers have been developed for high-performance computing (HPC) with parallel processing capabilities, including pre- and post-processing with an advanced visualization based on tools such as PATRAN, AVS, etc. In order to investigate the capabilities of HPC, a computer complex consisting of several supercomputers (CRAY-T90/T3E/J90) with parallel vector processing (PVP) and massively parallel processing (MPP) was established at the Research Center Jülich (FZJ); the computer complex is integrated into a connecting high-speed network (gigaring). Depending on the specific computer platform with shared or distributed memory, different parallelization concepts of reactive field codes have been realized, especially in the massively parallel mode. Effective parallelization routines are available for load balancing, synchronization, and communication of the allocated processors, e.g., see [5.147] and [5.148].

In order to cover a wide range of combustion modes, several field codes are applied at this computing cluster, each being specific for describing a particular phenomenon:

- the *CFX code* from AEA Technology Ltd. with an implemented eddy dissipation concept for the simulation of hydrogen deflagrations within complex geometries;
- the *AIXCO-2D* code with a flamelet concept for the simulation of a DDT process ahead of the flame with shock wave reflection and auto-ignition processes;
- the *DET-2D* code with a global reaction model for the simulation of stable detonation processes in hydrogen-air mixtures; and
- the *IFSAS-2/3D* code with an induction time model for describing both, shock ignition and detonations of single- and multi-phase flows as well as fluid-structure calculations.

For a detailed description and classification of these codes, refer to the references listed in Table 5.4.0-1.

More recently, first standard versions of reactive field codes have been established on massively parallel supercomputers with promising test results, as follows: First, the reactive Navier-Stokes flow solver code CFX-5 with combustion modelling was ported to the T3E using domain decomposition and PVM (parallel virtual machine) tools ([5.149], [5.150]). Second, the reactive Navier-Stokes flow solver code AIXCO with the flamelet concept was restructured on the T3E using multi-block grids and MPI tools (message passing interface). Third, the reactive Euler solver code DET with high-speed combustion modelling was optimized on the T3E using HPF tools (high-performance FORTRAN). These new parallel code versions showed in tests cases for slow, fast, and rapid flames a proper performance, quite good speed, and scaling with increasing number of processor nodes and grid sizes, [5.151]. For example, Figure 5.3.6.1-1 displays the measured performance of the DET code for parallel processing on the T3E with nearly linear speeding up to 100 processor nodes. In this test case 500 000 cells were used for a fine grid resolution of a detonation wave propagating over obstacles in a channel.

[*] Contributed by Dr. W. Rehm, Research Center Jülich/Forschungszentrum Jülich (FZJ), Germany

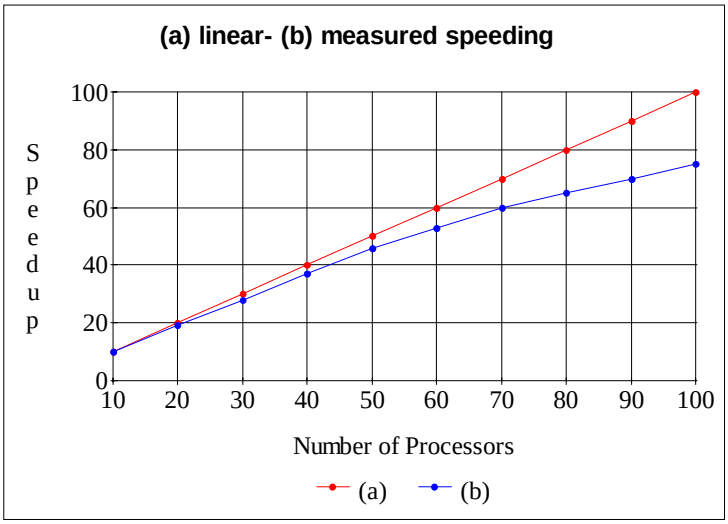

Figure 5.3.6.1-1 Parallel performance of the reactive Euler solver DET-2D/HPF on the CRAY-T3E for a detonation test case in a channel with obstacles using 500000 cells

5.3.6.2 Specific studies and sample-of-proof tests

The complexity of explosion phenomena may involve many combustion processes ranging from deflagrations to detonations, producing static or dynamic loadings on the safety enclosure, which depend on the mixture sensitivity and the geometrical configuration. For the safety analysis of accidental consequences, special numerical models have been accomplished for specific studies related to DDT phenomena, introducing high-performance computations with parallel processing. The modern field code cluster (MFCC) used comprises special reactive Navier-Stokes solvers as well as reactive Euler solvers, which were tested in combination on coarse- and fine-grid levels. As a sample of proof tests, benchmark calulations were performed for integral large-scale explosion tests of the RRC in Moscow (RUT Facility, see Figure 5.2.3.2-30) and for detailed small-scale laboratory tests of the Shock Wave Laboratory in Aachen, ([5.51], [5.152]). For the RUT Test Facility, the following specific post-test analyses were produced for combustion modes in hydrogen-air mixtures in the range 10-15-20 vol % H_2 [5.118]:

- Deflagration mode: turbulent flame acceleration over obstacles with flame velocities in the range 250-500-1000 m/s;
- Transition mode: DDT with shock wave focusing and auto-ignition conditions for mild and strong limits between 850 and 1200 K;
- Detonation mode: Ignition with detonation propagation and resulting pressure and impulse history in different positions up to 50 to 75 bar.

Flame acceleration. Three-dimensional simulations were performed using the CFX code for the flame acceleration over repeated obstacle arrays (35 m x 2.25 m x 2.5 m) with the flame propagation into the cavity (10.55 m x 2.5 m x 6.25 m) and into the outlet channel (25 m x 2.25 m x 2.5 m), whereby the

RUT-23 test was modelled with 11 vol % H_2 in air and 30% to 60% BR. The turbulent combustion model (RNG/EDC) was fine-tuned concerning the empirical constants in the reaction parameters of the source term. Examples of pressure and temperature contours are shown in Figure 5.3.6.2-1 for a simplified 2D simulation. These CFX results were compared with the AIXCO-2D results, which are based on the flamelet model with flame tracking and an empirical burning law. Both codes are in good qualitative agreement and agree quantitatively quite well with the measurements, concerning the flame velocity in the first channel and the pressure-time history in the cavity (e.g., see Figure 5.3.6.2-2). The mean grid resolution was of the order of 10 cm (flame quenching and re-ignition were not simulated in these tests).

DDT conditions. Based on the above reference cases, conditions for defagration- to-detonation transition were analyzed in more sensitive hydrogen-air mixtures. For this purpose, the code AIXCO-2D was adapted to the RUT-22 test with 14 vol % H_2 in air and 60% BR. In the numerical simulation, the flame propagated as a deflagration with about 800 m/s from the channel into the cavity. A transition from deflagration to detonation can occur by shock wave focusing and auto-ignition in the unburnt gas ahead of the flame (i.e., in preconditioned fresh gas pockets). The numerical results showed that the calculated shock reflection temperatures approach the auto-ignition conditions with increasing mixture sensitivity or grid resolution. For this reason, separate grid refinement studies were performed applying the IFSAS code and using adaptive mesh refinement with a maximum resolution in the cavity of the order of 1 mm. In this way, it is in principle possible to resolve DDT processes as far as shock wave focusing with auto-ignition and detonation propagation for various initial and boundary conditions are concerned. Typical test results are shown in Figure 5.3.6.2-3 for shock wave collision in the corner of the cavity and initiation of detonation in a 15 vol % H_2-air mixture, assuming a sustainable propagation.

Gas dynamic effects. In paramter and sensitivity studies, the gas dynamic effects on auto-ignition conditions were analyzed, using the parallel code DET with fine grid resolution in the cavity and the outlet channel of the order of 1 cm. The inlet conditions were specified at the end of the acceleration channel entering into the cavity and were varied in a wide range for the inlet parameters: pressure, velocity, and temperature. These test results reveal that high reflected shock pressures between 30 and 40 bar (factor 5) are necessary to reach auto-ignition temperatures between 850 and 1200 K in a 15 vol % H_2-air mixture. Figure 5.3.6.2-4 shows the reflected shock wave temperatures versus time in two corners of the cavity. The parameter is the inlet velocity of the burnt gas with 7.5 bar and 1000 K for an unburnt gas at 1 bar. The sequential combination of the parallel AIXCO code (Navier-Stokes solver) with the parallel DET code (Euler solver) via an interface allows the numerical simulation of DDT conditions for flame acceleration, shock ignition, or hot jet ignition at different model levels with grid refinement. In sensitivity studies with the parallel DET code, it was observed that the cavity can burn out rapidly by DDT and that a supersonic flame enters into the outlet channel. In addition, multiple ignitions can occur in the cavity. It was found that a DDT near a corner produces higher pressures but lower impulses compared with a DDT far from a corner in the cavity and vice-versa (turbulent mixing triggering DDT was not taken into account in these studies).

Ignition aspects. An important aspect for the onset of detonation concerns the sufficient resolution of the shock wave collision in correlation with the ignition process for detonation formation in H_2-air mixtures at ambient conditions. Strong and mild ignition processes were observed in shock tubes, whereby measured ignition delay times are not consistent with theoretical predictions in the low-temperature regime. The measured ignition delay times can be used for fitting reaction kinetic data. In a first step, a global reaction model with induction delay was implemented in the parallel Euler code DET with modified Arrhenius parameters and validated with shock tube experiments, performed at SWL-Aachen. Ignition delay times were measured in a 15% hydrogen-air mixture in a quadratic shock tube (5.4 cm x

6.4 m), using a plane end wall with a narrow gap (e.g., similar to the RUT geometry on a small scale). The numerical simulation was performed with a fine grid resolution of the order of 0.5 mm and resulted in a reasonable qualitative and quantitative agreement with the measurements for strong ignition behind the normal reflected shock. The CJ detonation velocity was about 1550 m/s. Characteristic numerical schlieren pictures (i.e., density gradients) for the DDT experiment are shown in Figure 5.3.6.2-5. The comparison of measured and calculated pressure transients is presented in Figure 5.3.6.2-6.

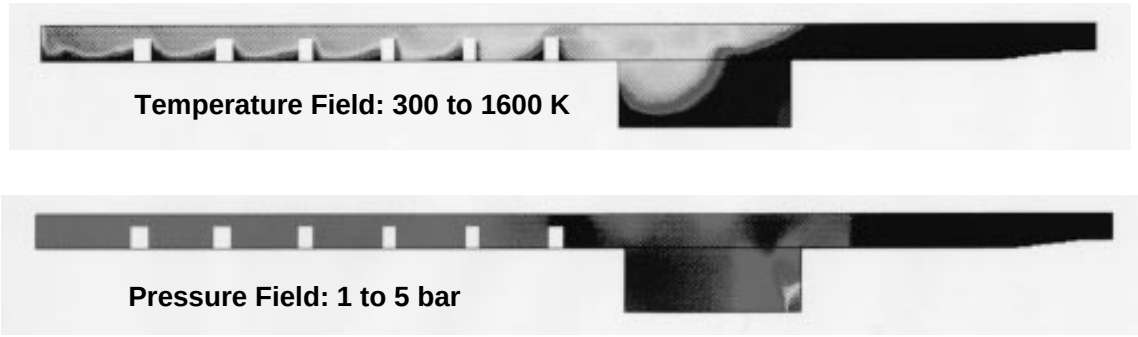

Figure 5.3.6.2-1 CFX temperature and pressure contours of the RUT-23 deflagration test with 11% hydrogen in air at NTP and BR = 60% at about 1 s

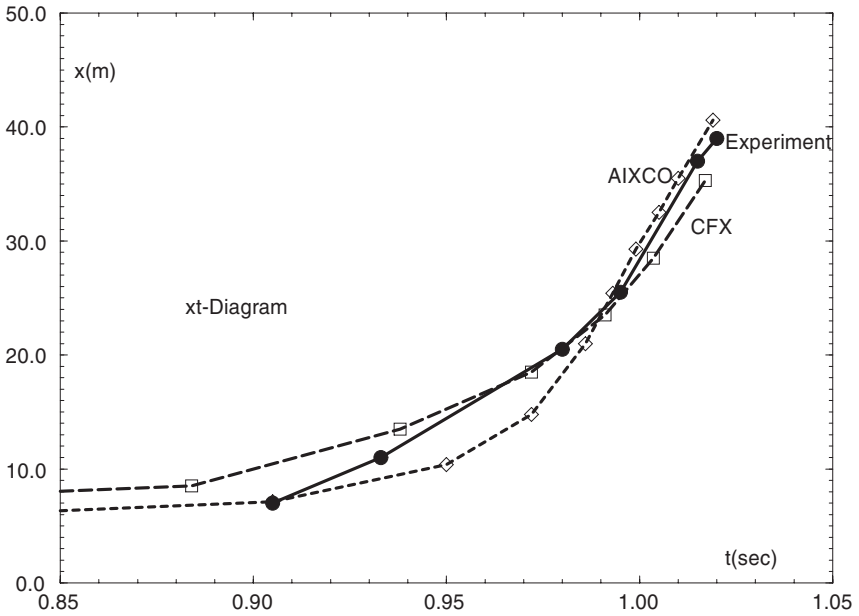

Figure 5.3.6.2-2 Comparison of experimental and numerical results with the codes CFX and AIXCO for RUT-23 deflagration test with 11% hydrogen in air at NTP and BR = 60%

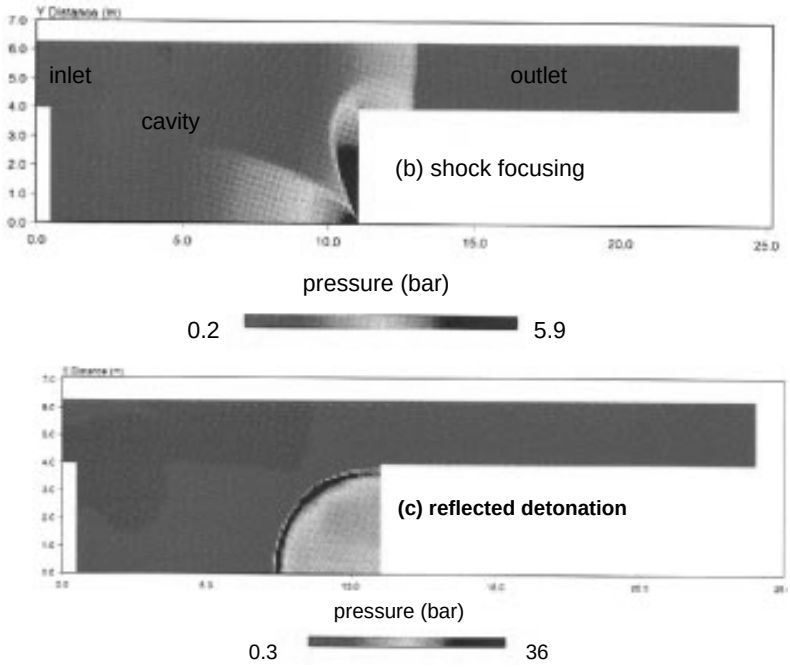

Figure 5.3.6.2-3 Pressure contours of the IFSAS code for transition from deflagration-to-detonation by shock wave focusing with auto-ignition in the RUT cavity (15% hydrogen)

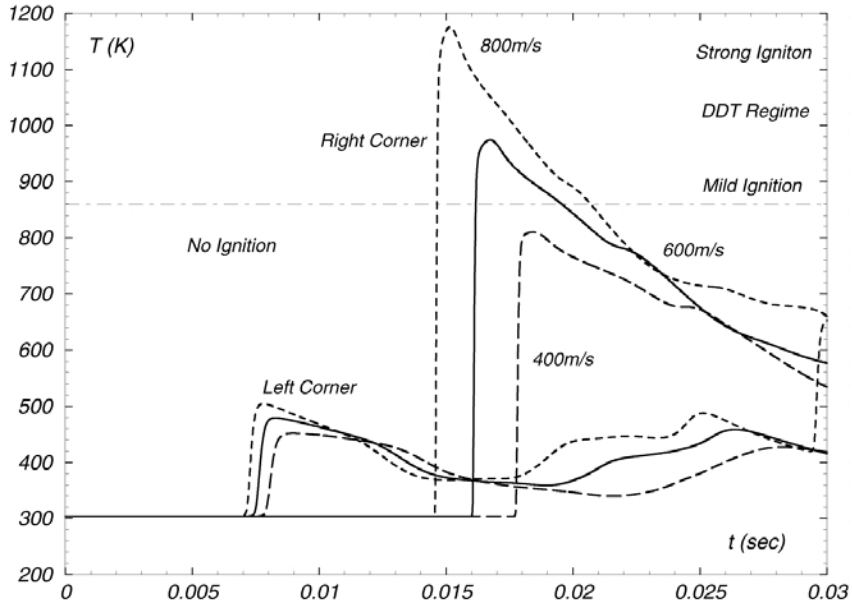

Figure 5.3.6.2-4 Parameter study of the parallel DET code for DDT conditions by shock wave focusing for mild and strong ignition temperatures in two corners of the the RUT cavity (15% H_2-air at NTP for p(in) = 7.5 bar, T(in) = 1000 K) and v(in) as parameter

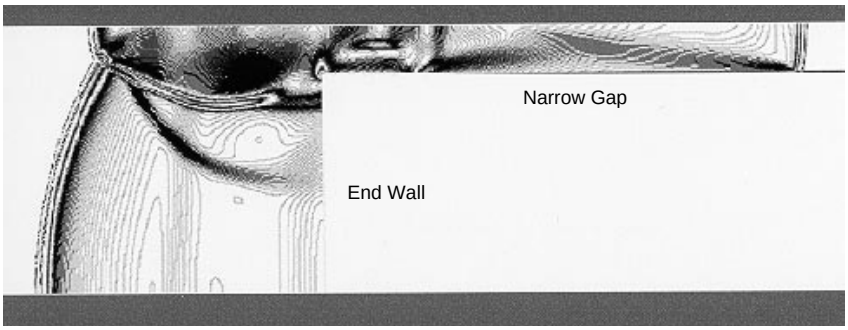

Figure 5.3.6.2-5 Numerical schlieren picture of the parallel DET code for DDT experiments in a quadratic shock tube with a narrow gap performed at SWL (15% H_2)

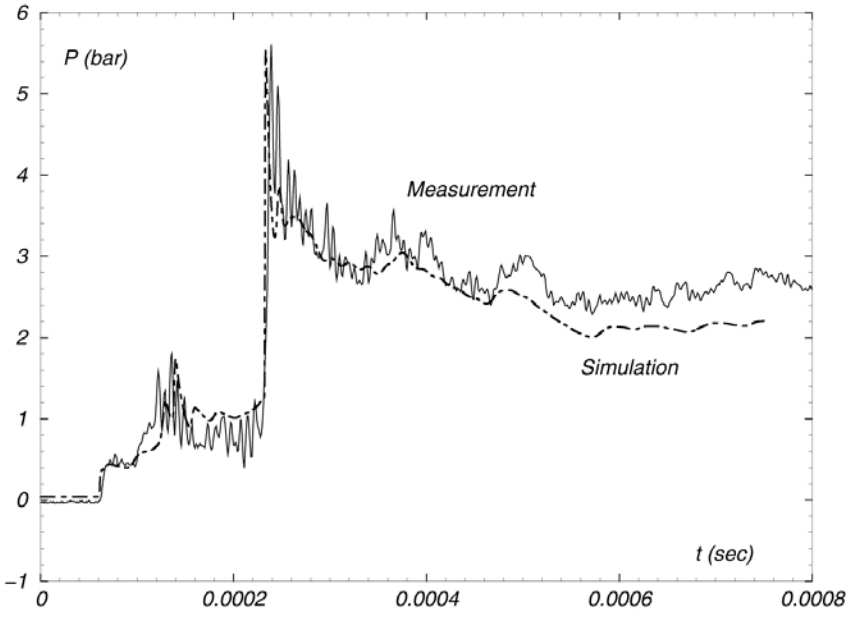

Figure 5.3.6.2-6 Comparison of experimental and numerical pressure transients for strong ignition and detonation formation with the parallel DET code (15% H_2)

5.4 Summary

This chapter has compiled both an overview of available experiments on FA and DDT, which are applicable for code validation, and the validation of the various codes with different levels of complexity.

The experiments presented addressed shock-focusing, flame acceleration, and transition to detonation in obstructed areas, and flame propagation in complex and large-scale geometries with various levels of detail in the instrumentation - all these parameters depend mainly on the size of the facility. At the small-scale facilities, it is possible to investigate the flame propagation highly resolved with different types of transducers or to visualize the flame propagation itself by means of sophisticated optical measurement techniques. A disadvantage of small-scale combustion experiments is the influence of relatively high heat losses and possible boundary layer influences on the combustion process. These influences decrease with increasing scale of the facility. On the other hand, large-scale tests generally do not allow the application of modern optical diagnostic techniques to characterize flow fields or reaction progress. Large-scale experiments usually employ conventional instrumentation such as pressure transducers, photo diodes, thermocouples, and ionization gauges, which provide local information at different points of the test facility. The investigated gas mixtures consisted mainly of dry hydrogen-air or hydrogen-air-steam mixtures. Moreover, the influence of diluents on the combustion process was investigated in some experiments, e.g., CO_2 in the test series conducted in the Battelle Model Containment [5.77 – 5.82].

Our main knowledge of flame acceleration and transition to detonation is based on experimental results from test facilities with volumes in the range of $0.01\ \mathrm{m}^3$ (explosion tubes) up to about $500\ \mathrm{m}^3$ (RUT Facility, Kurchatov Institute) in hydrogen-air-mixtures with and without steam as well as temperatures between ambient and 100^o C. Concerning an accident scenario, elevated initial pressures up to 3 bar are expected. Here, the database is still very poor because only few experiments [5.153] have been conducted.

It appears that the database available today on flame acceleration, local ignition, detonation onset, and shock-focusing contains a wide range of examples covering all relevant major processes. Nevertheless, there are still some unsolved topics as far as re-ignition, quenching, elevated initial pressure, and, in particular, scaling are concerned.

The model validation performed up to date with the described database may be summarized as follows: In the area of flame acceleration lumped-parameter (LP) and CFD approaches have been pursued. The LP class of tools allows rough but quick assessments of possible flame acceleration phenomena in a large number of accident sequences.

In the CFD class of tools, model validation has concentrated on flamelet models, eddy breakup (EBU) and statistical probability density function (PDF) type of combustion models, implemented in Reynolds-averaged Navier-Stokes codes for the simulation of various turbulent combustion regimes. It could be shown that the EBU approach is able to provide reasonable agreement with experimental data, if either free model constants are benchmarked on experiments with different scales [5.128], or a theoretical extension is implemented in the code [5.120], which leads to a model without any free constants.

The validation of the presumed PDF approach [5.129 – 5.131] without any free model constants showed promising results as it could be realized for small- and medium-scale turbulent combustion experiments. A further improvement of both numerical methods and model optimization will allow the application to large-scale problems within a reasonable running time.

Compared to FA, the prediction of DDT events is generally in a much less-advanced stage although the principal mechanisms are mostly understood. It is necessary to discriminate DDT on reflection from the more complicated case of DDT near a turbulent flame brush. Today, CFD tools allow us to reproduce DDT in reflection in small-scale 3D geometries or in medium-scale 2D configurations. It appears that one- or few-step chemistry models are sufficient to reproduce the occurrence and timing of the local explosion and the succeeding detonation propagation. Simulation of DDT in or near a turbulent flame brush is a more complicated problem that still requires substantial development in theoretical models, numerical techniques, and computational resources.

Table 5.4.0-1 List of codes. This list shall only give an exemplary overview of typical codes which are currently applied for the simulation of turbulent combustion or detonations. A very comprehensive list of multi-purpose field codes can be found on the World Wide Web under the URL: http:\\www.cfd-online.com

Code	Reference	Note
Lumped-Parameter Codes		
COCOSYS/(RALOC)	GRS, Germany	
MELCOR	USNRC, USA	
CONTAIN	Sandia National Laboratories, USA	
JERICHO	IPSN, France	
Muphi-Burn	NUPEC, Japan	
Hybrid CFD-Lumped-Parameter Codes		
GOTHIC	Numerical Applications Inc.	
TONUS	CEA, France	
CFD Codes		
FLACS	Christian Michelsen Research	
AutoReaGas	TNO and Century Dynamics Ltd.	
CFX	AEA Technology Ltd., UK	
CFX-TASCflow	AEA Technology Ltd., UK	
EXSIM	Aalborg University Esbjerg, DK	
Fluent	Fluent Inc., USA	
IFSAS	Combustion Dynamics Ltd., Canada	Flow-solver and Fluid-structure interaction
COM3D	Kurchatov Institute, Russia / FZK, Germany	
COMET	ICCM GmbH, Germany	
FIRE	AVL List GmbH, Austria	
Bassim	Battelle IT, Germany	
Gasflow	FZK, Germany	
AIXCO-2D	RWTH-Aachen, Germany	explicit Na-St. solver
DET-2D/3D	FZK and FZJ, Germany	explicit Euler solver
STAR-CD	Computational Dynamics Ltd., UK	
ACE+	CFD Research Corporation, USA	
GLACIER, Banff	Reaction Engineering Int., USA	
PHOENICS	Cham Ltd., UK	

5.5 Nomenclature

a	Sound speed in unburnt mixture
a_0	Sound speed in front of the flame
b, c	Constants
c	Heat capacity
c	Reaction progress
$\tilde{c}$	Reaction process
c_F	Reaction rate constant
d	Tube diameter
d_i, d_0	Diameters of orifice and obstacle
d/λ	DDT limit criterion
f	Stretching factor
i	Specific enthalpy
p_0	Initial pressure of unburned hydrogen-air mixture
k	Constant
k	Turbulent kinetic energy
l	Turbulence integral length scale
l_F	Laminar flame thickness
m_F	Mass fraction of fuel
m_O	Mass fraction of oxidizer
m_P	Mass fraction of products
p	Pressure
s	Step between obstacles
s/δ	Relative step between obstacles
t	Time
u,	Turbulent fluctuating velocity
u'	Turbulence intensity
u_m	Fluid Velocity
u_n	Normal flame velocity
u_v	Visible flame velocity
v	Specific volume
w_{H_2O}	Chance of the reaction rate
x	Running distance
A	Area
A, B, C	Constants
BR	$= 1 - (d_i/d_0)^2 = 1 - F_i/F_0$ – blockage ratio
C	Mole Fraction
D	Diameter
D_{ie}	Threshold Damköhler number

F	Covered area
F/s_f	Ratio of relector covered area to cross-section of the test channel
F_i, F_0	Areas of orifice and obstacle
FF	Flame front
FF_i	Flame front inside
G	Mass flow
$H_{1..5}$	Constants
I	Enthalphy
K	Karlovitz flame stretch factor
L	Flame-front position
L	Integral Length Scale
L	Total length of a channel
L/D	Length-diameter ratio
L_e	Lewis number
L_r	Length of reflector
L_{obs}	Length of obstructed part of a channel
L_{obs}/s	Density (compactness) of obstacles
M, m	Mass
M	Mach number
M_{min}	Minimum Mach number
M_t	Mach number corresponding to the appearance of the self-ignition
M_{tr}	Mach number corresponding to the transient regime of self-ignition
P	Pressure
P_1	Initial pressure
P_4	Maximum pressure reached
Q	Heat
R	Radius of curvature
R_e	Reynolds number
S	Burning velocity
S_L	Laminar flame velocity
T	Temperature
T_0	Initial temperature of unburned hydrogen-air mixture
T_A	Activation temperature
U	Inner energy
V	Volume
W	Volume displacement work
γ	Specific heat
δ	$= d_0$ – tube diameter flame thickness
ϵ	Density radio
ε	Dissipation rate

λ	Detonation cell width
ρ	Density
ρ_b	Density of combustion products
ρ_u	Density of the unburnt mixture
σ	Expansion ratio after burning
η	Dynamic viscosity
τ	Time of existence of zones of increased temperature
τ_i	Ignition delay time
τ_{CH}	Chemical induction time
τ_t	Turbulent time scale
ν	Kinematic viscosity
Θ	Time of chemical reactions
$\%\mathrm{H_2}$	Volume fraction of hydrogen in mixture
$\%\mathrm{H_2O}$	Volume fraction of water steam in mixture
$\%\mathrm{N_2}$	Volume fraction of nitrogen in mixture
$\%\mathrm{CO_2}$	Volume fraction of carbon dioxide in mixture

5.6 References

[5.1] A. Borisov, B. Gelfand and G. Skatchkov, Current topics in shock waves: Ignition of gaseous combustible mixtures in focused shock waves. In: *17th International Symposium on Shock Waves*. American Institute of Physics, New York, 1990, 696–701.

[5.2] B. Gelfand, S. Medvedev and S. Tsiganov, Three cases of shock waves focusing in combustible media. In: *18th International Symposium on Shock Waves*. (K. Takayama, (editor)), Vol. 2. Springer Verlag, 1992, 837–842.

[5.3] B. Gelfand, S. Khomik, S. Medvedev, A. Polenov and W. Breitung, Selfignition of combustible mixture behind shock waves reflected at non-flat surfaces at high initial pressure. In: *20th International Symposium on Shock Waves*, California Institute of Technology, Pasadena, CA, USA. 1995, 251.

[5.4] S. Medvedev, A. Polenov, B. Gelfand and S. Khomik, Experimental evidences on peak temperature at shock wave focusing. In: *20th International Symposium on Shock Waves*, California Institute of Technology, Pasadena, CA, USA. 1995, 131–132.

[5.5] C. K. Chan, Collision of a shock wave with obstacles in combustible mixture. Comb. & Flame, Vol. 100, 1995, 341–348.

[5.6] C. K. Chan, D. Lau, P.A. Thibault and J.D. Penrose, Ignition and detonation initiation by shock focussing. In: *AIP Conf. Proc.: Current topics in shock waves*. (Y. M. Kim, (editor)), American Institute of Physics, New York, USA. 1990, 696–701.

[5.7] A.A. Borisov, B. E. Gelfand and G. I. Skatchkov, Selfignition of gaseous mixtures by focusing of reflected shock waves. Chimicheskaya phisika, Vol. 7, 1988, 1387–1392.

[5.8] C. K. Chan, A. Guerro and D. Mc-Cooeye, Shock induced transition to detonation. In: *Paper at 2nd Canadian / German workshop*, 1993.

[5.9] O. V. Achasov, S. A. Labuda, O.G. Penzijakov and R. M. Puskin, Shock waves initiation of detonation in semiclosed cavity. Chimicheskaya phisika, Vol. 12, 1993, 714–716.

[5.10] M. Rose, P. Roth and U. Uphoff, Ignition of reactive gas by focusing of shock wave. In: *16th ICDERS*, Krakow, Poland. 1997, 554–556.

[5.11] V. Yu. Gidaspov, I. A. Ivanov and I. A. Krinkov, Numerical modeling of detonation in focusing channel. Mathematical modeling, Vol. 4, 1992, 85–88.

[5.12] B. E. Gelfand and W. Breitung, Detonation ignition characteristics of H_2 + Air mixtures under conditions of shock focusing. Inst. of Chemical Physics, RAS & Inst. Neutronenforschung und Reaktortechnik, FZK, , 1993.

[5.13] B. E. Gelfand and W. Breitung, Complete experimental investigation of shock wave focusing phenomena in H_2 + Air mixtures with additives. Inst. of Chemical Physics, RAS & Inst. Neutronenforschung und Reaktortechnik, FZK, , 1994.

[5.14] B. E. Gelfand, S. V. Khomik, S. P. Medvedev, A. N. Polenov, A. M. Bartenev, W. Breitung and A. Veser, Investigation of hydrogen +air fast flame propagation in tubes with multidimensional endplates. In: *Proc. Intl. Symp. on hazard, prevention and mitigation of industrial explosions*, Vol. 2, Safety Cons. Eng., Schaumburgh Ill., USA. 1998, 434 – 456. see also:

Abstracts of Intern. Colloq.: Advances in experimentation / computation of detonation, ENAS Publ., 1998, p. 65.

[5.15] B. E. Gelfand, A. N. Polenov, S. P. Medvedev, S. W. Khomik, A. M. Bartenev and H. Groenig, The selfignition of homogeneous gaseous mixtures near nonflat surfaces. Dokl. RAS, Vol. 359, 1998, 490–493.

[5.16] M. Rose, P. Roth and U. Uphoff, AMR calculation of ignition and detonation formation in reactive gas by shock wave focusing. In: *Abstracts of Intern. Colloq.: Advances in experimentation / computation of detonation*. ENAS Publ., 1998, 17–18.

[5.17] A. M. Bartenev, B. E. Gelfand, S. P. Medvedev, , A. N. Polenov, S. W. Khomik, H. Groenig and H. Olivier, Numerical modeling of ignition and detonation under focusing conditions. In: *Abstracts of Intern. Colloq.: Advances in experimentation / computation of detonation*. ENAS Publ., 1998, 26–27.

[5.18] B. E. Gelfand and W. Breitung, DDT experiments with focusing of H_2 + Air blast waves. Inst. of Chemical Physics, RAS & Inst. Neutronenforschung und Reaktortechnik, FZK, , 1998.

[5.19] G. Ciccarelli, Critical tube diameter measurements in high-temperature hydrogen-air mixtures. FIN L-1924, , 1998.

[5.20] B. E. Gelfand, O. Popov, S. P. Medvedev and S. W. Khomik, The features of hydrogen+oxygen mixture selfignition at high pressure. Dokl. RAS, Vol. 349, 1996, 482–485.

[5.21] B. E. Gelfand, O. Popov and S. W. Khomik, Selfignition of hydrogen-air mixtures at high pressure. Dokl. RAS, Vol. 330, 1993, 457–459.

[5.22] R. Blumental, K. Fieweger, G. Adomeit, B. E. Gelfand and K. Komp, Self-ignition of hydrogen + air mixtures at high pressure and low temperature. In: *20th International Symposium on Shock Waves*, CalTech, Pasadena, CA, USA. 1995, 175–176. See also, Shock Waves, 1996, vol.2, World Sci., p. 935-940.

[5.23] B. Gelfand, O. Popov, A. Kusharin, G. Agafonov and W. Breitung, High-temperature self-ignition and detonation of hydrogen+air mixtures with NO_x additives. In: *Proc. 15th ICDERS*, Boulder, Colorado, USA. 1995, 473–475.

[5.24] B.E. Gelfand, O. E. Popov, S. P. Medvedev, S. V. Khomik, A. Yu. Kusharin and G. L. Agafonov, Self-ignition of hydrogen-oxygen mixtures at high pressure. In: *CD-ROM Proc. 21st Inti. Symp. on Shock Waves*, 1997, paper 2400.

[5.25] B.E. Gelfand and W. Breitung, Measurement of hydrogen-air ignition length under severe accident conditions. In: *Proceed. Engl.-Germ. Symp. on combustion*, 1993, 419–420.

[5.26] R. Blumental, K. Fieweger and G. Adomeit, Self-ignition of hydrogen+air mixtures. In: *Paper at 11th World Hydrogen Energy Conference*, 1996.

[5.27] R. Blumental, K. Fieweger, K. Komp and G. Adomeit, Gas dynamic features of self-ignition of non-diluted fuel / air mixtures at high pressure. Comb. Sci. and Technol., Vol. 113/114, 1997, 137–166.

[5.28] J. Lu, A. K. Gupta, A. A. Pouring and E. L. Veating, A preliminary study of chemically enhanced auto-ignition in an internal combustion engine. In: *Proc 14th ICDERS*, Vol. 1, Coimbra, Portugal. 1993, 1–10.

[5.29] A. V. Eremin, V. Yu. Velikodny and V. S. Ziborov, Nonequilibrium of H2 / O2 mixtures in the weak wave front. In: *Proc 16th ICDERS*, Crakow, Poland. 1997, 597.

[5.30] C. Viguier, D. Desbordes, L. F. Figuera Da Silva and L. Guerrad, Oblique shock wave induced supersonic combustion and oblique detonation in H2 / air and H2 / O2 mixtures. In: *2-nd Intern. meeting: properties of reactive fluids and their application to propulsion*, ENSMA, France. 1996.

[5.31] B. E. Gelfand and W. Breitung, Measurement of H2 + Air ignition length under severe accident conditions. Inst. of Chemical Physics, RAS & Inst. Neutronenforschung und Reaktortechnik, FZK, , 1992.

[5.32] B. E. Gelfand and W. Breitung, Investigation of spontaneous detonation ignition under non-uniform pressure and temperature conditions. Inst. of Chemical Physics, RAS & Inst. Neutronenforschung und Reaktortechnik, FZK, , 1993.

[5.33] B. E. Gelfand and W. Breitung, Measurements and prediction of detonation of H2 + H2O +Air mixtures with accident relevant additives (CO, CO2, NOx). Inst. of Chemical Physics, RAS & Inst. Neutronenforschung und Reaktortechnik, FZK, , 1994.

[5.34] B. E. Gelfand and W. Breitung, Suppression of explosive phenomena by CO2 admixing. Inst. of Chemical Physics, RAS & Inst. Neutronenforschung und Reaktortechnik, FZK, , 1996.

[5.35] C. Viguier, L. F. Figuera Da Silva, D. Desbordes and B. Deshaies, Onset of oblique detonation waves. In: *26th Intl. Symp. on Combustion*. The Combustion Inst., Pittsburgh, USA, 1996, 3023– 3031.

[5.36] D. L. Baulch, C. J. Cobos, R. A. Cox R.A., C. Esser, P. Frank, Th. Just, J. A. Kerr, M. J. Pillig, J. Troe, R. W. Walker and J. Warnatz, Evaluated kinetic data for combustion modelling. J. Phys. Chem. Ref. Data, Vol. 21, 1992, 411–736.

[5.37] H. G. Wagner, personal communication. 1997.

[5.38] G. Ciccarelli, J. L. Boccio, T. Ginsburg, C. Finfrock, L. Gerlach, K. Sato and A. M. Kinoshita, High-temperature hydrogen+air+steam detonation experiments in the BNL small - scale development apparatus. BNL-NUREG-52414, NUREG/CR - 6213, , 1994.

[5.39] R. J. Kerr, CHEMKIN - II: A fortran chemical kinetic package for analysis of gas-phase chemical kinetics. Sandia Nat. Lab. Report: SAND 89-8001, , 1989.

[5.40] F. Mayinger, G. Strube and R. Beauvais, Derzeitiger Wissenstand über den Verlauf der Grenze für den Deflagrations-Detonations-Übergang (DDT) im Dreistoff-Diagramm [Current knowledge about deflagration to detonation transition (DDT) in the trenary mixture diagram]. TU München, Abschlussbericht, BMU-SR-403, , 1988.

[5.41] F. Mayinger and N. Brehm, Grenze für den Übergang von der Deflagration in die Detonation (DDT) in H_2-Luft-Wasserdampf–Gemischen [Limit for the transition from deflagration to detonation (DDT) in H_2-air-steam mixtures]. TU München, Abschlussbericht, BMFT 150 0712 4, , 1988.

[5.42] J. H. S. Lee, R. Knystautas and A. Freiman, High speed turbulent deflagration and transition to detonation in H_2 + Air mixtures. Comb. & Flame, Vol. 56, 1984, 227–239.

[5.43] W. Breitung, P. Royl and A. Veser, Results of hydrogen behaviour and mitigation in severe PWR accidents. FZTU Karlsruhe, Report 5914, , 1997.

[5.44] F. Mayinger and G. Strube, Struktur und Brenngeschwindigkeiten hochturbulenter Wasserstoff-flammen [Structure and burning velocity of highly turbulent hydrogen-air flames]. TU München, Abschlussbericht, BMTF-GRS-150 0769, , 1990.

[5.45] F. Mayinger and N. Brehm, Zündgrenzen von Wasserstoff in aerosolhaltiger Atmosphäre [Ignition limits of hydrogen in an aerosol atmosphere]. TU München , Abschlussbericht , BMTF-GRS-15006150, , 1987.

[5.46] B. E. Gelfand and W. Breitung, Laminar and turbulent flame propagation in H_2 / Air / Steam mixtures at accident relevant pressure and temperature conditions. Inst. of Chemical Physics, RAS & Inst. Neutronenforschung und Reaktortechnik, FZK, , 1995.

[5.47] R. Beauvais, F. Mayinger and G. Strube, Severe accident in a light water reactor influence at elevated initial temperature on H_2 combustion. In: *2nd ASME-JSME conference*, Vol. 1, 1993, 425–433.

[5.48] R. K. Kumar and E. M. Bowles, Flame acceleration in H_2 / air / steam mixtures in the presence of repeated obstacles in a closed volume. In: *CEC-Workshop "Hydrogen behaviour and mitigation in water-cooled nuclear power reactors"*. European Commission, Brussels, Belgium, 1992, 129–140.

[5.49] R. K. Kumar, Combustion of H_2 / Air / steam mixtures in presence of repeated obstacles in a confined volume. Comb. Sci. and Technol., Vol. 126, 1997, 23–52.

[5.50] B. E. Gelfand and W. Breitung, Investigation of H_2 + Air fast flame propagation and DDT in tube with multidimensional endplates. Inst. of Chemical Physics, RAS & Inst. Neutronenforschung und Reaktortechnik, FZK, , 1997.

[5.51] S. B. Dorofeev, V. P. Sidorov and A. B. Dvoinishnikov, DDT in large confined volumes of lean H_2 + Air mixtures. Comb. & Flame, Vol. 104, 1996, 95–110.

[5.52] C. K. Chan and W. A. Dewitt, DDT in end gases. In: *26th Intl. Symp. on Combustion*. The Combustion Inst., Pittsburgh, USA, 1996, 2679–2684.

[5.53] G. Ciccarelli, J. L. Boccio and T. Ginsberg, The influence of initial temperature on flame acceleration and DDT. In: *26th Intl. Symp. on Combustion*. The Combustion Inst., Pittsburgh, USA, 1996, 2973–2979.

[5.54] G. Ciccarelli, J. L. Boccio, T. Ginsberg, C. Finfrock, L. Gerlach, H. Tagawa and A. Malliakos, The effect of initial temperature on flame acceleration and DDT phenomenon. NUREG/CR-6509, BNL-NUREG-52515, , 1998.

[5.55] G. Ciccarelli, J. L. Boccio, T. Ginsberg, C. Finfrock, L. Gerlach, H. Tagawa and A. Malliakos, The effect of lateral venting on DDT in hydrogen - air - steam mixtures at various initial temperatures. NUREG/CR-6524, BNL-NUREG-52518, , 1998.

[5.56] N. Ardey, *Struktur und Beschleunigung turbulenter Wasserstoff-Luft-Flammen in Räumen mit Hindernissen [Structure and acceleration of turbulent hydrogen-air flames in obtacle obstructed rooms]*. PhD thesis, Technische Universität München, 1998.

[5.57] N. Ardey and F. Mayinger, Einfluß Containment-typischer Strömungshindernisse auf die Ausbreitung trubulenter Wasserstoff-Luft-Flammen [Influence of containment typical obstacles on the propagation of turbulent hydrogen-air flames]. Abschlußbericht zum Forschungsvorhaben BMFT, Nr. 150 0957, TU München, , 1998.

[5.58] A. Eder and M. Jordan, Application and Potentials of Optical Measurement Techniques for the Investigation of Transient Combustion Phenomena. In: *Applied Optical Measurement Techniques*. (D. Mewes and M. Lehner, (editors)). Springer-Verlag, Heidelberg, 1999.

[5.59] F. Mayinger, (editor), *Optical Measurement Techniques*. Springer-Verlag, Heidelberg, 1994.

[5.60] A. Eder, M. Jordan and F. Mayinger, Einfluß von hindernis-induzierter Turbulenz auf die Beschleunigung von H2- und CH4-Luftflammen in geschlossenen Behältern [Influence of turbulence due to obstacles on the acceleration of H2- and CH4-air flames in closes vessles]. In: *Proc. der 6. Fachtagung Lasermethoden in der Strömungsmeßtechnik der GALA e.V.* GALA, 1998. ISBN: 3-8265-4287-8.

[5.61] A. Eder, B. Edlinger, M. Jordan and F. Mayinger, Investigation of Transient Flame Development using a Combination of Advanced Optical Measurement Techniques. In: *Proc. of the 8th Int. Symp. on Flow Visualisation*, Sorrento, Italy. 1998.

[5.62] M. Jordan, R. Tauscher and F. Mayinger, New Challenges in Thermo-Fluiddynamic Research by Advanced Optical Techniques. In: *Proc. of the 15th UIT National Heat Transfer Conference*, Torino, Italy. 1997.

[5.63] C. Gerlach, A. Eder, M. Jordan, N. Ardey and F. Mayinger, Advances in Understanding Flame Acceleration for the Improving of Combustion Efficiency. In: *Energy Conservation Through Heat Transfer Enhancement of Heat Exchangers*, Cesme, Turkey. Nato Advanced Study Institute, 1998.

[5.64] M. Jordan, *Ignition and Combustion of premixed turbulent jets (in German)*. PhD thesis, Technische Universität München, 1999.

[5.65] M. Jordan, N. Ardey and F. Mayinger, Effect of the molecular and turbulent transport on flame acceleration within confinements. In: *Proc. of the 11th Int. Heat Transfer Conference*, Kjongju, Korea. 1997.

[5.66] I.S. Zaslonko, V.P. Karpov, S.M. Frolov, M. Jordan, A. Eder and F. Mayinger, Flame-Jet Ignition of Fuel Air Mixtures. Experimental Findings and Modeling. In: *Proc. of the 16th Int. Conl. on the Dynamics of Explosions and Reactive Systems (ICDERS-16)*, Heidelberg, Germany. 1999.

[5.67] M. Jordan, A. Eder, B. Edlinger and F. Mayinger, Turbulent Quenching and Acceleration of Flames by Highly Blocking Obstacles. FISA Symposium 1999, to be published.

[5.68] M. Jordan, N. Ardey, C. Gerlach and F. Mayinger, Quenching Effects at Jet-Ignition of Lean Hydrogen- and Methane-Air Mixtures. In: *Proceedings of the 10th Int. Symp. on Transport Phenomena in Thermal Science and Process Engineering*, Vol. 1, Kyoto, Japan. 1997, 19–24.

[5.69] G. W. Koroll, R. K. Kumar and E. M. Bowles, Burning velocities of hydrogen-air mixtures. Combustion and Flame, Vol. 94, 1993, 330–340.

[5.70] N. Peters, Cours sur la combustion turbulent. Institut de l'Ecole Normale Superieure, Paris, 1997.

[5.71] R. Beauvais, *Brennverhalten vorgemischter, turbulenter Wasserstoff-Luft-Flammen in einem Explosionsrohr [Compustion properties of premixed, turbulent hydrogen-air flames in an explosion tube]*. PhD thesis, Technische Universität München, 1994.

[5.72] R.G. Abdel-Gayed and D. Bradley, Combustion Regimes and the Straining of Turbulent Premixed Flames. Combustion and Flame, Vol. 76, 1989, 213–218.

[5.73] R. P. Lindstedt and V. Sakthitharan, Time Resolved Velocity and Turbulence Measurements in Turbulent Gaseous Explosions. Combustion and Flame, Vol. 114, 1998, 469–483.

[5.74] D.R. Greig and C.K. Chan, Burning of Near-Flammability H2-air Mixtures in Interconnected Vessels. AECL report, COG-97-474, , 1998.

[5.75] R.K. Kumar, J. Loesel-Sitar, W.A. Dewit, E.M. Bowles and B. Thomas, Experiments in the Large-Scale Vented Combustion Test Facility: Series S01-Quiescent Vented Combustion Tests with Central Ignition in Hydrogen-Air Mixtures in the Full- Volume Geometry. AECL, COG-96-578, , 1997.

[5.76] J. Loesel-Sitar, W.A. Dewit, E.M. Bowles and B. Thomas, Experiments in the Large- Scale Vented Combustion Test Facility: Series S03-Vented Combustion Tests at $100^{\circ}C$ in Hydrogen-Air-Steam Mixtures in the Full-Volume Geometry. AECL report, COG-99-135, , 1999.

[5.77] T. Kanzleiter, Hydrogen Igniter Experiments Performed in the Model Containment Utilities Program. Battelle Institute, Final Report No. BF-V67.503-01, , 1992.

[5.78] T. Kanzleiter, Hydrogen Igniter Experiments Performed in the Model Containment Hx Tests. Battelle Institute, Final Report No. BleV-R66.985-01, , 1992.

[5.79] T. Kanzleiter, Experiments on the Efficacy of Hydrogen Mitigation Methods within a Multi-Compartment Containment Geometry. Battelle Institute, Final Report No. BleV-R67.036-01, , 1991.

[5.80] T. Kanzleiter and J Tenschert, Experiments on Hydrogen Deflagrations in Compartments with Obstacles. Battelle Ingenieurtechnik GmbH, Final Report No. BF-R68.145-01, , 1995/1997.

[5.81] T. Kanzleiter, DIVA - Versuche zur H2-Deflagration in einer Inertgas-verdünnten Sicherheitsbehülter-Atmosphäre [DIVA - H2-deflagration experiments in a containment, diluted with inert gas]. Battelle Ingenieurtechnik GmbH, Final Report No. BF-V 68.338-1, , 1996.

[5.82] J. Tenschert, Wasserstoff-Deflagrations-Experimente in einer kleinmaßstäblichen Versuchsanlage DN400 [Hydrogen deflagration experiments in the small-scale test facility DN400]. Battelle Ingenieurtechnik GmbH, Reports BF-R68.145-302, BF-R68.145-303, BF-R68.145-304, , 1995.

[5.83] L. Valencia, Wasserstoffdeflagrationsversuche in großer 3-Raumgeometrie im HDR-Containment [Hydrogen deflagration experiments in the large-scale 3D HDR containment]. In: *Jahrestagung Kerntechnik*, Karlsruhe. 1992.

[5.84] T. Hashimoto, K. Inagaki and J. Ogata, Large-Scale hydrogen Combustion Test at NUPEC. In: *Proceedings of the International (5 countries) Cooperative Exchange Meeting on Hydrogen in Reactor Safety*, Toronto, Canada. 1997.

[5.85] MELCOR 1.8.4, User's Guide. USNRC, Office of Nuclear Regulatory Research, NUREG/CR-6119, Rev.1, 1998.

[5.86] COCOSYS V1.1, Program Reference Manual. GRS, , 1999.

[5.87] M. Heitsch, Das Verbrennungsmodell DECOR für das Programmsystem RALOC mod4 [The combustion model DECOR for the RALOC mod4 code]. GRS-A-2292, , 1995.

[5.88] M. Heitsch, A Model of Vented Hydrogen Deflagrations in a Containment. Nuclear Technology, Vol. 114, 1996, 68–76.

[5.89] G.W. Koroll, R.K. Kumar and E.M. Bowles, Burning Velocities of Hydrogen-Air Mixtures, Combustion and Flame. Combustion and Flame, Vol. 94, 1993.

[5.90] M. Heitsch, Begleitung und Analyse großmaßstäblicher Wasserstoff- Verbrennungsversuche im Rahmen der Zusammenarbeit mit NUPEC (MITI) Japan [Analysis of large-scale deflagration experiments within the scope of cooperation with NUPEC (MITI) Japan]. GRS-A-2397, , 1996.

[5.91] A. Geist et al., PVM User's Guide and Reference Manual. RNL/TM-12187, Oak Ridge National Laboratory, , 1994.

[5.92] H. Paillre et al., Development of hydrogen distribution and combustion models for the multi-dimensional/lumped parameter TONUS code. 1997. Proc. 8th NURETH Conf., Kyoto, JAPAN.

[5.93] K.K. Murata et al., Users Manual for CONTAIN 1.1 : A Computer Code for Severe Nuclear Reactor Accident Containment Analysis. Sandia National Laboratories SAND87-2309, NRC Report NUREG/CR-2309, 1989.

[5.94] J. Gauvain and J.P. LHériteau, JERICHO, a code for computation of containment thermal hydraulic behaviour during a severe accident in a NPP. 1989. Proc. Int. Conf. NURETH 4, 909-914, Karlsruhe, Germany, October 10-13.

[5.95] M. Plys et al., MAAP4 model and validation status. 1993. Proc. 2nd Int. Conf on Nuclear Engineering, San Francisco, USA, March 21-24.

[5.96] H. Jahn et al., Description of the RALOC/FIPLOC family - Part 2 : Physical modeling of thermal hydraulics and integration methods. GRS Report, GRS-A-1426, 1988.

[5.97] J. R. Travis, HMS: a computer program for transient three dimensional fluid flows with chemical reactions and fuel sprays. NRC Report, NUREG/CR-4020, 1984.

[5.98] T. L. Georges et al., Containment Analysis with GOTHIC. 1991. Proc. 27th Nat. Heat Transfer Conf., Minneapolis, Minnesota, USA.

[5.99] A. Majda and J. Sethian, The Derivation and Numerical Solution of the Equations for Zero Mach Number Combustion. Combustion Science and Technology, Vol. 42, 1985, 185–205.

[5.100] A. Beccantini et al., Upwind flux splitting schemes for the 1D Euler equation : Application to shock tube and blast wave model problem. CEA internal report, 1997.

[5.101] A. Beccantini et al., A two-dimensional high order unstructured grid solver for unsteady shock propagation problems. CEA internal report, 1998.

[5.102] P. Verpeaux et al., A Modern approach of computer codes for structural analysis. 1989. Proc. of the 10th Conf. On structural Mechanics in Reactor Technology, Anaheim, USA.

[5.103] C.K. Chan, J. Loesel-Sitar, R. Beauvais and F. Mayinger, Modeling maximum flame speed. Nuclear Engineering and Design, Vol. 166, 1998, 463–470.

[5.104] G. E. Andrews, D. Bradley and S. B. Lwakabamba, Turbulence and turbulent flame propagation: A critical Appraisal. Combustion & Flame, Vol. 24, 1975, 285–304.

[5.105] F. Mayinger, R. Beauvais, G. Strube and N. Ardey, Einfluss der Temperatur auf die Grenzen für den Übergang zur Detonation in Wasserstoff/Luft/Wasserdampf-Gemischen AND Einfluss der Strömungsstruktur auf die Ausbreitung von Wasserstoff-Luft Flammen [Influence of Temperature on the Transition to Detonation in Hydrogen/Air/Steam Mixtures AND Influence of the Fluid Flow on the Propagation of Hydrogen-Air Flames]. 1995. BMFT 1 500 824 and BMFT RS 1500 810.

[5.106] G.W. Koroll, R.K. Kumar and E.M. Bowles, Burning velocities of hydrogen-air mixtures. Combustion & Flame, Vol. 94, 1993, 330–340.

[5.107] L.S. Kozachenko and I.L. Kuznezov, Burning velocity in a turbulent stream of a homogeneous mixture. Combustion, Explosions, Shock waves, Vol. 1, 1965, 22ff.

[5.108] N. Peters, New developments in the theory of premixed turbulent combustion. 1997. Cours sur la combustion turbulente, Institut de lEcole Normale Suprieure, Paris, FRANCE.

[5.109] C.K. Chan, Flame acceleration and transition to detonation experiments at AECL. 1995. Hydrogen combustion working group meeting, Tokyo, JAPAN.

[5.110] M. P. Sherman, S. R. Tieszen and W. H. Benedick, FLAME Facility. 1975. NUREG CR-5275.

[5.111] T. Hirose, H. Ogasawara (NUPEC) and J. Ogata (MHI), Large scale hydrogen combustion test. 1995. Hydrogen combustion Working group Meeting, Tokyo, JAPAN.

[5.112] B. Edlinger, C. Poruba, A. Eder, F. Mayinger, U. Bielert, A. Veser, A. Kotchourko, W. Breitung, P. Royl, W. Scholtyssek, H. Wilkening, T. Huld, M. Movahed, F. Dabbene and E. Studer, Multi-dimensional simulation of hydrogen distribution and combustion in severe accident. EU contract FI4S-CT-95-0001, Final Report (to be published), 1999.

[5.113] S.B. Dorofeev, A.S. Kotchourko, A.A. Efimenko and B.B. Chaivanov, Evaluation of hydrogen explosion hazard. Nuclear Engineering and Design, Vol. 148, 1994, 305–316.

[5.114] J. E. Shepherd, Chemical kinetics of hydrogen-air-diluent detonations. Progress in Astronautics and Aeronautics, Vol. 106, 1986, 263–293.

[5.115] G. Ciccarelli et al., High temperature hydrogen-air-steam detonation experiments in the BNL Small-Scale Development Apparatus. BNL-NUREG-52414, , 1994. NUREG CR-6213.

[5.116] J.H.S. Lee, R. Knystautas, C. Guirao, W.B. Benedick, J.E. Shepherd and P. A. Freiman, H2-Air Detonations. 1982. SAND82-1864C.

[5.117] D. W. Stamps, Detonation cell widths in hydrogen-air-diluent mixtures. 1990. SAND90-2251C.

[5.118] W. Breitung, I. Coe, H. Grönig, L. He, R. Klein, H. Olivier, W. Rehm, E. Studer and B. Wang, *Models and Criteria for Prediction of Deflagration-to-Detonation Transition (DDT) in Hydrogen-Air-Steam Systems under Severe Accident Conditions*. Projekt FI4S-CT96-0025 - Final Report. European Commission, Brussels, 1999.

[5.119] S.B. Dorofeev, A. Kotchourko, A. Lelakin, A. Baitin and A. Efimenko, Development of numerical programs for 3d reactive flow simulation in complex containment geometry. Turbulence Modeling. Final report for FZK, Kurchatov Institute Moscow, , 1994.

[5.120] A. Kotchourko, W. Breitung and A. Veser, Reactive Flow Simulations in Complex 3d Geometries using the COM3D Code. In: *Jahrestagung Kerntechnik*, Karlsruhe, Germany. May 18-20 1999, 173.

[5.121] A. Veser, A. Kotchourko and W. Breitung, Experiments on Turbulent Combustion and COM3D Verification. ibid, .

[5.122] V. Yakhot and S.A. Orszag, Renormalization group analysis of turbulence. I.Basic theory. J.sci. Comput., Vol. 1(3), 1986.

[5.123] A. Harten, High resolution schemes for hyperbolic conservation laws. J.Comput. Phys., Vol. 49, 1983, 357–393.

[5.124] A. Kotchourko, W. Breitung, A. Veser and S.B. Dorofeev, Tube experiments and numerical simulation on turbulent hydrogen-air combustion. In: *21st Symp. (Int.) on Shock Waves*, Great Keppel Island, Australia. 1997.

[5.125] W. Breitung, S.B. Dorofeev, A.A. Efimenko, A.S. Kotchourko, R. Redlinger and V.P. Sidorov, Large-scale confined hydrogen-air detonation experiments and their numerical simulation. In: *20th Symp. (Int.) on Shock Waves*, Pasadena, CA, USA. 1996.

[5.126] AEA Technology Ltd., Oxfordshire, United Kingdom, *CFX4.2, Solver Manual*, 1997.

[5.127] G.L. Schott and J.L. Kinsey, Kinetic studies of hydroxyl radicals in shock waves, II. Induction times in the hydrogen-oxygen reaction. J. Chem. Phys., Vol. 29, 1958, 1177–1182.

[5.128] K. Fischer et al., Verification and further development of a predictive multidimensional model for hydrogen deflagration in a multiple compartment LWR-containment. Final report BF-R68.121, Battelle, Eschborn, Germany, , 1996.

[5.129] B. Durst and F. Mayinger, Einfluß Containment-typischer Strömungshindernisse auf die Ausbreitung von Wasserstoff-Luft-Flammen – Band II: Lokale Strömungsmessungen und dreidimensionale Modellierung der turbulenten Verbrennung [Influence of containment typical obstacles on the propagation of turbulent hydrogen-air flames – vol II: measurement of flow velocity and modelling of turbulent combustion]. Abschlußbericht zum Forschungsvorhaben BMFT, Nr. 150 0957, TU München, 1999.

[5.130] B. Durst. PhD thesis, Technische Universität München, 1999. To be published.

[5.131] B. Durst, N. Ardey and F. Mayinger, Interaction of Turbulent Deflagrations with Representative Flow Obstacles. In: *Proceedings of the OECD/NEA/CSNI Workshop On the Implementation of Hydrogen Mitigation Techniques*, Winnipeg, Manitoba. 1996, 433–447.

[5.132] S. B. Pope, The Statistical Theory of Flames. Phil. Trans. R. Soc. London, Vol. A 291, 1979, 529–568.

[5.133] K. N. C. Bray, Turbulent Flows with Premixed Reactants. In: *Turbulent Reacting Flows*. (P. A. Libby and F. A. Williams, (editors)), Topics in Applied Physics, chapter 4, 115–183. Springer Verlag, Berlin, Heidelberg, 1980.

[5.134] R. Borghi, Turbulent Combustion Modelling. Prog. in Energy and Combust. Sci., Vol. 14, 1988, 245–292.

[5.135] F. C. Lockwood and A. S. Naguib, The Prediction of Fluctuations in the Properties of Free, Round-Jet, Turbulent, Diffusion Flames. Combust. and Flame, Vol. 24, 1975, 109–124.

[5.136] R. J. Kee, J. F. Grcar, M. D. Smooke and J. A. Miller, A FORTRAN Program for Modeling Steady Laminar One-Dimensional Premixed Flames. Sandia National Laboratory, Technical Report SAND85-8240, 1985.

[5.137] R. J. Kee, F. M. Rupley and J. A. Miller, CHEMKIN-II: A FORTRAN Chemical Kinetics Package for the Analysis of Gas-Phase Chemical Kinetics. Sandia National Laboratory, Technical Report SAND89-8009, 1989.

[5.138] U. Maas, *Mathematische Modellierung instationärer Verbrennungsprozesse unter Verwendung detailierter Reaktionsmechanismen [Mathematical modelling of transient combustion processes using detail reaction mechanisms]*. PhD thesis, Universität Heidelberg, 1988.

[5.139] U. Maas and J. Warnatz, Ignition Processes in Hydrogen-Oxygen Mixtures. Combust. and Flame, Vol. 74, 1988, 53.

[5.140] A. Eder, B. Edlinger and F. Mayinger, Einfluß Containment-typischer Strömungshindernisse auf die Ausbreitung von Wasserstoff-Luft-Flammen, Vol.III,Maßstabseffekte und Anlaufvorgänge [Influence of containment typical obstacles on the propagation of turbulent hydrogen-air flames – vol III: Scaling and run-up effects]. TU München, Abschlussbericht, BMFT 1500957, , 1998.

[5.141] A. Eder, C. Gerlach and F. Mayinger, Determination of Quantitative Criteria for the Transition from Deflagration to Detonation in H2/Air/H2O-Mixtures. In: *Proceedings of the 22nd International Symposium on Shock-Waves*, London, UK. 1999.

[5.142] A. Eder, C. Gerlach and F. Mayinger, Experimental Observation of Fast Deflagrations and Transition to Detonations in Hydrogen-Air-Mixtures. In: *Proceedings of the Symposium on Energy Engineering in the 21st Century, to be published*, Hong Kong. 2000.

[5.143] W. Rehm, M. Heitsch, W. Jahn and F. Semler, Numerical Investigations of Gas Mixing and Deflagration-to-Detonation Effects Using Multi-Dim. Computational Fluid Dynamic Tools. In: *3rd Int. CFX Users Conference*. AEA Harwell, UK, 1997, 393–413.

[5.144] W. Rehm, R. Klein, N. Peters, P. Thibault and C. Chan, Effects of DDT on Hydrogen Explosion Loads in Large Scale Enclosures. Pilot Project Final Report, Contract No. FI3S-CT92-0003, Brussels, Aug. 25, '95, 1995.

[5.145] W. Rehm, P. Royl, F. Fineschi, M. Heitsch, K. Reinders and W. Breitung, Combustion Phenomena in Nuclear Reactor Containments. In: *FISA-95 Symposium, EC Research on Severe Accidents*. European Commission, 1996, 330–357. ISBN 92-827-6980-1.

[5.146] R. Klein, W. Breitung, W. Rehm, H. Olivier, L. He, P. Armand and M. Ang, Models and Criteria for Prediction of Deflagration-to-Detonation Transition (DDT) in Hydrogen-Air-Steam Systems under Severe Accident Conditions. In: *FISA-97 Symposium, EC Research on Severe Accidents*. European Commission, 1997.

[5.147] F. Hoßfeld, E. Maehle and E.W. Mayr, PASA '96, Parallel Systems and Algorithms. In: *Proc. of the 4th Workshop*. Research Center Jülich, Germany, 1996, 393–413.

[5.148] M. Gerndt, Compilers for Parallel Computers. In: *Proc. of the Sixth Workshop*, Vol. 21. Research Center Jülich, Germany, 1996.

[5.149] F. Unger, Port of the CFX-5 to the CRAY System at FZJ. AEA Technology Otterfing, Germany, Technical Report, 1998.

[5.150] M. Kuntz and W. Rehm, Combustion Modelling in CFX-5. In: *CFX User Conference, Friedrichshafen*. AEA-Technology, 1999.

[5.151] W. Rehm, M. Gerndt, W. Jahn, F. Semler and I. Jones, CFD Simulation of Deflagration-Detonation Processes Using Vector- and Parallel Computing Systems. Journal for Applied Mathematical Modelling, Vol. 22, 1998, 811–822.

[5.152] B. Wang, M. Weber and H. Olivier, Ignition Phenomena and Detonation Formation in H2-Air and H2-Air-Steam Mixtures. RWTH-SWL, Aachen, Germany, , 1998.

[5.153] A. Veser, W. Breitung and G. Engel, Hydrogen combustion experiments. Projekt Nukleare Sicherheitsforschung, Jahresbericht 1997, 1998, 82. Report FZKA-6126.